MIKRONIEK

PROFESSIONAL JOURNAL ON PRECISION ENGINEERING

2019 (VOL. 59) ISSUE 6

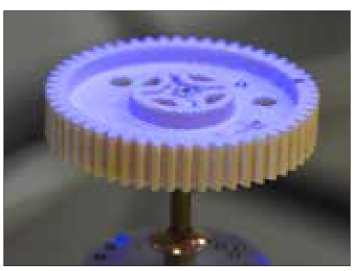

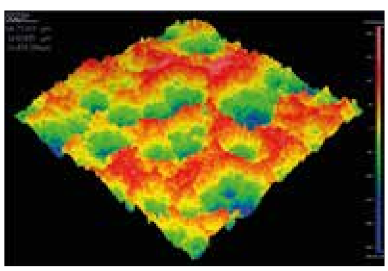

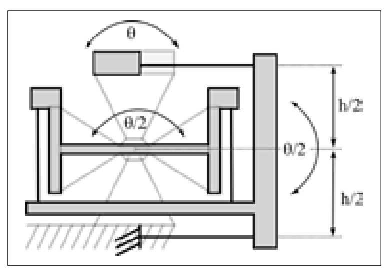

- THEME: ENERGY (MICRO & MACRO)
- NOVEL INTERVENTIONAL X-RAY SYSTEM ARCHITECTURES
- 2019 PRECISION FAIR IMPRESSIONS
- MULTIPLE-NOZZLE RECOATER

MIKRONIEK IS A PUBLICATION OF THE DUTCH SOCIETY FOR PRECISION ENGINEERING WWW.DSPE.NL

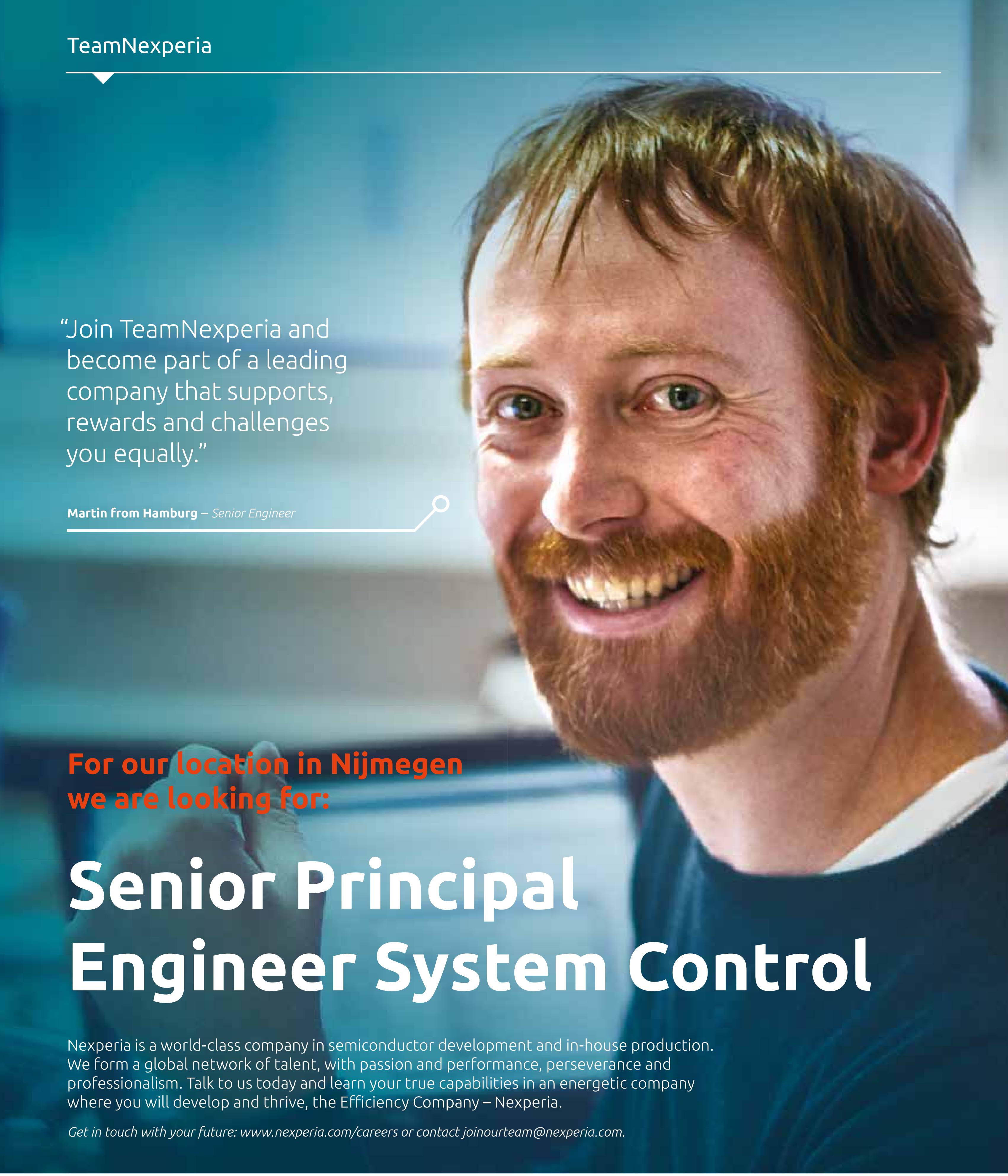

nexperia

EFFICIENCY WINS.

IN THIS ISSUE

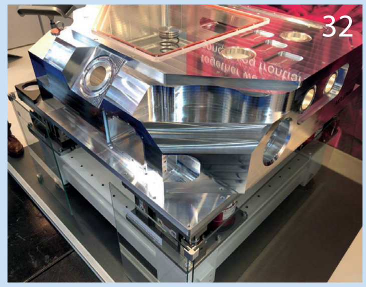

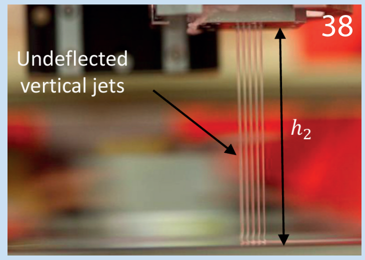

FEATURES

PUBLICATION INFORMATION

Objective
Professional journal on precision engineering and the official organ of DSPE, the Dutch Society for Precision Engineering. Mikroniek provides current information about scientific, technical and business developments in the fields of precision engineering, mechatronics and optics. The journal is read by researchers and professionals in charge of the development and realisation of advanced precision machinery.

DSPE
YOUR PRECISION PORTAL

Publisher
DSPE
Annemarie Schrauwen
High Tech Campus 1, 5656 AE Eindhoven
PO Box 80036, 5600 JW Eindhoven
info@dspe.nl, www.dspe.nl

Editor
Hans van Eerden, hans.vaneerden@dspe.nl

Advertising canvasser
Gerrit Kulsdom, Sales & Services
+31 (0)229 – 211 211, gerrit@salesandservices.nl

Design and realisation
Drukkerij Snep, Eindhoven
+31 (0)40 – 251 99 29, info@snep.nl

Subscription
Mikroniek is for DSPE members only.
DSPE membership is open to institutes, companies, self-employed professionals and private persons, and starts at € 80.00 (excl. VAT) per year.

Mikroniek appears six times a year.

ISSN 0026-3699

The main cover photo (by Thomas Tolstrup, featuring solar collectors) is courtesy of Heliac. Read the article on page 8 ff.

SAVING ENERGY, SECURING PRECISION

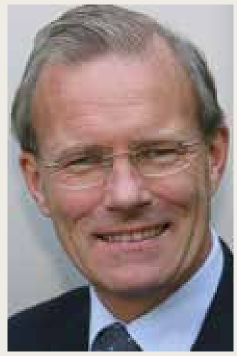

Precision engineering and today's energy challenges related to climate change and limited material resource availability appear to be unrelated. But think one level deeper. Over the last centuries, mankind has been able to generate valuable products in smaller and smaller dimensions. Large windmills and boats became steam engines and then petrol engines made with millimeter precision. Products made by craftsmen became mass-produced items. In these products, every component has to have accurate dimensions to be exchangeable with other components and to fit in any other part with micrometer precision. Today, we produce valuable products with nanometer precision. We are even able to process food using 3D printers with microlitre-precision dosing of ingredients, after eons of bulk production of food the size of decilitres on your daily plate.

The basic reason behind this trend is that on a general level the cost of a product is related to the amount of material required to build that product. If one writes off the design costs in three years and the manufacturing equipment costs in seven years, the only remaining costs are those of the material and the logistics of handling. If you make the products smaller and smaller, they will become cheaper. Once you make them smaller, however, precision aspects become more important.

We expect this trend to accelerate. Where the fourth industrial revolution is about digitalisation, the fifth will be about sustainability. CO_2 costs today are at a level of 30 euro/ton, i.e. 3 eurocent/kg. Realistic price levels will look more like 10 eurocent/kg, and it is possible that they will reach 300 euro/ton or 30 eurocent/kg. Petrol taxes today are already 1 euro/litre, so why should CO_2 waste costs be so low? If CO_2 costs increase to the level of 10 eurocent/kg or more, the use of new materials will become significantly more expensive, as mining and processing involve a lot of CO_2 emissions. The costs of these will add up to the cost price of materials. More refurbishment and recycling, etc., will be the first simple steps in avoiding these increasing costs, but shrinking the size of a product to a smaller dimension ultimately reduces the amount, and therefore the costs, of the materials required.

It can be expected that future products will be designed with minimal material usage. This might result, in motion systems for example, in less weight and less required energy. As stated above, however, think deeper: less material might result in less stiffness, whereas the same positioning precision will still be needed. A smarter digitalised solution might help, but one way or another precision engineering skills will be necessary for finding the proper solutions with fewer materials. Lastly, as an ultimate consequence, precision skills will remain important even during the coming years/decade when a fifth industrial revolution will change our industry once again.

Prof.dr.ir. Egbert-Jan Sol
Programme director Smart Industry, TNO Industry
egbert-jan.sol@tno.nl, www.smartindustry.nl

CLASSIFYING MINIATURISED GENERATORS

Although motion energy harvesting at the small scales has been a research topic for over 20 years, the implementation of such generators remains limited in practice. One of the most important contributing factors here is the poor performance of these devices under low-frequency excitation. In this research, a classification of miniaturised generators is proposed based on the dynamics of the nonlinear systems. This provides insight in the performance of different types of designs, which can be used to develop new designs with better efficiencies under realistic conditions.

THIJS BLAD AND NIMA TOLOU

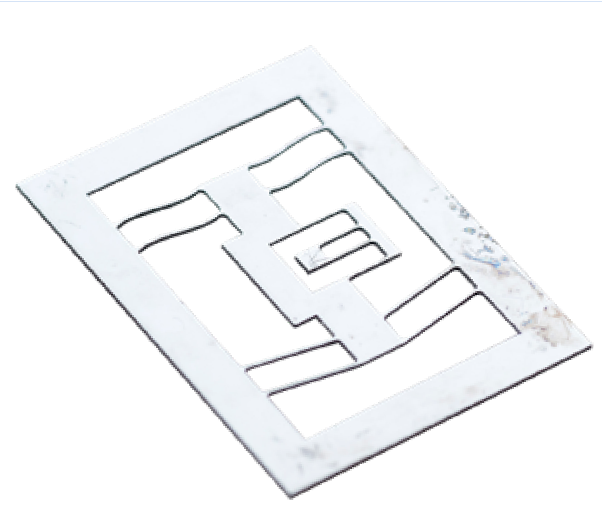

Glossary

- Vibration energy harvester: Device that delivers an electrical output as a result of applied mechanical vibrations.
- Transducer: Part that converts energy from one form to another.
- Piezoelectricity: Electric charge that accumulates in certain solid materials in response to applied mechanical stress.
- Resonance: Phenomenon of amplification that occurs when the frequency of a periodically applied force is close to a natural frequency of a system.
- Bandwidth: Range of frequencies for which a satisfactory performance is obtained.
- Frequency up-converter: Device that incorporates a mechanism that takes a low-frequency input and delivers an output with increased frequency.

AUTHORS' NOTE

Thijs Blad (Ph.D. student) and Nima Tolou (assistant professor) are both associated with the Mechatronic System Design group in the Department of Precision and Microsystems Engineering, Delft University of Technology, Delft (NL).

t.w.a.blad@tudelft.nl
www.pme.tudelft.nl

Introduction

Small generators that harness ambient sources of energy can be attractive alternatives to batteries as wireless power supplies for low-power electronic devices. Of all ambient energy sources, kinetic energy in the form of motion or vibration is generally the most versatile and ubiquitous energy source available [1].

Generators that aim to use this source are grouped under the term vibration energy harvesters and have been investigated for over 20 years since the early work of Williams and Yates in 1996 [2], who investigated the piezoelectric, electromagnetic, and electrostatic transduction mechanisms for the purpose of vibration-to-electric energy conversion.

Generally, the power that can be harvested is in the range of micro- to milliwatts and may fluctuate greatly when the ambient motions are constantly changing. However, the expanding number of wireless devices and the great advances in their power consumption are continuously increasing the interest in the field of energy harvesting.

The most attractive applications are found in environments where battery replacement is expensive, inconvenient and/or prohibited by regulations. Examples of such applications are medical implants such as pacemakers, or wireless sensor networks composed of many small sensor nodes that can be used for the monitoring of structural health in buildings or for the tracking of goods.

In many of these applications it is reasonable to assume future power requirements in the order of a few microwatts. Given that a buffer is used to deal with fluctuations in generated power, this is certainly within reach for energy harvesters of modest sizes in many realistic vibration environments. In the case of the pacemaker, it was already demonstrated in vivo [3] that relevant amounts of energy can be harvested from the motion of the heart itself.

Working principles

Powering these devices requires the transformation of virtually useless energy from an ambient source into useful electric power. For this transformation two things are fundamentally required: an ambient source with a relevant amount of available energy and a device that can facilitate this transformation with a relevant efficiency.

The basic working principle of the vibration energy harvester shown in Figure 1 is as follows. The housing of the generator is mounted on a vibration source. Inside the generator is a suspended inertial element (proof mass) that moves relative to the housing as a result of the applied motion. This relative motion results in an electrical power output due to a transducer such as a piezoelectric material.

Relevant parameters for the maximum power output are the dimensions and mass of the generator as well as the frequencies and accelerations of the applied vibrations. Furthermore, the actual power output is greatly dependent on the dynamic response of the generator to the applied vibrations. In cases where a vibration is applied with a fixed frequency and acceleration, a generator can be designed based on linear models to operate at resonance such that satisfactory power output is ensured. Using this strategy, generators have been reported with efficiencies up to 30% of the theoretical maximum [4].

However, in practical applications the generators will be exposed to vibrations with frequencies and amplitudes that change over time. Although excellent performance was achieved through a resonance-based strategy, the bandwidth over which this performance was found was extremely narrow.

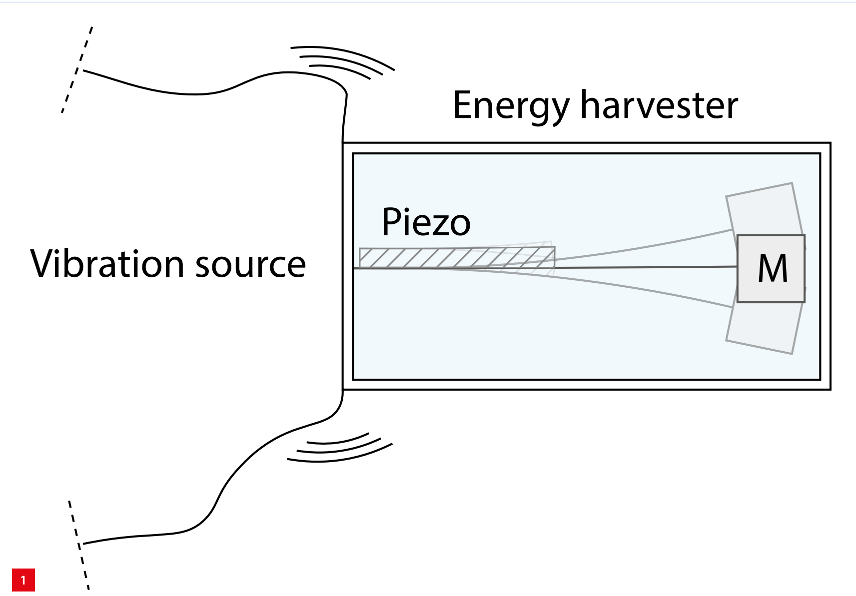

1

General concept of vibration energy harvesting using a piezoelectric transducer; the device is mounted on a vibrating source and generates output power as a result of internal motion.

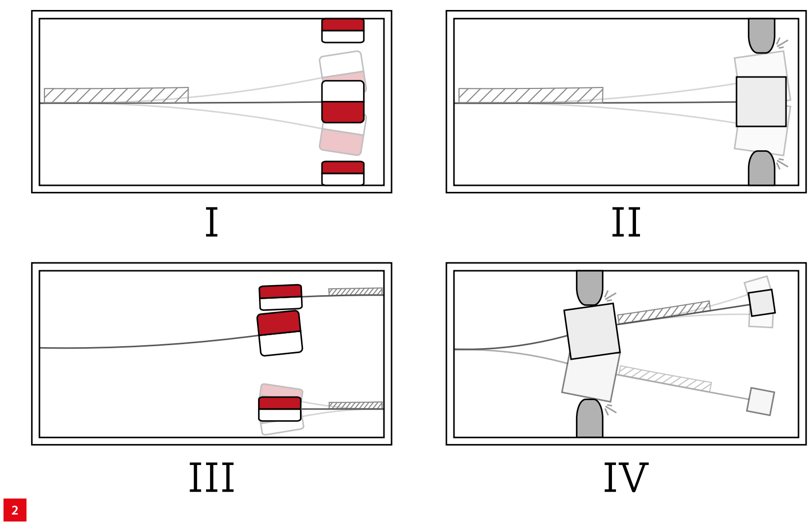

2

Classification of miniaturised generators under low-frequency excitation.
Single-degree-of-freedom generator:
I) using soft stoppers;
II) using hard stoppers.
Frequency up-converter:
III) using plucking;
IV) using impact.

Therefore, in realistic cases these devices may not deliver the required performance. To overcome this problem, more complex mechanisms with nonlinear elements are being developed and investigated. These mechanisms open up a range of nonlinear dynamics and have the potential to demonstrate relevant power outputs under realistic conditions. However, the design of their dynamic response is vastly more complex compared to the linear case, and as a result, the efficiencies of these types of systems are typically much lower.

Overview

When the size of the energy harvester approaches the amplitude of the applied vibrations (as can be the case with miniaturised generators under low-frequency excitation), the internal motion must be limited. The implementation of the motion limiter is an important design aspect and affects the dynamics of the device. Based on the dynamics found in these systems, the miniaturised nonlinear generators can be classified in the groups shown in Figure 2.

Single-degree-of-freedom generators (I + II)

The first class of nonlinear energy harvesters contains the generators with a single degree of freedom (DoF), which is used directly for the energy conversion. In this class we find two groups of devices: I) those that use soft stoppers, and II) those that use hard stoppers, to limit the internal motion.

Soft stoppers rely on a gradually increasing stiffness to limit the internal motion. In the design illustrated in Figure 2.I a moving magnet experiences a repulsive force from the oppositely-poled magnets at the motion limits. The closer the centre magnet moves towards the motion limits, the greater this repulsive force becomes.

The other group features devices with a very rapid stiffening effect at the end of their range of motion. In Figure 2.II it can be seen that a mechanical contact is used to produce the behaviour of a hard stopper.

Frequency up-converters (III + IV)
The other class of systems is the frequency up-converters. These are multi-DoF systems that use an inertial mass to excite a secondary oscillator. The energy is harvested from the motion of the secondary oscillator, which oscillates with an increased frequency compared to the frequency of the driving motion.

The first group of frequency up-converters comprises the systems that excite their secondary oscillator through plucking. The design illustrated in Figure 2.III consists of an inertial mass which snaps back and forth between two secondary oscillators, attaching magnetically. When the inertial mass detaches, the secondary oscillator starts oscillating at its natural frequency, which generates the output power.

The other group of frequency up-converters uses the impact of an impact member to excite the secondary oscillator. In Figure 2.IV a secondary oscillator is mounted in series with the inertial mass. Under a driving motion, the inertial mass makes contact with the mechanical stops at the end of its range of motion. As a result of this impact, the secondary oscillator begins to oscillate in its own natural frequency.

Conclusions
It was found that the efficiencies of nonlinear energy harvesters are typically reported between 0.1 and 1%. In general, generators found in groups I and II report higher efficiencies compared to those of groups III and IV. Reasons for this could be the significantly larger amount of reported work on the single-DoF generators and the increased complexity of the dynamics of frequency up-converters.

However, it was found that the frequency up-converters are likely to demonstrate a better performance when approaching greater degrees of miniaturisation. Furthermore, it was found that the nonlinearities that result from the stoppers or the use of frequency up-conversion, greatly improve the efficiency of the energy harvester over a much wider bandwidth compared to the linear systems.

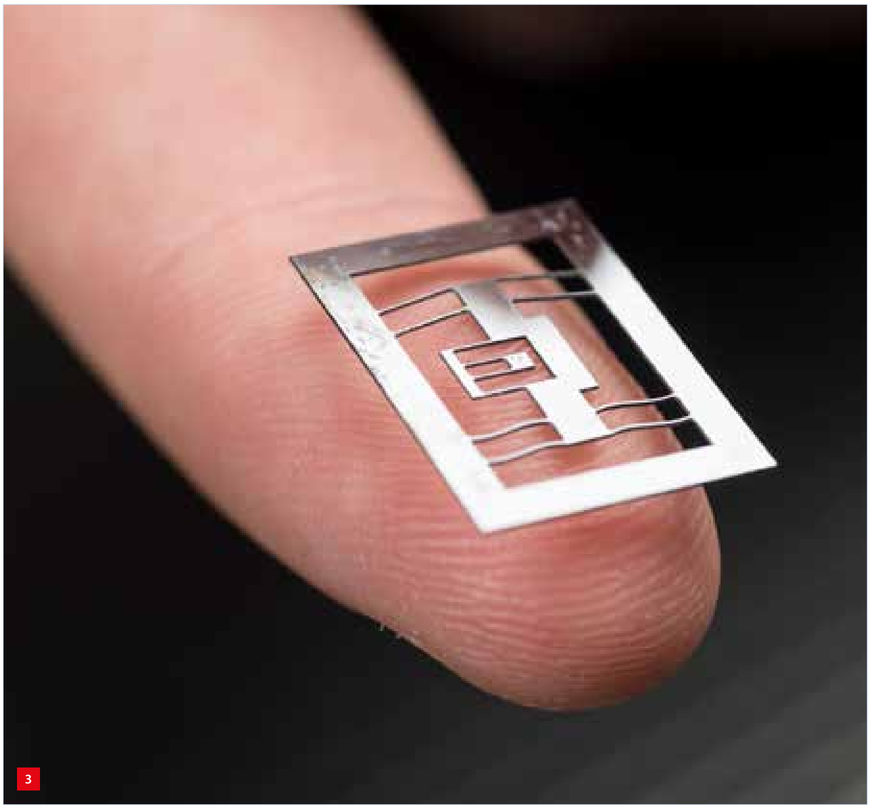
3

Possibly the future of miniaturised generators; a class-IV energy harvester.

Future work
The focus of future work is to systematically benchmark the performance of typical nonlinear generator designs under varying conditions and at different scales to gain better insight in the design parameters and their sensitivities. This can be used to develop more accurate models to estimate the performance of vibration energy harvesters under realistic conditions. Using these models, we aim to develop better designs of miniaturised generators (Figure 3) to build the next generation of energy harvesters.

REFERENCES

[1] Mitcheson, P.D., Yeatman, E.M., Rao, G.K., Holmes, A.S., and Green, T.C., "Energy Harvesting From Human and Machine Motion for Wireless Electronic Devices", *Proceedings of the IEEE*, 96 (9), pp. 1457-1486, 2008.

[2] Williams, C.B., and Yates, R.B., "Analysis of a micro-electric generator for microsystems", *Sensors and Actuators A: Physical*, 52 (1), pp. 8-11, 1996.

[3] Zurbuchen, A., et al., "Endocardial Energy Harvesting by Electromagnetic Induction", *IEEE Transactions on Biomedical Engineering*, 65 (2), pp. 424-430, 2018.

[4] Blad, T.W., and Tolou, N., "On the efficiency of energy harvesters: A classification of dynamics in miniaturized generators under low-frequency excitation", *Journal of Intelligent Material Systems and Structures*, 30 (16), pp. 2436-2446, 2019.

WIND, STORAGE, SOLAR, OFFSHORE AND BEYOND

The euspen Special Interest Group meeting on Precision Engineering for Sustainable Energy Systems took place at the University of Strathclyde, Glasgow, UK on 9-10 October 2019. Distinguished delegates from all over the world shared their experiences and ideas to identify areas of improvement for increased production and high-quality renewable energy systems with low costs.

After the welcome speech by euspen's President, Prof. Enrico Savio, University of Padua, Italy, the Principal and Vice-Chancellor of the University of Strathclyde, Prof. Sir Jim McDonald addressed the importance of precision engineering for renewable energy systems and expressed his desire to take the message from the SIG meeting to the Scottish and UK government in his role as President of the UK Royal Academy of Engineering and co-chair of the Scottish Government's Energy Advisory Board.
Dr. Marieke Beckmann from National Physical Laboratory, UK presented the urgent need for renewable energy systems to address social and economic challenges. She also highlighted the need for advanced metrology systems in the development of renewable energy systems across wind, solar, wave, etc.

Presentations

The two-day programme of six lecture sessions, a poster session and a commercial session provided a rich mix in four broad categories: Wind, Storage, Solar, Offshore and beyond. With growing concern about the necessity of green energy, the programme was strongly focused on the barriers, technological improvements and future challenges for these renewable energy systems.

Wind

The first session started with a discussion of trends by Prof. W.E. Leithead of the University of Strathclyde. Wind energy faces challenges including reliability, high cost, maintenance, etc. Despite these challenges, energy bodies over the world have set their future development goals in the wind sector. Prof. Alex Slocum, MIT, USA addressed the importance of total design for future wind energy systems.

A Competence Center for Wind energy (CCW) was presented by Prof. Frank Härtig, PTB, the National Metrology Institute of Germany. The centre comprises three major sections. It can accurately measure the 3D geometries of large components with diameters up to 4 m. The wind tunnel allows to generate homogeneous wind fields with speeds in the range of 1-30 m/s. Finally, the torque measuring unit can measure torques up to 5 MN·m and hopefully the range up can be extended to 20 MN·m in future. The talk highlighted the importance of applying digital technology based on measured big data for future wind energy systems, as well as the need of unifying the definition of digital twin in this field.

1

Heliac from Denmark has developed an extremely efficient solar collector based on the large-area precision manufacturing of light-guiding polymer Fresnel lenses on glass. (Photos: Thomas Tolstrup, Heliac)

EDITORIAL NOTE

This event report was contributed by euspen (European Society for Precision Engineering and Nanotechnology).

www.euspen.eu

Wind turbine hub precision manufacturing with a mobile CNC machine was presented by Alessandro Checchi of the Technical University of Denmark (DTU). The prototype of a mobile CNC machine with enhanced manufacturing capabilities was designed and implemented. The design models' validations show good agreement. Enhanced reliability of wind energy systems requires better quality assurance by traceable metrology for large drivetrain components. For this, Dr. Harald Bosse of PTB introduced some novel measurement standards.

Storage

In this session, several energy storage methods were introduced: pumped hydro, gravity and electrolyser. Prof. Maximilian Fleischer, chief key expert from Siemens, explained how power generation and consumption are mismatched today due to residual loads. Economical usage of this excess energy from renewables is important where the storage technologies can play an important role to solve this problem. A pumped hydro power plant can be an effective storage solution.

Cheng Cheng, from the Australian National University, focused on the potential of off-river pumped hydro systems with 100% renewable energy, which can be the lowest-cost energy storage system. About 616,000 possible off-river sites (between 60° North and 56° South latitude) over the world have already been identified.

On the other hand, chemical storage systems such as proton-exchange membrane (PEM) electrolysers can be alternative solutions because of their reduced size. Dr. Arend de Groot of TNO, the Netherlands discussed the supply chain development for PEM electrolysers. Finally, Miles Franklin of Gravitricity, UK presented a storage system based on gravity. They are developing this technology, which can be very effective for small-range application.

Solar

Solar is one of the important sources of renewable energy and the technology is now well developed and reliable. Prof. Tapas Mallick of the University of Exeter, UK discussed the challenges, opportunities and integration of solar energy technologies.

Dr. Henrik Pranov of Heliac, Denmark presented large-area precision manufacturing of light-guiding lenses for solar heat (Figure 1). These polymer Fresnel lenses on glass were tested at DTU and proved to constitute extremely efficient solar collectors. They deliver heat at the same cost as natural gas. Pranov also demonstrated a rock-based system to store solar or excess process heat where the charging and discharging takes place by condensation or evaporation, respectively.

Prof. Liam Blunt from the University of Huddersfield, UK presented the roll-to-roll production and in-process metrology for thin-film photovoltaics carried out in the EU-funded NanoMend project. He reported initial measurements taken on prototype films and the correlation of water vapour transmission with defect density, and also described an in-process, high-speed, environmentally robust optical interferometer instrument developed to detect defects on the polymer film during manufacture.

Offshore and beyond

Prof. Alex Slocum of MIT talked about energy harvesting and storage-system-stabilised offshore wind turbines. He presented a symbiotic energy harvesting idea to lower the cost where the offshore wind turbine structure supports the wave and hydro energy systems. The main challenge to this symbiotic system is the weight restriction. Dr. Zhiming Yuan of the University of Strathclyde presented several offshore renewable energy hybrid models. Integration can yield a platform that can serve multiple purposes including water breaking and aquaculture. His colleague Dr. David Butler discussed manufacturing challenges for lifetime extension of renewable energy systems, through refurbishing or remanufacturing of system parts. And Dr. Cameron Johnstone from the same university nicely wrapped up the meeting with an update of wave and tidal energy development.

Conclusion

The two-day programme generated a variety of discussions on the status, challenges and opportunities for renewable energy systems. They are becoming matured with a huge amount of ongoing research and developments. Overall, the SIG meeting was successful and inspiring. All the delegates felt the same as Prof. Alex Slocum (Figure 2) wished, "we are all responsible for the canvas of life – we can work together to create a beautiful future for the planet and all its lifeforms."

2

Prof. Alex Slocum, MIT: "We are all responsible for the canvas of life – we can work together to create a beautiful future for the planet and all its lifeforms."

ADVANCED METROLOGY FOR ENERGY EFFICIENCY

Lightweighting is a priority for automotive OEMs in their quest to adhere to exacting engine efficiency and emission guidelines. More and more, massive iron engines and components are replaced with aluminium and lightweight alloys that match the strength of iron without the negative weight implications. Cutting-edge optical metrology tools can facilitate the manufacture of lightweighted engine components.

MICHAEL SCHMIDT

There have been many initiatives in recent years aimed at reducing vehicle emissions and increasing overall efficiency. This has required the automotive sector to focus enormous resources on optimising engine performance. Be it due to concerns over climate change or insulating economies against the vagaries of fuel costs and possible fuel shortages; the race is on to make vehicles considerably more efficient while at the same time maintaining a level of required functionality and attractiveness to stimulate sales and profitability.

Thermal barrier coatings

Focusing on efficiency, automotive OEMs are looking to reduce weight and at the same time, enhance the efficiency of engine performance. One area of focus in line with these goals is the replacement of cast-iron cylinder liners used in aluminium cylinder blocks with more thermally efficient and lighter-weight materials. Various viable alternative materials and solutions exist that must be wear- and scuff-resistant as well as having a low friction coefficient, one such being thermal barrier coatings (TBCs).

TBCs are the choice for many automotive OEMs today, effectively, coating the cast aluminium block bores with a spray of wear-resistant, ceramic or composite material. This material will harden to form a much thinner surface – relative to a liner – in the aluminium cylinder. To date, the most commercially viable of these are being applied through the use of the plasma spray process, which yields superior wear resistance compared to iron, enabling aluminium alloy engines to utilise robust tribological materials within the harsh environments of combustion chambers.

However, there are also some inherent issues with the spray-coating process that require the implementation of rigorous quality management procedures and measuring protocols. For example, at the high velocity with which the coating is applied to the cylinder wall, a splatter morphology occurs, leading to possible inconsistent coating.

Surface metrology

Properties of the coating such as porosity, micro-hardness, thickness, adhesion, and strength are essential metrics in assessing its viability and provide important tools for evaluating which process parameters need to be changed to achieve an optimum coating [1].

The non-deterministic porosity distribution across the surface of the cylinder after spraying requires the use of a metrology technology that is able to reliably, repeatably and accurately measure the three phases required to produce a finished lined cylinder:
- mechanical activation;
- thermal spray application;
- post-spray finishing.

Any metrology solution used to assess the surface characteristics of a spray-lined cylinder must be able to make highly accurate measurements at all three of the phases of the process, each stage transitioning from extremely rough to very smooth. This dynamic range of surface textures requires a metrology solution such as the one developed by Zygo using its coherence scanning interferometry (CSI) technology (see the box). CSI can capture data pertaining to a vast array of surface heights and textures and is used in Zygo's range of 3D optical profilers.

3D optical profilers

CSI extends interferometric techniques to surfaces that are complex in terms of roughness, steps, discontinuities, and structure. Additional benefits include the equivalent of autofocus at every point in the field of view and suppression of spurious interference from scattered light.
CSI technology is at the heart of all Zygo's 3D optical

AUTHOR'S NOTE

Michael Schmidt is market development manager at Zygo Corporation, headquartered in Middlefield, CT, USA. Zygo, part of the Ultra Precision Technologies Division of Ametek, is a worldwide supplier of optical metrology instruments, high-precision optical components and complex electro-optical systems.

michael.schmidt@zygo.com
www.zygo.com

CSI: coherence scanning interferometry explained

CSI uses the principle of optical interference to compare a part that needs to be measured to a 'perfect' reference surface; Figure 1 shows a typical set-up. Interferometry divides a light source into two paths and compares the light reflected from a test surface to light reflected from a reference surface. The two reflections combine at a detector where they interfere with each other, and a pattern of light and dark intensities is created. That interference pattern represents the surface topography of the test surface

In the system, light comes from an illuminator based on white LEDs. That light travels through illumination optics to the objective. The objectives in Zygo's optical profilers not only provide magnification like a regular light microscope, but they also contain the reference surface. This makes them an interferometer, or an interferometric objective.

The objective has a beam splitter which divides the incoming light into two paths: a test path which goes to the part being measured, and a reference path which goes to the perfect mirror. When the distance between the beam splitter and the reference surface is the same as the distance between the beam splitter and the test surface, the light that is reflected off of these two surfaces will interfere, creating a series of alternating light and dark called an interference signal.

The interference signal only happens when the test and reference legs of the interferometer have the same length, so if one of those lengths is changed, complex topography can be explored. This is called scanning, and it is done by moving the entire objective perpendicular to the test part.

The interference signal is imaged onto a camera and each pixel processes the signal it sees to produce its own height value, and then all the heights for all the pixels are combined to create a map for the surface being tested.

Because CSI uses white light, the interference signal is localised, which means that it only happens when the test and reference legs are the same length. Because of this, surfaces that are rough or structured with steps or other discontinuities can be measured.

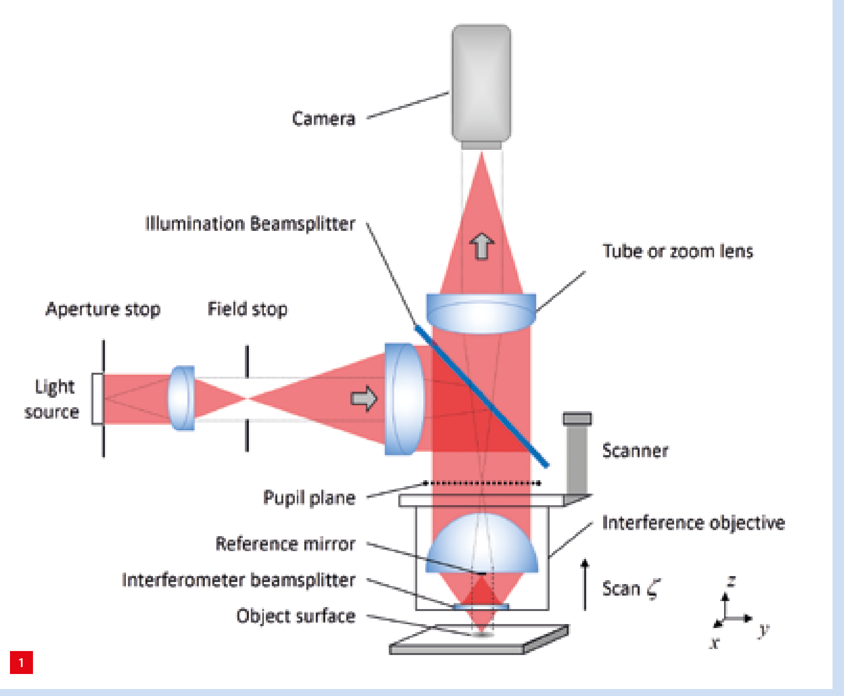

1 Typical set-up for coherence scanning interferometry; see the text for explanation.

As an all-optical technology, CSI is completely non-contact, and Zygo's CSI instruments can measure virtually any material and texture from rough to smooth, shaped to flat, and opaque to transparent. CSI is also very precise with nanometer or sub-nanometer height precision and a fast, consistent measurement speed (1.9 million pixels in just a few seconds) at all magnifications, unlike other techniques where the height precision and speed depend directly on the magnification.

Comparing confocal scanning microscopy with CSI, both have the ability to stitch multiple images, are characterised by high-magnification, high-resolution imaging, and are suitable for rough and steeply sloped surfaces. However, CSI can in addition be used on super-smooth or optically transparent surfaces, and with CSI measurement speed and instrument precision is independent of objective numerical aperture and magnification. Also, unlike confocal scanning microscopy, CSI is appropriate for low-magnification, large-field-of-view imaging (< 5x).

profilers, delivering sub-nanometer height precision at all magnifications, and analysis of a broader range of surfaces (from rough to super-smooth, including thin films, steep slopes, and large steps) quicker and more precisely than other commercially available technologies. This makes it ideally suited to applications such as the spray-lined cylinder application, which is detailed below.

Alternative technologies, such as fax film, rely on affixing a thin sheet of plastic to the cylinder surface and applying a solvent to soften and conform the sheet to the surface. When removed and sufficiently hardened, it is then manually inspected under a microscope. This method,

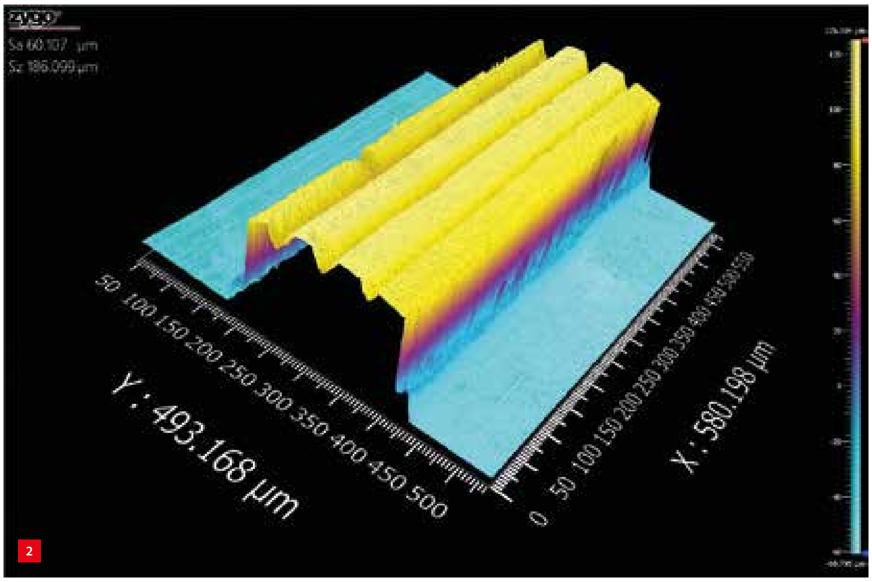

CSI scan of the mechanically activated surface that will provide the anchor for the thermal barrier coating to adhere to the cylinder wall surface. The height scale runs from –60 to +125 µm.

though used extensively, is messy, and can result in very subjective results. When looking specifically at the metrology demands connected with the analysis of the spray-coating of cylinders, Zygo's CSI 3D optical profilers benefit from being non-contact, thereby eliminating any chance of the inadvertent compromising of surface integrity. In addition, CSI technology enables the highest vertical resolution measurement agnostic of the interferometric objective.

Other optical measurement technologies may perform sub-optimally when the surface texture is considered quite smooth. Focus variation technologies, for example, require some level of texture on the surface to be able to resolve the surface.

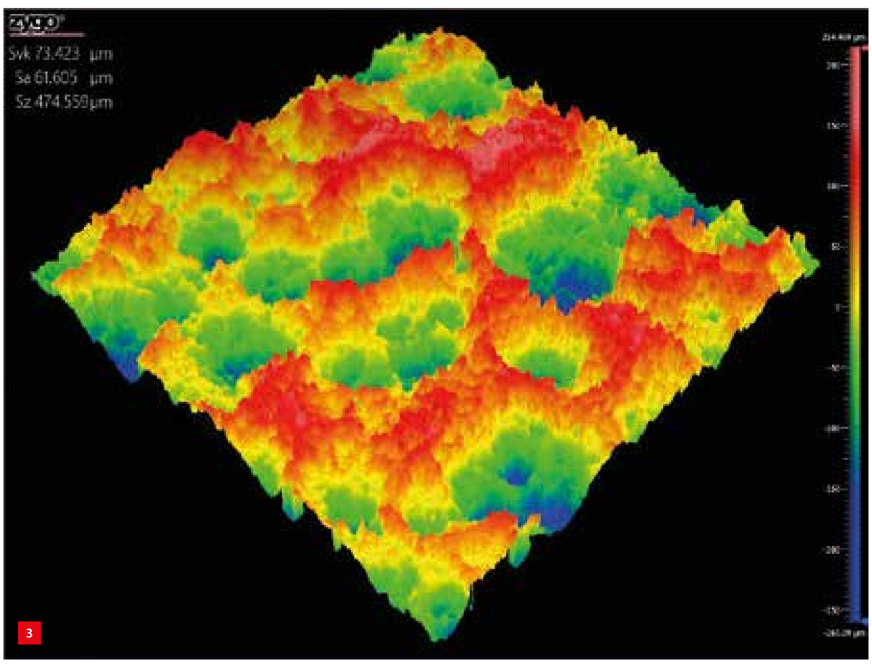

Measurements of the dark, rough features after the TBC application can provide process engineers information on the formation and distribution of surface porosity. The height scale runs from –260 to +214 µm, the XY dimensions are approx. 1 mm x 1 mm.

Zygo's Mx™ software powers complete system control and data analysis, including interactive 3D maps, quantitative topography data, intuitive navigation, and built-in statistical process control (SPC), control charting, and pass/fail limits. As a result, hundreds of parameters can be reported when measuring surface structure and texture across varying surface scales, including areal surface roughness to ISO 25178 standards, and 2D profile standard compliance to ISO 4287/4288.

Spray-lined cylinder application

Mechanical activation

For the mechanical activation / pre-coating stage of the process, the cylinder walls need to be scored (Figure 2), which needs to be strictly controlled as this dictates the amount of TBC that will be applied. Too thin, and there's the possibility that the TBC can flake off. Too thick, and the honing process can remove the peaks that contain the TBC, either scenario potentially compromising the quality and efficiency of the cylinder coating process.

For such step-height-type measurements, Zygo's CSI technology enables the company's optical profilers to speedily measure structures higher than 250 µm with their extended scan capabilities accurately and repeatably.

Thermal spray application

After the TBC application, automotive OEMs need to assess how the pores have developed (Figure 3). The variety of pore sizes – ranging from 50 μm^2 to over 1 mm^2 – will help determine the lubricity retention of this newly sprayed surface. Because these pre-honed coatings are typically very rough and have low reflectivity, typical CSI systems will have difficulty acquiring data from the surface. With Zygo's implementation of CSI, such surfaces are easily measured, producing consistent metrics for process engineers.

Post-spray finishing

Finally, it is necessary to analyse the finished surface texture (Figure 4) of the cylinder post-spraying, checking crosshatch (a textured pattern on a cylinder wall used to retain oil for proper lubrication of the cylinder and piston rings), as well as the final porosity (pore density, pore volume by area, and change of pore size by cylinder depth).

To conclude

Transitioning from the very rough surface measurement pre-honing to the final assessment of extremely smooth honed surfaces displays the full dynamic range of the Zygo CSI-based optical profiler systems. The development of specialised hardware and software enhancements has significantly improved this capability, enabling measurements of previously inaccessible steep surfaces and super-polished surfaces with one metrology solution.

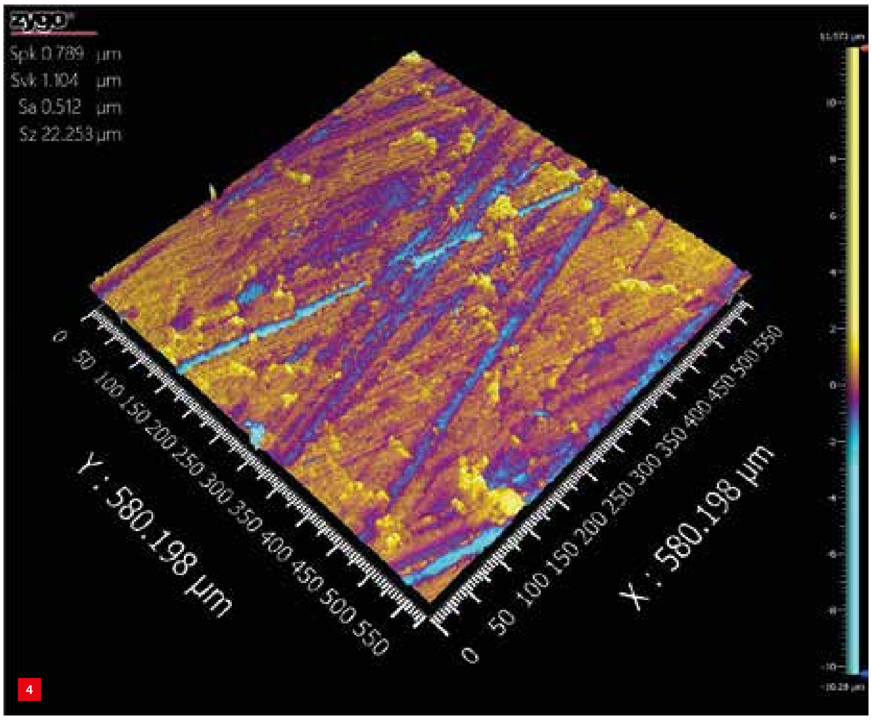

Honing generates the proper stratified surface for the sliding ring/cylinder interface. Quantifying the lubricity by direct measurement of porosity will assist with honing process control. The height scale runs from –10 to +12 µm.

REFERENCE

[1] Robinson, D., Ramsunder, P., and Samantaray, C., "Analyzing Porosity in Thermal Barrier Coatings: Edge Detection of Images using MATLAB", *121st ASEE Annual Conference and Exposition*, Indianapolis, IN, USA, 2014.

VIABLE ALTERNATIVES FOR GLASS AND STEEL

Replacing metal by engineering plastics can help to make car bodies lighter in order to reduce fuel consumption and CO_2 emission. To that end, SABIC is collaborating with automotive manufacturers and developing high-performance resins. SABIC uses metrology solutions from GOM to prove that these resins are viable alternatives for glass and steel.

Partners

In 2007, SABIC first started to consider optical metrology to enable growth through application development, including design aspects, process development, application performance and predictive engineering. There were several reasons to choose for GOM as part of this growth strategy.

GOM systems enable a fast validation of different designs in various environmental conditions. It is also possible to do correlation studies with predictive engineering, for example, when measuring shrinkage, warpage or strain evolution. Furthermore, many of SABIC's customers were already working with GOM systems, which makes comparing and discussing measuring results much easier.

SABIC is a global leader in diversified chemicals headquartered in Riyadh, Saudi Arabia. It manufactures on a global scale a variety of products: chemicals, commodity and high-performance plastics, agri-nutrients and metals. The company has more than 35,000 employees worldwide and operates in more than 50 countries, with innovation hubs in five key geographies.

GOM develops, produces and distributes software, machines and systems using 3D coordinate measurement technology and 3D testing based on latest research results and innovative technologies. With more than 60 sites and more than 1,000 metrology specialists based throughout the world, GOM guarantees professional advice as well as support and service, as witnessed by more than 17,000 system installations serving product quality and manufacturing process improvement in the automotive, aerospace and consumer goods industries.

WWW.SABIC.COM
WWW.GOM.COM

EDITORIAL NOTE

This article was contributed by GOM.

Resins in automotive parts

The LEXAN™ and NORYL™ materials produced in the SABIC's Bergen op Zoom (NL) plant consist of granulate, small grains to be processed further, for example, in injection moulding, extrusion and film blowing. There are numerous applications for LEXAN™ resins. Within the automotive industry, these include headlamp lenses, helmet visors and windscreens. The main advantages of using these resins are their environmentally conforming flame retardancy, scratch resistance, toughness, heat resistance, weatherability, biocompatibility, optical quality, and compliance with stringent FDA and USP requirements.

NORYL™ resin is an extremely chemical-resistant material with the stiffness, impact resistance and heat performance required for online painting. The low density of unfilled NORYL GTX™ resin can result in weight savings of the part of up to 25% compared to glass- or mineral-filled resins. When used for car fenders, the NORYL™ resin is on average 50% lighter than steel. GOM systems are used to measure and analyse both of SABIC's materials and prove that they are viable alternatives for glass and steel – meeting standards and achieving the desired benefits.

Testing a plastic tailgate prototype

A typical example of replacing metal by engineering plastics is a completely metal-free tailgate with a reduction of 30% in weight. Instead of retrofitting an existing metal product, SABIC redesigned the new tailgate in plastic, NORYL™ and STAMAX™ resins, from scratch. Even the glass window of the tailgate has been replaced by transparent polycarbonate. High stiffness can be obtained by applying a rib structure. A new design like this must be tested thoroughly.

To test the quality of this new plastic tailgate, prototypes have been subjected to torsional loads and thermal conditions, using new products with glass windows, plastic windows and even without windows for comparison. Figure 1 shows thermal test results from measurements in three

Thermal test results from TRITOP measurements.

different directions and as vector representation; these results were obtained using GOM's TRITOP optical 3D coordinate measuring machine (CMM). The deformation grades are indicated by colour. The products were tested inside a climate chamber, where a number of measurements were taken within 10-20 s after opening the climate chambers doors. These measurements were done in different temperature conditions; Figure 2 shows the deformation of the tailgate.

These tests cannot be done with a conventional CMM, according to a SABIC application testing specialist. The only alternative to TRITOP is a measurement with high-temperature LVDTs, linear variable differential transformers, a type of electrical transformers used for measuring linear displacement, but this is very time-consuming and an inaccurate measuring method compared to photogrammetry. Using TRITOP means simply making a series of photographs with one single hand-held camera.

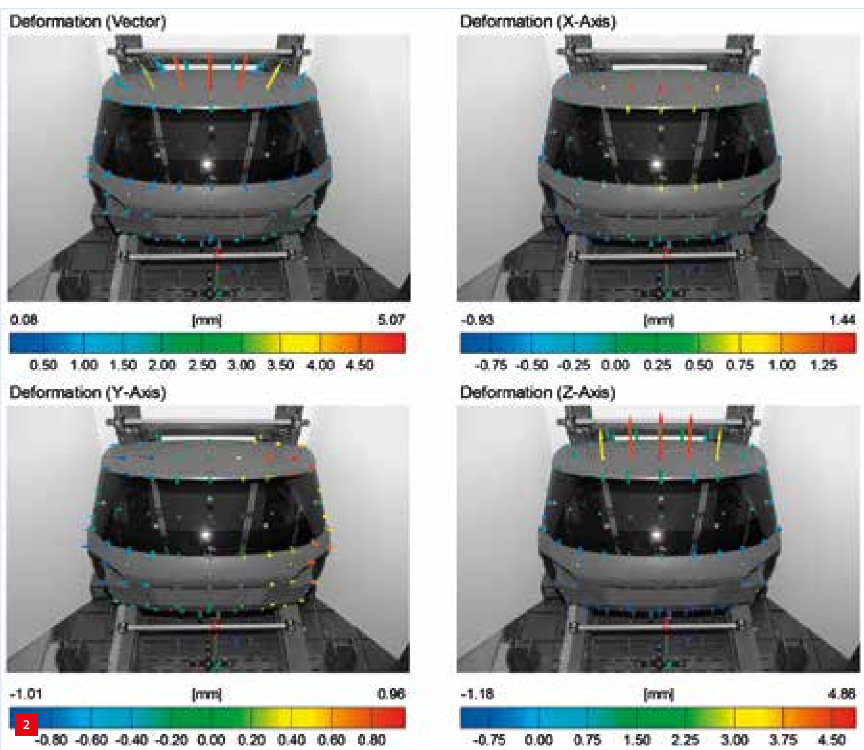

Deformation of the tailgate during elevated temperature exposure (max. 60 °C).

Before taking photos, the object has to be prepared by fixing uncoded markers, being the 3D measuring points, directly on the tailgate, and by fixing coded markers for picture stitching on the part surroundings. Also, scale bars are positioned close to the workpiece to determine the size of the object. With a stably positioned workpiece, the measurement technician takes a series of at least three measurements from different directions.

The images are automatically evaluated in the work station using TRITOP Professional software. A mathematical algorithm computes a precise model from ray intersections, camera positions, lens distortions and object coordinates. The coded and uncoded markers and the scale bars placed next to the object are included in this computation.

Testing strength of a composite beam

Instead of doing only 3D static tests, it also became important for the SABIC Global Application Technology Department to do 3D dynamic tests. Using the ARAMIS 3D motion and deformation sensor, they investigate mechanical and thermal properties of SABIC plastics as well as their use in customer products, for example the behaviour of products under the influence of forces, pressures and temperature differences. The ARAMIS system helps defining deformations during various experimental loading conditions. For SABIC, this leads to a better understanding of the material characteristics, but the data can also be shared with customers proving that the material fulfils all their requirements.

The ARAMIS 3D testing system from GOM has been especially developed for materials research and component testing. It consists of a stereo camera system which delivers precise 3D coordinates based on triangulation, using stochastic patterns or reference point markers. These non-contact sensors measure full-field 3D strain and deformation of soft and rigid materials under mechanical or thermal load. Thanks to the high-speed 3D camera, the surface deformation can be observed in real time.

Figure 3 shows how plastic samples were tested for stiffness and strength under different temperature conditions in an ARAMIS creep-testing set-up. A special project was created to investigate the usability of strengthening a composite beam using unidirectional laminate across the full specimen length, instead of only using chopped glass fibres as reinforcement. For this analysis, the object was also subjected to a four-point bending test, see Figure 4 and 5, and a high-speed impact test.

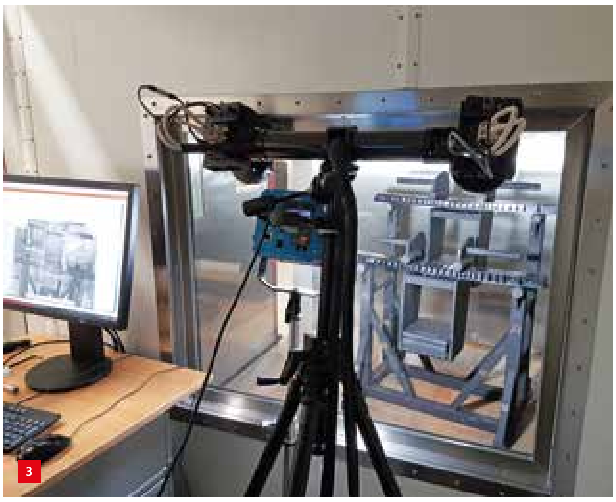

3

Experimental plastic samples are tested for stiffness and strength under different temperature conditions (above 60 °C) in an ARAMIS creep testing set-up.

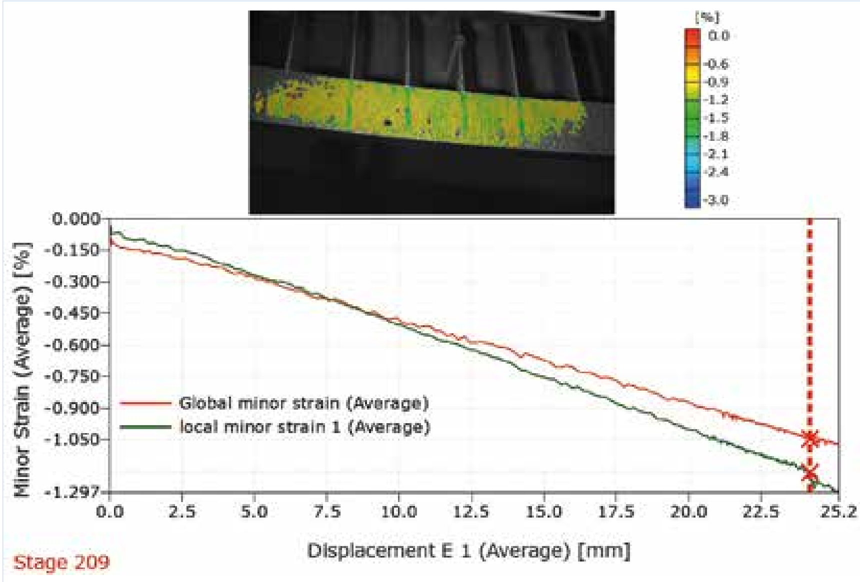

5

Relation between the average strain and displacement during the four-point bending test of the composite beam.

ARAMIS Professional software offers numerous possibilities to show measuring results. Figure 5 displays some results showing the relation between the average strain and the displacement during the four-point bending test of the composite beam. The colour plot of Figure 6 shows the breaking point as a red dot during the high-speed impact test. These ARAMIS results will help improving strength and stiffness of SABIC future products.

Measuring wear of gear wheels

In addition to TRITOP and ARAMIS systems, SABIC is also using the ATOS Triple Scan optical measuring system (two cameras recording precise fringe patterns projected onto the surface) to compare the data of the 3D measurement with a CAD file for full-field inspection. SABIC uses the ATOS Triple Scan both in a manual set-up for single parts and automated in an ATOS ScanBox machine for multiple parts. The ATOS Triple Scan gives the opportunity to measure both small and large parts, for full-field measurements and not just point-based measurements as with the tactile coordinate measuring machine, according to a SABIC application testing specialist. The overview of the full-field data provides a direct indication of what is wrong compared to the CAD data and does not leave any blind or unchecked areas.

SABIC is also active in the field of materials for dynamic bearings. Examples are LNP™ Lubricomp™ and LNP™ Lubriloy™ compounds with integrated Teflon-like lubricating material at molecular level. Such materials can be used in dry-running gears where external application of oil or grease is not permitted. Customers apply such driving systems in healthcare and food service sectors with regulatory requirements for cleanliness and safety. The SABIC Application Testing Center uses the ATOS Triple Scan to measure the wear of these gear wheels after lifecycle tests (Figure 7 and 8).

The ATOS works with blue-light technology. Due to the narrow-band blue light of the LED projection unit, measurements can be carried out regardless of ambient

4

Four-point bending test of a composite specimen.

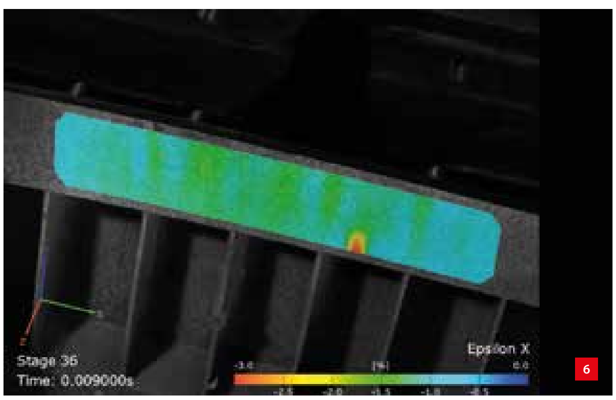

6

On the colour plot, the breaking point can be seen as a red dot during the high-speed impact test.

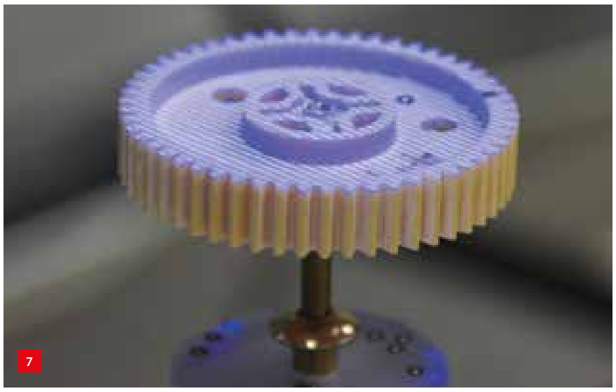

7

Gear wheel onto which a fringe pattern is projected.

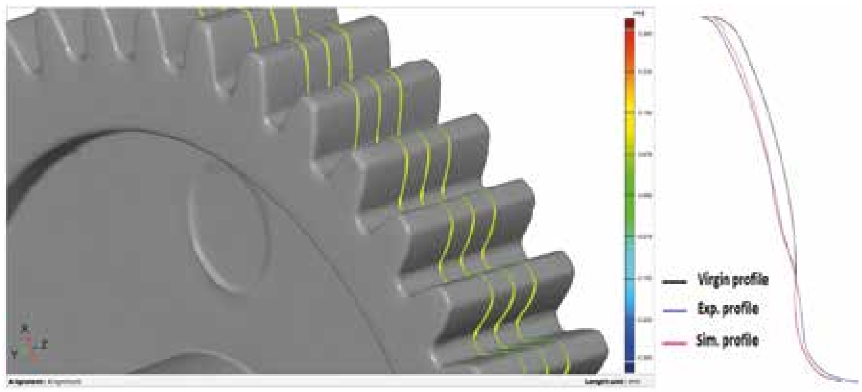

9

Section-based inspection on teeth of a gear wheel. See text for explanation.

lighting conditions and surface structure. A complete 3D scan of the gear wheel was obtained in five minutes. See Figure 9 for the result of a running test on a gear wheel. A best-fit was created between CAD data and the measuring results of the worn gear wheel. The amount of wear could be calculated and shown in different colours, which makes it easy to understand the results and find out what is happening. In extreme zones, about 400 μm wear was established for a gear wheel with 17 teeth.

8

Measurement of a gear wheel with an ATOS Triple Scan.

The graph on the right in Figure 9 shows a virgin gear (in black) being compared with the wear captured with the scan (in blue) and the simulation (in red). It can be observed that the wear is very close to the simulated data. These measurements help with finetuning gear lifetime prediction models which rely on accurate wear coefficients, a SABIC application testing specialist explains. These coefficients are best determined on real gear wear profiles.

Conclusion

Altogether GOM's various measuring options rapidly help to solve measuring challenges and analyses. SABIC supports actions in the precision engineering industry to replace heavy metal parts by light-weight plastic ones. "By using GOM systems, we took the next steps in advanced dimensional performance evaluations", concludes the SABIC team leader application testing. "We started with tactile measurements for warpage and shrinkage studies. Moving to ATOS and TRITOP, gave us more flexibility, improved accuracy and time-savings, which was much needed. With ARAMIS, we made the next step toward more localised deformation and strain measurements during loading conditions on complex moulded parts."

NOVEL SYSTEM ARCHITECTURES

Interventional X-ray systems are used to acquire 2D and 3D images of complex anatomical structures (e.g. the cardiovascular system). These images provide a clinician with feedback in a medical procedure, which enables advanced minimally invasive treatments. Hereby, they have become an indispensable tool in many clinical disciplines. However, architectural innovations over past decades have been limited, while developments in imaging equipment, software, and medical treatments were not. This leaves a desire for an improved mechatronic architecture, that better balances performance, clinical usability, and cost. Three novel designs are presented, aimed at improving the interventional X-ray system on multiple, application-specific levels.

JEFFREY VAN PINXTEREN, HANS VERMEULEN AND ROB VAN LOON

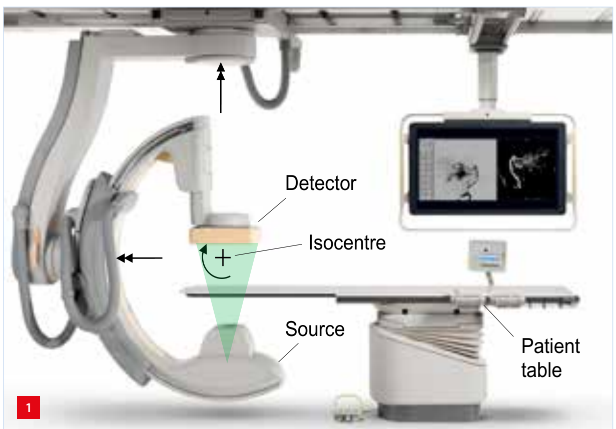

Typical interventional X-ray system.

C-arm architecture

Today's interventional X-ray systems have many imaging functionalities, e.g. (contrast-enhanced) 2D imaging, fluoroscopy (real-time imaging), and 3D computed tomography. All of these require 2D X-ray images to be taken at various projection angles. To this end, interventional X-ray systems (Figure 1) contain a C-shaped arm, to which an X-ray source and detector are connected. The C-arm is part of a series of rotational and translational motion stages, connected by long and slender structural elements.

This mechatronic architecture enables the imaging equipment to be positioned over extensive 3D trajectories, while somewhat limiting the obstruction to clinicians and medical equipment. However, it also entails a large structural mass (~1,200 kg) and relatively low stiffness. The resulting structural deflections, combined with backlash from form-closed roller guidance systems, cause a (reproducible) misalignment of the X-ray beam of up to ~10 mm. This translates to an excess radiation dose of approximately 10%, and introduces a need for extensive and time-consuming geometric calibration.

AUTHORS' NOTE

Jeffrey van Pinxteren (Ph.D. student) and Hans Vermeulen (professor) are members of the Control Systems Technology group at Eindhoven University of Technology, Eindhoven (NL). Rob van Loon is senior mechanical designer for image-guided therapy systems at Philips Healthcare, Best (NL)

j.a.w.v.pinxteren@tue.nl
www.tue.nl/cst
www.philips.com

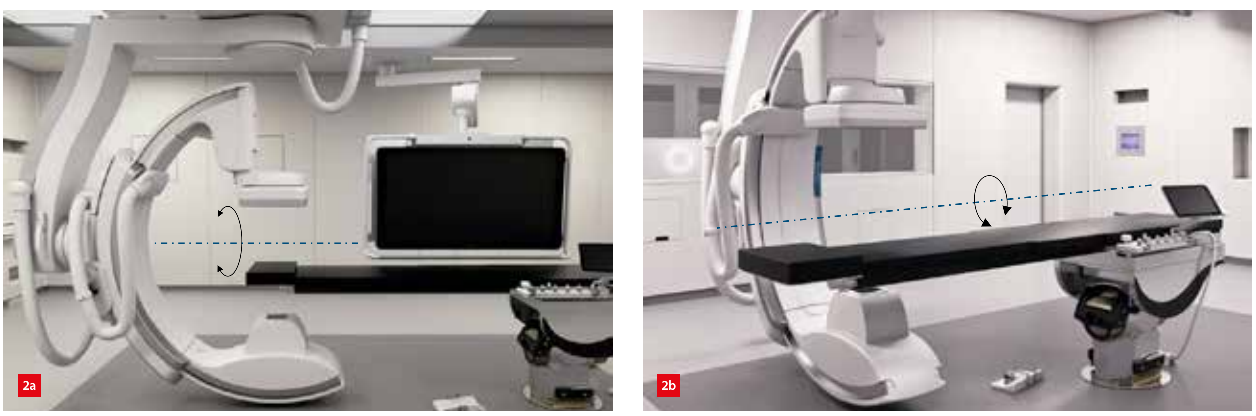

C-arm position.
(a) For 3D propeller scan.
(b) For 3D roll scan.

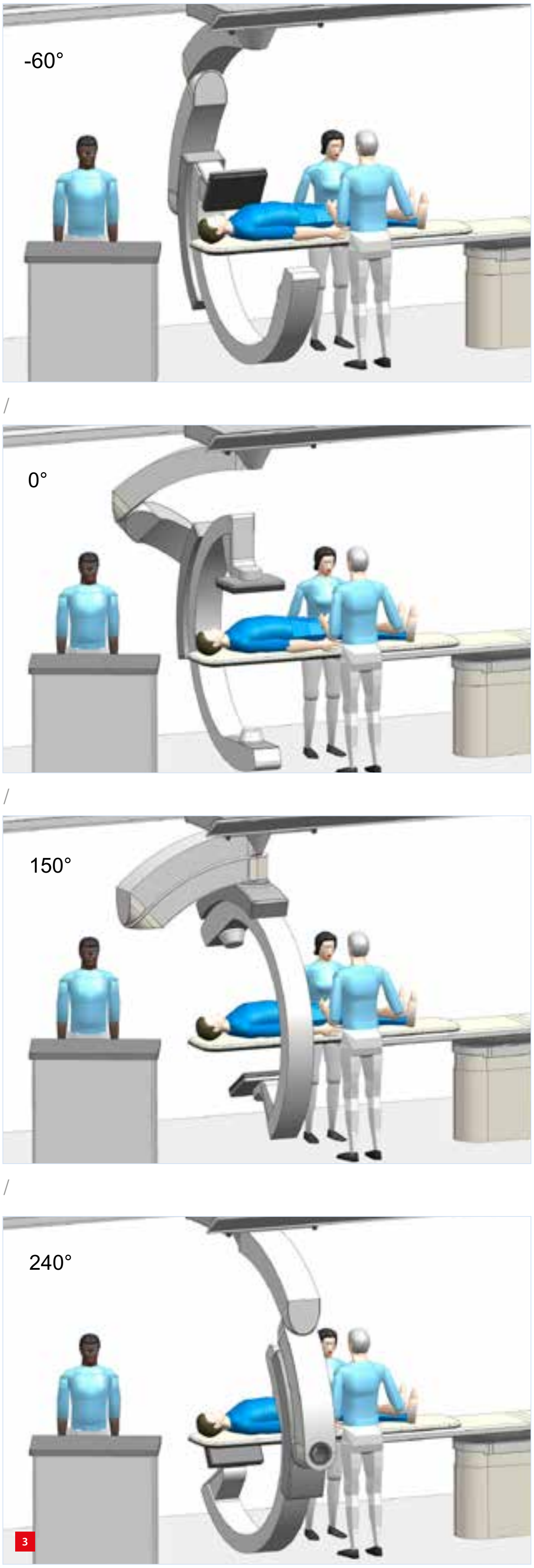

System 1: Additional rotational joint allows for a 300° extended 'roll' scan, from –60° to +240°.

3D computed tomography

The use of 3D reconstructions (3D images) has been proven to be an asset in an increasing number of clinical disciplines. For this application, reconstruction algorithms combine multiple 2D images, taken at various angular projections. Typically, two scanning motions can be distinguished.

A propeller scan (Figure 2a) is carried out with the C-arm at the head end of the table. The large scan range (+/–120°) allows for the use of exact reconstruction algorithms [1], and application-specific scan trajectories [2]. Both factors contribute to achieving high-quality 3D images with minimal artefacts (such as streaks).

A roll scan (Figure 2b) is performed with the C-arm at the side of the table. This type of scan requires a smaller footprint in the operating room, and leaves valuable space at the head end of the table (e.g. for anaesthesia). However, the C-arm roll guidance has a smaller (+/–90°) range of motion, which dictates the use of approximate reconstruction algorithms. 3D images generated by the roll scan are therefore of lower quality compared to the propeller scan, and less suited for procedures involving soft tissue imaging.

System 1: Dual-stage design

The first novel alternative (system 1) aims to combine the image quality of the propeller scan with the clinical usability of the roll scan. Its mechanical structure (Figure 3) features an additional joint in the arm that connects the C-arm to the ceiling. The axis of this rotational joint coincides with the isocentre, i.e. the (virtual) centre of all rotation axes of the imaging system. Therefore, in combination with the existing rotational joints, it forms an additional spherical motion stage. This dual-stage design allows for an extended 'roll' scan over a 300° range (–60° to 240°), with a 55% smaller footprint compared to the propeller scan (Figure 2a). The scanning motion is performed from the side of the table, which leaves valuable space at the head end, and allows for full body coverage.

In system 1, more than half of the 3D scan range is covered by the spherical motion stage. The range of motion of the C-arm roll guidance can therefore be limited to clinically relevant 2D projection angles only (+/–60°). This enables structural improvement of the C-arm and its roll guidance. For this, a kinematic roll guide design was made [3], which eliminates backlash and ensures continuous contact with all rolling elements. Aluminium tubular profiles form the base of a stiff and lightweight boxed structure for the C-arm and roll guide.

a floor-mounted base, which can rotate around a second, vertical axis. In this design, the propeller DoF is omitted, so that there is no more out-of-plane rotation of the C-arm with respect to the gravitational vector. This eliminates torsional deformation of the C-arm due to gravitational and inertial loads (~60% of worst-case C-arm deflection). Furthermore, it enables space at the sides of the C-arm to be used for a stiff construction of the base. Together, this results in a lightweight system (~500 kg), with improved X-ray alignment and image quality. Such a lightweight, less complex system does not only reduce the cost of production. It also allows for simpler and less costly transport and installation.

System 2: 2D and 3D imaging capabilities at reduced cost and installation requirements.

Combined, these aspects lead to 30% less deflection of the C-arm due to gravitational and inertial forces. The amount of excess radiation, used to guarantee full detector coverage, can therefore be decreased. In this way, unnecessary radiation dosage for both the patient and medical staff is reduced. Initial design iterations indicate that a 40% mass reduction is achievable for the C-arm and roll guidance. Similar results are expected for the complete system.

System 2: Novel floor-mounted base

Typical interventional X-ray systems are able to move the C-arm in three rotational degrees of freedom (DoFs). Two of these DoFs (roll and propeller movement, Figure 2) are used to move the imaging equipment spherically around the patient. The third DoF (rotation around vertical axis) is used only to position the C-arm at either side of the table. System 2 (patent applied for) aims to decrease the system cost and installation requirements, while maintaining and adding to the current imaging capability.

To achieve this, it is based on only two rotational DoFs to move the C-arm (Figure 4). For the first DoF, the C-arm is supported by a roll guidance. This guidance is part of

The two rotational DoFs enable a similar spherical positioning of the C-arm as in the original system. Furthermore, all clinically relevant projection angles can be achieved with multiple C-arm postures (Figure 4, lower images). This allows a clinician to choose a neutral position for the system at the left or the right side, or at the head end of the table. From this neutral position, clinically relevant projection angles can be achieved by rotating the base within a 135° range (Figure 4, indicated on the floor in blue).

For high-quality 3D reconstructions of the upper body, both rotational DoFs can be used simultaneously in a novel, dual-axis 3D scan (Figure 5). This scan starts at a –105° roll angle (Figure 5, top). While rotating around the vertical axis over 180°, the C-arm is moved to a near neutral roll angle, and back to –105° (Figure 5, middle and bottom). Combined, this results in a close-to-circular scan path of 210° (–105° to +105°), allowing exact reconstruction algorithms to be used ([1], minimising artefacts).

System 3: Advanced mechatronic alignment

Both system 1 and 2 use a structural beam to physically connect and align the X-ray source and detector. Despite their slender construction, this beam, and part of the

System 2: Dual-axis 3D scan, for high-quality 3D images of upper body.

motion stages, take up valuable space around the patient table. System 3 (patent applied for) provides a revolutionary alternative which optimises both the clinical workflow and the imaging performance (Figure 6).

System 3 features two separate positioning systems which move the X-ray source and detector, respectively, over six DoFs (Figure 6). Both systems were designed to make optimal use of the space available in the operating room, and to limit obstruction to the medical procedure and staff. The upper positioning system contains a

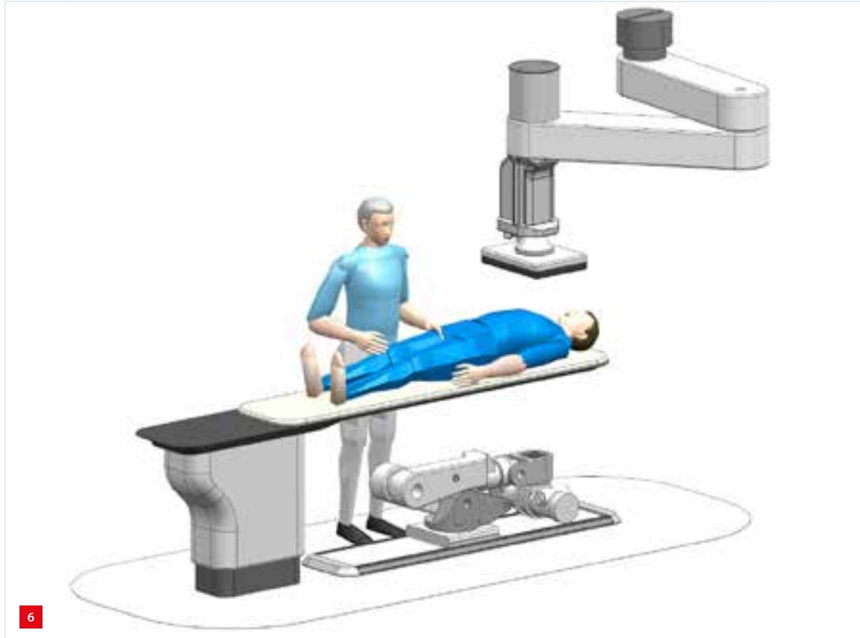

System 3: Two separate positioning systems to move the X-ray source and detector.

SCARA arm, which provides for three DoFs in the horizontal plane. A vertical translation module, and two rotational joints are used to couple the detector to the SCARA arm.

This layout ensures that most moving components operate above head height (2.10 m, Figure 7). Components that do move into the workspace are placed intuitively, above the detector. The lower positioning system features a custom, 6-DoF articulated arm. It is mounted to a linear translation stage beneath the patient table, creating a redundant kinematic layout. This enables system movements to be programmed

System 3: Upper positioning system operates above 2.10 m; lower positioning system moves beneath the patient table.

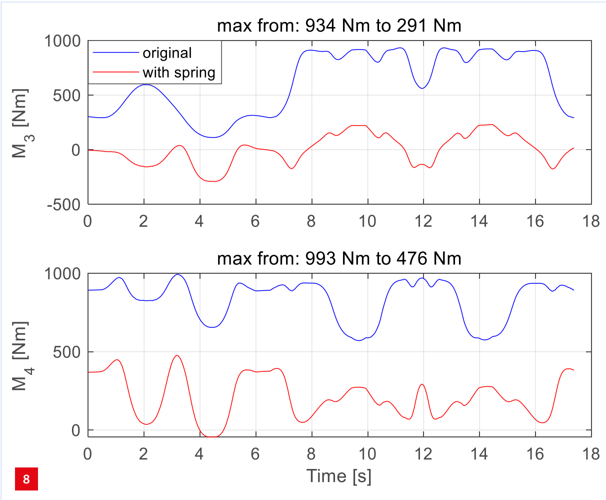

Torque values for the most heavily loaded joints, with (red lines) and without (blue lines) weight compensation.

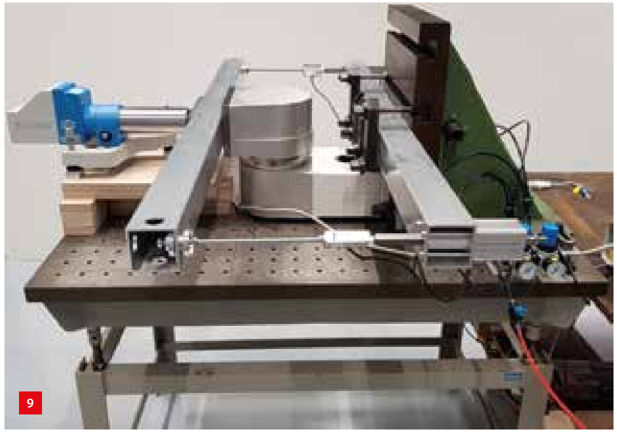

Test set-up for rotational joint of the lower positioning system. (Acknowledgement to TU Eindhoven Equipment & Prototype Center)

such that the articulated arm operates underneath the patient table, for all projection angles (Figures 6 and 7).
The 6-DoF motion capability of system 3 provides for additional functionality, on top of the ability to move the imaging equipment along spherical, longitudinal, and lateral trajectories. Contrary to almost all C-arm systems currently available, it makes the height of the (virtual) isocentre adjustable (range of 100 mm). This enables a clinician to set the patient table to an ergonomically more comfortable working height, and adjust the isocentre accordingly.

Furthermore, quasi-static deflections in the mechanical structure can be compensated for. This enables the misalignment of the X-ray beam on the detector, and thereby the unnecessary radiation dose to be minimised. Initially, a model-based calibration will be applied to identify and reduce X-ray misalignments to ~2 mm, and to ensure compliance with regulations. Future research could focus on a measuring principle (e.g. [4]), that can quantify the actual misalignment during operation. This would allow for direct minimisation of the X-ray alignment error using a feedback control loop.

Feasibility study for system 3

System 3 is considered most promising for future applications. Therefore, a feasibility study is being carried out. Here, focus is on the lower positioning system, since it has the largest payload (40 kg X-ray source) and smallest design volume.

Based on initial mass estimates, a multi-body model is made in the simulation environment Matlab Simscape Multibody. Given a reference trajectory, this model computes force and torque values for all motion axes. Two rotational joints are identified to be most critical. The moment load on these joints is highest (~1,000 Nm), and dominated by gravity.

Weight compensation is therefore essential to achieve a lightweight design. For this reason, a gas spring is integrated between the base and the articulated arm (best visible in Figure 11, see below). This reduces the load on the critical rotational joints by a factor of 2 to 3 (Figure 8).

A detailed design of the lower positioning system is completed. It features stiff, thin-walled boxed structures, and modular drive-train designs with a high gear ratio. Both aspects contribute to a lightweight system design of 220 kg. The drive trains include two absolute encoders, and a passive safety brake.

A prototype of the critical rotational joints is realised. The angular stiffness (in tilt and drive direction) of this rotational joint is quantified using finite-element analysis (FEA) and measurements. The latter is done with an experimental set-up (Figure 9). Here, a moment loading is applied and measured using two pneumatic cylinders and two force transducers (AST KAP-E-1kN). The resulting angular deformation is measured using an electronic autocollimator (Möller Wedel Elcomat 2000).

The measured load-deflection diagrams are shown in Figure 10. Each measurement includes three complete hysteresis loops. For both directions, all measurements are repeated six times (3x forwards, 3x backwards). In tilt direction (Figure 10a), the deflection curve is modelled by a linear fit (black dashed lines). The resulting stiffness

Table 1
Measured vs. specified stiffness (k, see text for explanation) and hysteresis (s_v), in the drive direction.

	k_1 [Nm/rad]	k_2 [Nm/rad]	k_3 [Nm/rad]	s_v [rad]
Measurement	$2.05 \cdot 10^5$	$2.58 \cdot 10^5$	$3.71 \cdot 10^5$	$2.5 \cdot 10^{-4}$
Specification	$2.10 \cdot 10^5$	$2.90 \cdot 10^5$	$3.70 \cdot 10^5$	$2.9 \cdot 10^{-4}$

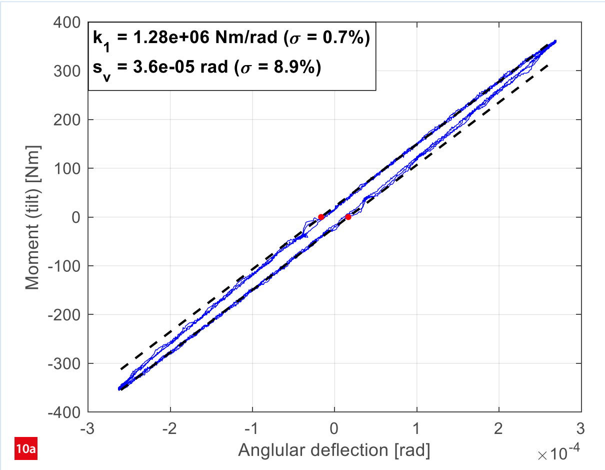

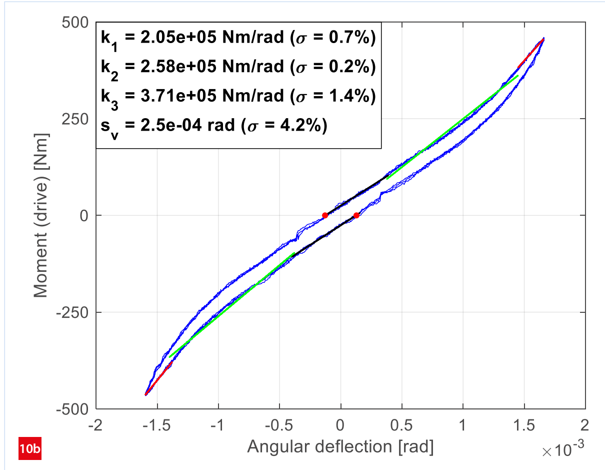

Measured load-deflection diagrams, with load in the specified direction of the rotational joint; see text for explanation.
(a) Tilting direction.
(b) Driven direction.

(k = 1.28·10^6 Nm/rad, σ = 0.7%) is within 10% of FEA results. In drive direction (brake applied), a nonlinear deflection curve is measured (Figure 10b). Estimates for the hysteresis (red dots) and the stiffness values in three load regions (k_1, black line; k_2, green line; and k_3, red line) correspond to specifications of the applied strain wave gearing (Table 1).

Using the measured stiffness values, a 4th-order representation of the two critical joints is included in the multi-body model. This shows pose-dependent dynamics, with a first eigenmode at ~10 Hz. Conventional non-collocated PID control is implemented to model the transient response to a relevant scan trajectory. Based on this, a factor of 5 improvement in positioning performance is expected compared to today's system.

Outlook

In the upcoming months, a second rotational joint and the weight compensation system will be realised. The resulting 2-DoF set-up (Figure 11) will be used to test positioning accuracy and reproducibility over large-range trajectories.

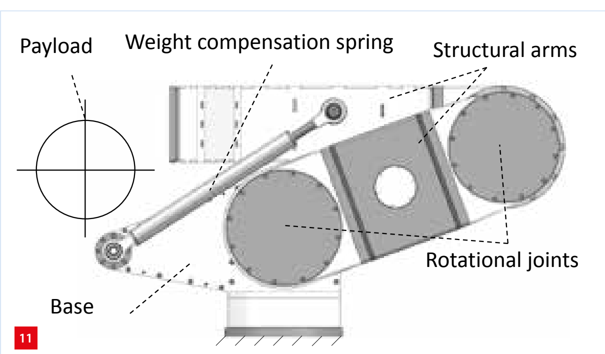

2-DoF set-up for repeatability tests over large-range trajectories.

Summary

This article presents three novel mechatronic architectures, designed to improve the interventional X-ray system in terms of performance, usability, and cost (see also [5]).

System 1 focuses on improved image quality and clinical usability of 3D scans (high-end applications). A dual-stage design allows for scanning motions up to 300°, with a 55% smaller footprint in the operating room. It is based on a kinematic roll-guide design, resulting in less nonlinear behaviour and improved alignment of the imaging equipment.

System 2 decreases cost and installation requirements, while maintaining and adding to the current imaging capability (low-end applications). By reconsidering the DoFs needed, a lightweight design was created (> 50% mass reduction), with an improved stiffness-to-mass ratio.

The third, and most revolutionary, system pursues high-end performance and optimised workflow. It features a compact and lightweight mechatronic design which makes optimal use of the space available in the operating room. To this end, the fixed C-arm was replaced by two separate positioning systems for the X-ray source and detector, respectively. Multi-body modelling and experimental validation of a prototype support the technical feasibility of system 3. A factor of 5 improvement in positioning performance is expected, compared to today's system.

REFERENCES

[1] Tuy, H.K., "An inversion formula for cone-beam reconstruction", *J. Appl. Math.*, 43, pp. 546-552,1983.
[2] Schernthaner, R.E., "Feasibility of a modified cone-beam CT rotation trajectory to improve liver periphery visualization during transarterial chemoembolization, *Radiology*, 277, pp. 833-841, 2015.
[3] Kregting, S.W., "Design of a C-arm and roll guide for an interventional X-ray system", Master's thesis, Eindhoven University of Technology, 2017.
[4] Gaasbeek, R.I., "Image-based estimation and nonparametric modeling: towards enhanced geometric calibration of an X-ray system", *Proc. 2015 IEEE Conf. Control and Appl.*, pp. 1063-1068, 2015.
[5] Pinxteren, J.A.W., "(R)evolutionary improvements in the design of interventional X-ray systems", *Proc. euspen 19th Int. Conf.*, pp. 534-537, 2019.

LARGE-STROKE, FLEXURE-BASED

The design of a flexure-based suspension for a high-torque, iron-core direct-drive motor is presented. Over the full, large range of motion, the design provides the high radial stiffness (> 1,000 N/mm) required for resisting the high magnetic forces from the permanent magnets and iron core. Furthermore, it maintains a constant position of the pivot axis within 0.1 mm, to meet alignment tolerances. A prototype was realised and experimental validations have confirmed its high radial stiffness and applicability for iron-core torque motors.

MARK NAVES, MARIJN NIJENHUIS, WOUTER HAKVOORT AND DANNIS BROUWER

Introduction

In high-precision applications, flexure-based mechanisms are used for their deterministic behaviour due to the absence of play and friction. To maintain these deterministic properties, the actuators of flexure-based precision systems should also be free of play and friction. To this end, direct-drive actuators are often used as they do not rely on tribological contacts. Common Lorentz-type actuators, such as voice-coil, linear ironless or rotary ironless (torque) motors, rely on a permanent magnetic field and coil windings (without an iron core) to provide actuation forces.

The absence of an iron core means on the one hand that there is no disruptive cogging or high parasitic magnetic forces. On the other hand, this absence results in a reduced strength of the magnetic field and reduced thermal dissipation, which decreases the maximum actuation force. Therefore, ironless actuators are not always able to provide sufficient actuation force for demanding applications.

In contrast, Lorentz-type actuators with an iron core, in which the coils are mounted in an iron lamination stack, have actuation forces that are up to a factor of two larger, although at the expense of parasitic magnetic forces [1]. These parasitic forces are proportional to the misalignment between the magnet track and iron core away from the equilibrium position, which results in a destabilising negative stiffness.

To compensate for this negative stiffness, a stiff-bearing construction is required. This is often too demanding for flexure mechanisms, however, due to their limited support stiffness, especially when considering large-range-of-motion applications. Furthermore, large-stroke flexure mechanisms often suffer from a limited load capacity, insufficient for the resulting reaction forces on the bearing construction.

Additionally, the nonlinear nature of the elastic deformations of the flexures also results in parasitic motion that easily exceeds the alignment tolerances of typical actuators, because the air gap between the magnet track and coil is often small. Lastly, due to the negative stiffness provided by the iron core, parasitic motion results in additional parasitic pull-in forces.

This article presents a flexure-based rotary actuator suspension with 60° range of motion. This actuator suspension was designed for use in a flexure-based, large-range-of-motion hexapod system (the T-Flex [2], videos in [3]) for which high actuator torque is required (up to 40 Nm).

Actuator

The direct-drive motor considered is an iron-core, permanent-magnet motor (Tecnotion's QTR-A-133-60), which allows for an ultimate torque of 55.5 Nm. The negative radial stiffness resulting from the iron core and permanent magnets is approximately 350 N/mm, while a radial alignment of < 1 mm is required to prevent contact between the rotor and stator. A schematic drawing with the main dimensions of the actuator is provided in Figure 1.

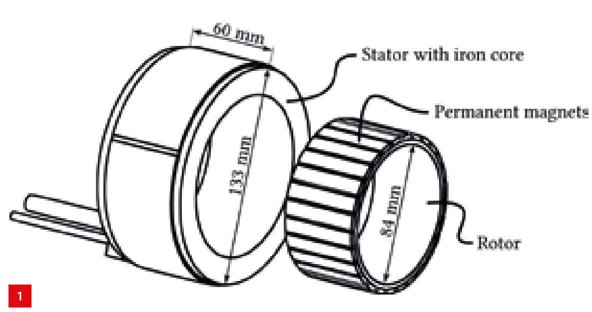

1

Exploded view of the QTR-A-133-60 torque motor with the main dimensions.

AUTHORS' NOTE

Mark Naves and Marijn Nijenhuis (both Ph.D. students), Wouter Hakvoort (assistant professor) and Dannis Brouwer (professor) are all members of the chair of Precision Engineering in the Department of Mechanics of Solids, Surfaces & Systems at the University of Twente (NL).

m.naves@utwente.nl
www.utwente.nl/en/et/ms3/research-chairs/pe

Flexure-based suspension

For commonly used flexure joints for a single rotational degree of freedom (DoF), such as the cross-spring pivot consisting of two (or more) separate leafsprings, the motion of the shuttle (in this case attached to the rotor) is typically approximated by a circular motion around a fixed axis of rotation. However, for larger deflection angles, the motion path of the shuttle deviates from this circular path, due to the non-linear nature of the elastic deformations of the flexures. For the considered range of motion of 60° (–30° to +30°), this deviation easily exceeds the required alignment tolerance of 1 mm between rotor and stator.

In order to minimise the parasitic motion of the rotor, the butterfly flexure hinge design was selected, as it is known for its small parasitic motion due to the smart compounding of the leafsprings [3]. This hinge effectively consists of a stacked arrangement of four cross-spring pivots with coinciding rotation axis, schematically illustrated in Figure 2. For this joint, the parasitic motion of the first and fourth cross-spring pivots is compensated for by the opposed parasitic motion of the second and third cross-spring pivots. Therefore, the parasitic motion is strongly reduced and its magnitude can be approximated by [4]:

$$d_{par} = \left(\frac{1}{cos(\alpha_2)} - \frac{1}{\cos(\alpha_1)}\right)\frac{9\lambda^2 - 9\lambda + 1}{120} L\theta^2$$

Here, $\lambda > 1$ in order to prevent interference between the individual cross-spring pivots in the stacked arrangement and α provides the angle between the individual leafsprings. Please note that this equation only provides the kinematic parasitic motion of the butterfly hinge, disregarding (magnetic) reaction forces on the system that will cause additional displacement. Considering a realistic value of $\lambda = 1.1$ combined with $\alpha_1 = 35°$ and $\alpha_2 = 55°$ and a range of motion of $\theta = 30°$, this results in a parasitic motion of $L/341$ [m], which is well below 1 mm for typical values for L.

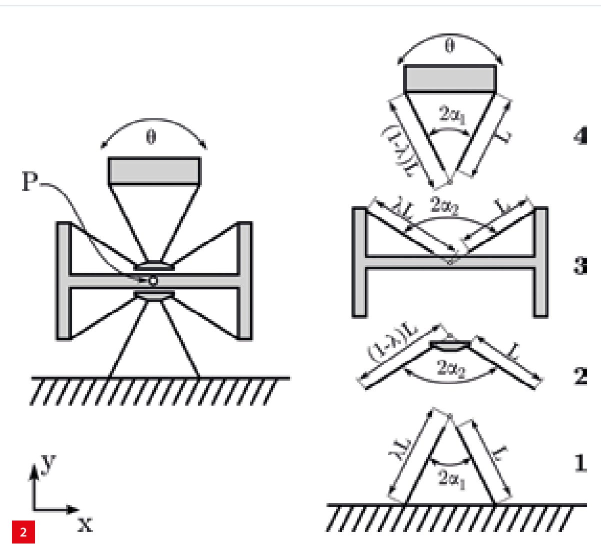

2

Schematic overview of the butterfly hinge with the rotation axis provided by P.

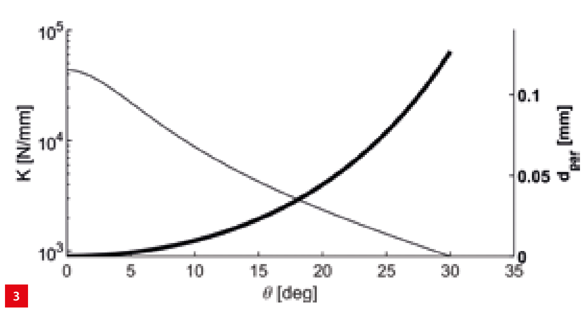

3

Support stiffness (K) and parasitic motion (d_{par}) of the optimised butterfly hinge.

For the design of the butterfly hinge, the width of the joint (the z-dimension in Figure 2) was fixed to 100 mm and the length (L) and thickness (t) of the flexures were optimised to maximise support stiffness in the most compliant direction (considering the full range of motion). For the optimisation, the flexible-multi-body package Spacar [5] was used, combined with an adapted Nelder Mead-based shape-optimisation algorithm [6]. As for material, tool steel (Stavax) was selected, with the allowable stress limited to 600 MPa, which is about 40% of the yield stress of the material.

The resulting support stiffness and parasitic motion of the optimised butterfly hinge (L = 35 mm and t = 0.33 mm), including the negative stiffness induced by the rotor magnets, is provided in Figure 3. At the maximum deflection angle of $\theta = 30°$, a radial support stiffness (K) of almost 1,000 N/mm (–350 N/mm negative stiffness included) was obtained, combined with a parasitic deflection of 0.12 mm, which is well below the allowed 1 mm.

For the butterfly hinge, it has to be noted that each intermediate body between each set of flexures has an unintended rotational DoF around the rotation axis of the joint, introducing three unconstrained DoFs. For most flexure-based mechanisms, underconstrained intermediate bodies dramatically deteriorate support stiffness (especially for large deflection angles) due to the coupling between external loads applied to the end-effector and the unconstrained DoFs of the intermediate bodies, similar to the compounded parallel leafspring guidance without slaving mechanism [7]. However, as the instant centre of rotation of each intermediate body and the end-effector coincide and hardly vary, external loads on the end-effector do not result in a reaction moment in the DoFs of the intermediate body.

With respect to the dynamic behaviour of the joint, however, the unconstrained intermediate bodies can result

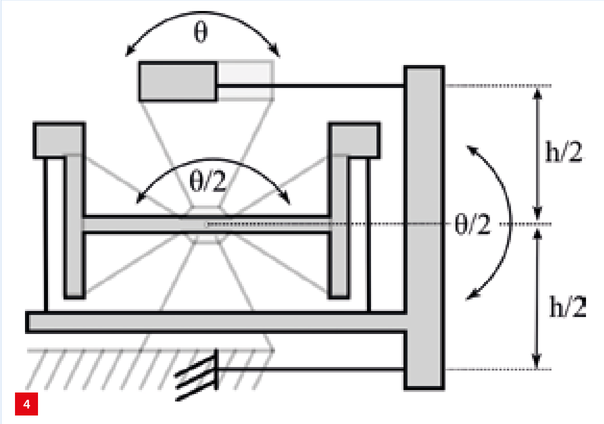

Schematic overview of a butterfly hinge with slaving mechanism.

in unwanted vibrations of the system. The two small intermediate bodies positioned between the first and second set of leafsprings and the third and fourth set of leafsprings have a high natural frequency in the unconstrained DoF, due to the low inertia with respect to the rotation axis of the joint.

Therefore, these unconstrained DoFs typically do not introduce unwanted vibrations in the frequency range of interest. The large intermediate body positioned between the second and third flexure set does potentially lead to unwanted vibrations due to its large size and high inertia.

In order to eliminate this underconstraint, an additional slaving mechanism can be added that couples the motion of the end-effector and the intermediate body with a ratio of two-to-one [3]. A schematic overview of a butterfly hinge with slaving mechanism is provided in Figure 4.

Prototype design

Based on the optimisation results, a prototype of the flexible actuator suspension for the selected torque motor was constructed. An exploded view of the prototype is provided in Figure 5, which shows the suspension for two actuators with parallel rotation axes.

In the design, two butterfly hinges (1) with a width of 50 mm and a slaving mechanism (2) are placed on either side of an aluminium rotor hub (3) that carries the rotor (4). The central 'large' intermediate bodies (5) that are slaved by the slaving mechanisms are interconnected with an aluminium body (6). This body is placed inside the rotor hub and provides a stiff connection between the intermediate slaved bodies.

Furthermore, a linear encoder (7) is placed on the rotor hub (concentric with the rotor) to provide sensing of the rotor position, and a mechanical stop (8) and optical switch (9) are added to prevent excessive rotation of the rotor. The stationary part of the actuator containing the coils, the stator (10), is fixed

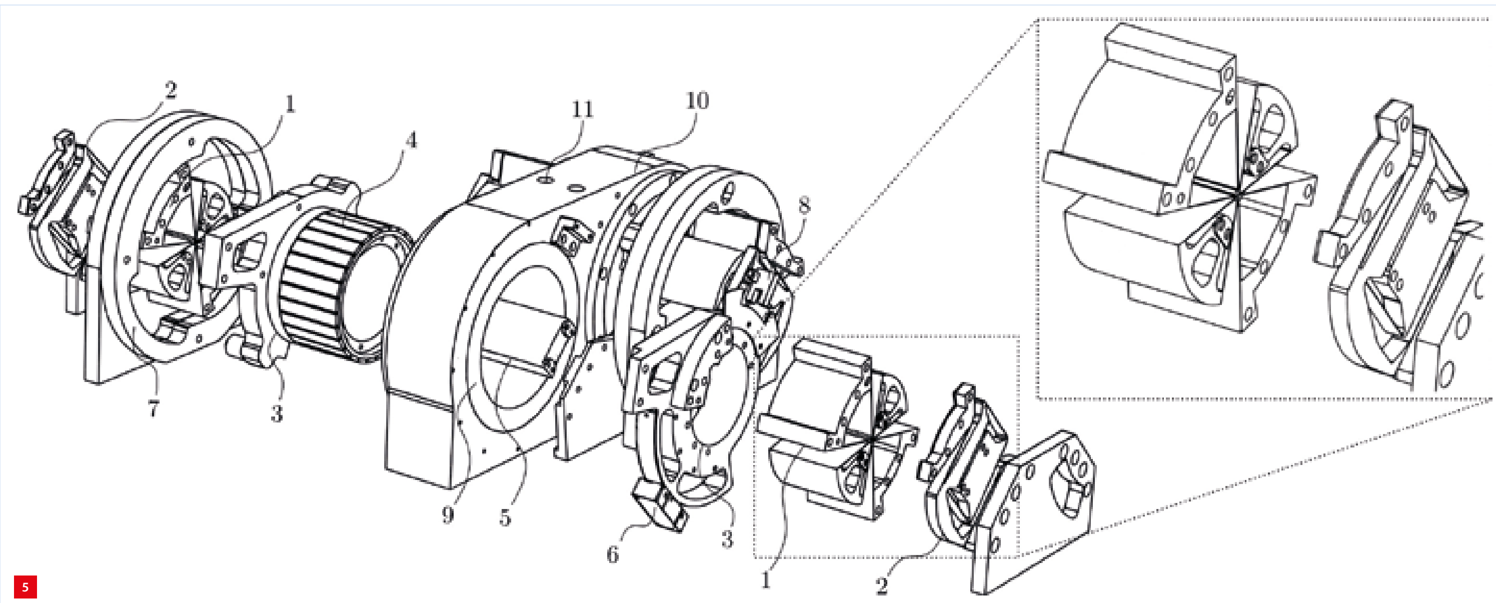

Two actuator suspensions with parallel rotation axis (front actuator suspension in exploded view).
1) Butterfly hinge.
2) Slaving mechanism.
3) Rotor hub connected to both butterfly hinges.
4) Permanent magnets of the rotor.
5) Body coupling intermediate bodies of both butterfly hinges.
6) Encoder.
7) Mechanical stop.
8) Optical switch.
9) Actuator's stator.
10) Stator housing.
11) Cooling channels.

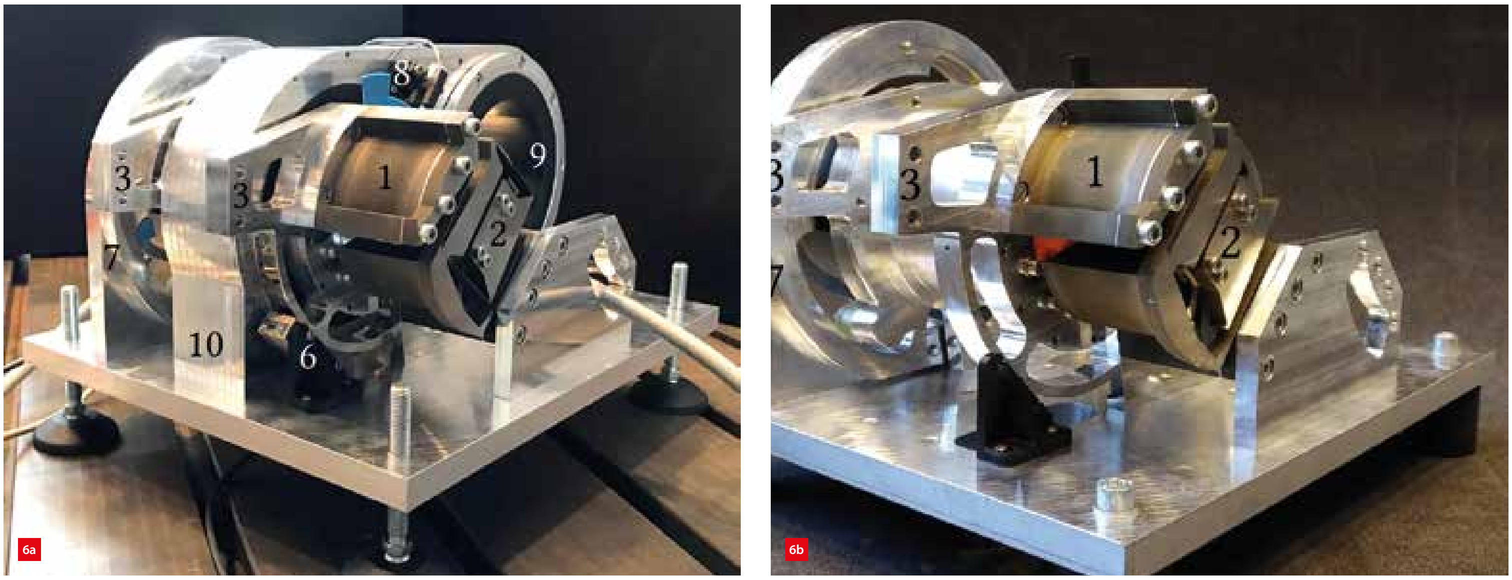

The assembled flexure-based actuator suspension, with 1) butterfly hinge, 2) slaving mechanism, 3) rotor hub, 6) encoder, 7) mechanical stop, 9) actuator's stator, and 10) stator housing.
(a) Overview.
(b) Trimmed view, with the torque motor and stator housing removed.

inside an aluminium frame (11). This frame holds the stator and improves the thermal dissipation for the actuator. Furthermore, the housing is equipped with cooling channels (12) to actively cool the stator for high-load applications.

An overview of the realised prototype is provided in Figure 6 and the video [V1] demonstrates the low hysteresis of the flexure-based design. It has to be noted that insertion of the rotor during assembly requires special attention and additional assembly tools to provide resistance to the negative radial stiffness and to ensure good alignment between the stator and rotor.

As two butterfly hinges at each side of the rotor are used for supporting the actuator, the system is overconstrained, which could result in excessive stress or increased stiffness in the DoF or even decreased stiffness in the support directions. Therefore, care was taken in the positioning of the two individual butterfly hinges to ensure good alignment between them. In particular, the locations of the rotation axis of both butterfly hinges require good alignment, which is ensured by using dowel pins for both hinges.

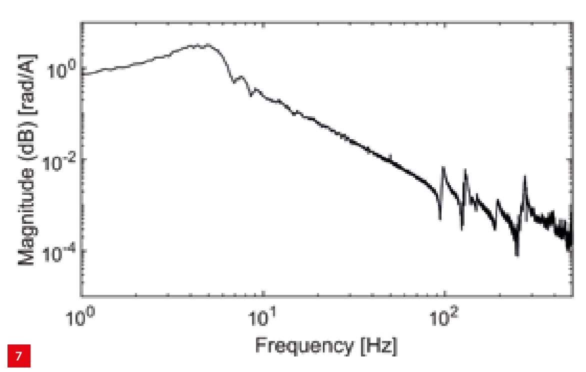

Transfer function from current (A) to rotor position (rad) at $\theta = 25°$, with the first parasitic eigenfrequency at 98 Hz.

Experimental validation

Support stiffness

To validate the support stiffness of the rotor suspension, the frequency of the first parasitic vibration mode of the end-effector was evaluated, which is directly related to the (critical) radial support stiffness. This parasitic vibration mode consists of a translational radial motion approximately parallel to the encoder head on the rotor hub, which can be sensed by the encoder.

To determine the stiffness, the frequency response from actuator current to rotation of the rotor was evaluated, which is provided in Figure 7. This frequency response was evaluated as close to the maximum deflection angle as possible while still allowing for sufficient range of motion for a sweep signal on the input current. From this data, the first (damped) eigenfrequency in the DoF of the system could be observed at about 5 Hz. At 98 Hz, the first parasitic eigenfrequency could be observed, which can be related to the off-axis support stiffness of the system.

In combination with the 3.0 kg mass of the end-effector, consisting of the rotor, rotor hub and a part of the butterfly hinges, this 98 Hz eigenfrequency provides a radial support stiffness of approximately 1,138 N/mm. This is in good agreement with simulations and confirms the intended high radial stiffness of the butterfly hinges (simulated value $K \approx 1{,}400$ N/mm at $\theta = 25°$, Figure 8). The slightly lower stiffness values in the measurement can be related to additional (i.e. non-zero) compliance of the frame parts, which was disregarded in the simulations.

Repeatability
As the system is free of play and friction (and therefore free of self-locking and limit cycling), its repeatability is directly determined by its stand-still performance. To test the repeatability, a representative load was attached to the rotor (a solid block of aluminium resulting in a total inertia of 0.066 kgm^2) and the rotor was moved to a setpoint while the positioning error was tracked. For the presented case, the rotor was moved from $\theta = -22.5°$ to $\theta = -2.5°$ in 0.2 s. The resulting error for a single movement is provided in Figure 8a, where motion starts at $t = 0$ s. Furthermore, a more detailed view of the position of the rotor between $t = 2$ s and $t = 2.5$ s is provided in Figure 8b.

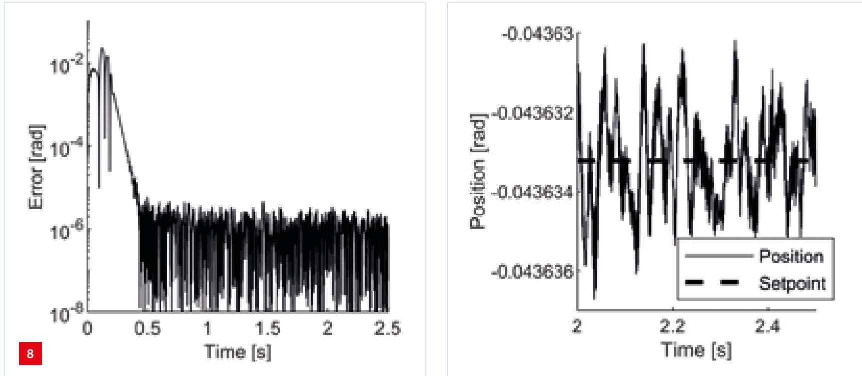

8

Position error for tracking a reference signal moving from $\theta = -22.5°$ ($t = 0$ s) to $\theta = -2.5°$ ($t = 0.2$ s).

From the results it can be observed that the position of the rotor has converged to the target position in about 0.5 s, after which it fluctuated around the target position with an average error of 1.1 µrad rms. These fluctuations in the position are caused by current fluctuations (current ripple) from the motor driver (±5 mA rms noise), resulting in deviations in the generated torque (motor constant 5.57 Nm/A).

As stated earlier, due to the absence of friction, no stick-slip behaviour is present in the flexure-based bearing suspension, resulting in no (mechanical) resistance to small current (torque) variations. Therefore, small fluctuations in the provided current directly cause rotor positioning errors that produce a vibrating motion around the reference position. The driver can be identified as the source of this error as these fluctuations are only present when the motor driver is active.

Stand-still performance can be improved by either reducing the noise output of the driver (dedicated electronics) or by reducing the sensitivity of the rotor position with respect to current fluctuations. The latter can be achieved by reducing the motor constant (i.e. selecting a different actuator) or by increasing the inertia of the system. However, this comes at the expensive of the maximum acceleration that can be achieved and does not affect the ratio between acceleration and stand-still performance.

Conclusion
A large-range-of-motion, flexure-based suspension for an iron-core, direct-drive torque motor with high power density has been designed. The system allows for 60° range of motion combined with an ultimate torque of 55 Nm, featuring high repeatability. The repeatability was measured at 1 µrad rms positioning error with a load of 0.066 kgm^2, at present restricted by current noise of the motor driver.

For the actuator suspension, a butterfly hinge has been modified and optimised to result in only 0.1 mm parasitic radial displacement over the range of motion, which limits pull-in forces typical for iron-core actuators. The radial support stiffness exceeds 1,000 N/mm. This provides adequate support stiffness to compensate for the negative stiffness induced by the iron core of the actuator.

Experimental validations have confirmed the support stiffness and proven the applicability of a flexure-based suspension for high-power-density, iron-core actuators.

REFERENCES
[1] Laithwaite, E.R., and Nasar, S.A., "Linear-motion electrical machines", *Proc. IEEE*, 58(4), pp. 531-541, 1970.
[2] Naves, M, Aarts, R.G.K.M., and Brouwer, D.M., "Maintaining high support stiffness – Large-stroke spherical flexure joint", *Mikroniek*, 59 (3), pp. 17-21, 2019.
[3] *www.utwente.nl/en/et/ms3/research-chairs/pe/T-Flex*
[3] Henien, S., "Short Communication: Flexure delicacies", *Mechanical Sciences*, 3, pp. 1-4, 2012.
[4] Hongzhe, Z., and Shusheng, B, "Accuracy characteristics of the generalized cross-spring pivot", *Mechanism and Machine Theory*, 45(10), pp. 1434-1448, 2010.
[5] Jonker, J.B., and Meijaard, J.P., "Spacar – computer program for dynamic analysis of flexible spatial mechanisms and manipulators", pp. 123-143 in Schiehlen, W. (ed.), *Multibody Systems Handbook*, Springer-Verlag, Heidelberg, 1990.
[6] Nelder, J. A., and Mead, R., "A Simplex Method for Function Minimization", *Computer Journal*, 7(4), pp. 308–313, 1965.
[7] Jones, R.V., "Some uses of elasticity in instrument design", *Journal of Scientific Instruments*, 39(5), pp. 193-203, 1962.

VIDEO
[V1] Fully flexure-based motor suspension
www.youtube.com/watch?time_continue=4&v=rzQorFtXK3I&feature=emb_logo

USING AUTOMATIONML FOR SYSTEM DECOMPOSITION, DOCUMENTATION AND CONTROL REPRESENTATION

As an Industry 4.0 case study, the system design of a mobile robot is presented for use in the RoboCup@Work competition. RoboCup@Work is an international competition, mainly for university students, that aims to bring research and education into the field of industrial automation. RoboHub Eindhoven, a student team at Fontys University of Applied Sciences, has built a custom-made robot for competing in RoboCup@Work. To make the best possible robot design and obtain a good system overview, a model-based breakdown was created in AutomationML, a sophisticated tool for system decomposition, documentation and representation of the control algorithm sequences.

ESMAEIL NAJAFI

Introduction

Industry has been making a switch from traditional mass production with people to a more modular production set-up that is automated. This is called the fourth industrial revolution, or Industry 4.0, and creates new challenges concerning the implementation of such a production set-up. Problems include object handling with differently-sized objects, computer vision to detect and scan objects, mobile platforms that can move objects around in the factory, and robot path planning for generating efficient routes while avoiding obstacles.

The international RoboCup competition was set up for tackling robotics challenges on many different levels and in various leagues, where the RoboCup@Work league [1] focuses on industry and aims to stimulate research into the aforementioned Industry 4.0 challenges. The underlying vision is to foster research and development that enables use of innovative mobile robots equipped with advanced manipulators for current and future industrial applications, in which robots cooperate with human workers on complex tasks ranging from manufacturing, automation and parts handling, to general logistics. The competition aims to simulate a factory environment, in which teams use a mobile robot that is equipped with a robotic arm and vision cameras to autonomously drive around and complete tasks.

This article presents an implementation of model-based design (MBD) for the RoboCup@Work competition as an Industry 4.0 case study. AutomationML [2] is the tool used for the documentation of system decomposition. By decomposing the challenge defined in the RoboCup@Work competition into a unified model, a breakdown of this challenge could be made. The decomposed model could be used to generate a systematic, high-level representation of the mobile robot for the competition tasks.

Model-based design

The RoboCup@Work competition covers three main tasks: navigation, manipulation and transportation. The robot (Figure 1) is subject to specific size restraints, because the competition is using a small-scale environment.

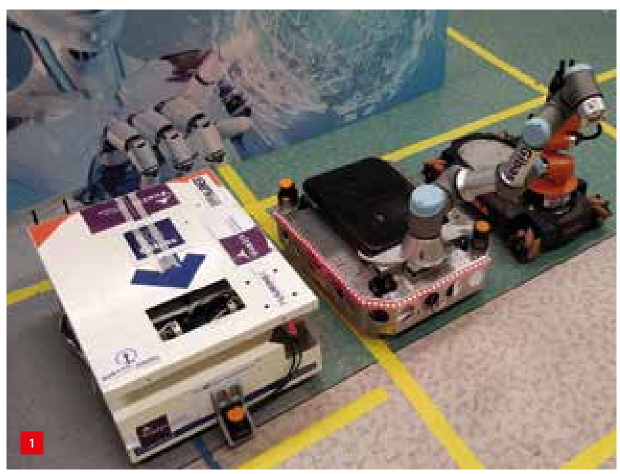

1 *RoboCup@Work line-up of the RoboHub Eindhoven student team [3].*

AUTHOR'S NOTE

Esmaeil Najafi obtained his Ph.D. in Systems and Control in the field of Robotics and Mechatronics at Delft University of Technology, Delft (NL). Then he joined Eindhoven University of Technology, Eindhoven (NL), as a post-doctoral researcher. Now he is a faculty member of the Mechatronics department at Fontys University of Applied Sciences, Eindhoven.

e.najafi@fontys.nl
www.fontys.nl

Model-based design is a methodology to find the solution to a problem by creating a proper model in four steps: modelling the system, designing a controller, simulating the controller, and deploying the controller. As such, the accuracy of the model, as the basic part of the MBD, is very important, because the controller design will be based on this model. Hence, finding an accurate model helps to design an efficient controller. In the implementation stage, there are some tools available to simplify the direct application of the control algorithm to the hardware, without having to convert to low-level hardware codes such as PLC, CNC or FPGA.

System structure

For designing the full system, the robot had to be placed in a virtual execution environment, like the Robotic Operating System (ROS) [4], with the static and dynamic variables that act on it externally. The system modelling language (SysML [5]) diagrams have been used to demonstrate the system structure, looking from the high-level to the low-level design.

Figure 2 illustrates the top level of the system. The SysML diagram offers all the functionality required for defining all parts of the system and provides a high-level decomposition of the robot model. When the mobile platform had reached the late design stage, the SysML diagram offered insights and could act as a basis for prototype building as well as hardware selection.
During the design phase, the requirements of the system were established, followed by the two main building blocks, i.e. the structure of the system and the behaviour in different stages of execution. The requirements block presents the system requirements and the general dependency between them in the design of the mobile platform. The two main building blocks were designed in parallel when the concept of the system had been defined, as the structure and behaviour are linked together, with respect to each system module.

The structure block presents the different modules that compose the system. In the current system, the focus was on the hardware comprising mechanical and electronic components. The structure block additionally presents the interfaces of each system module and the way they are connected to the other modules through the known communication, data, interface or physical protocol.
Based on a more general view of the structure of the system, the block definition diagram presents the dependencies of each module with respect to the roots of the system. The behaviour block presents multiple views of the execution flow of the system. The views of the behaviour can be processed individually, but the full execution loop is created by combining all the behaviour diagrams.

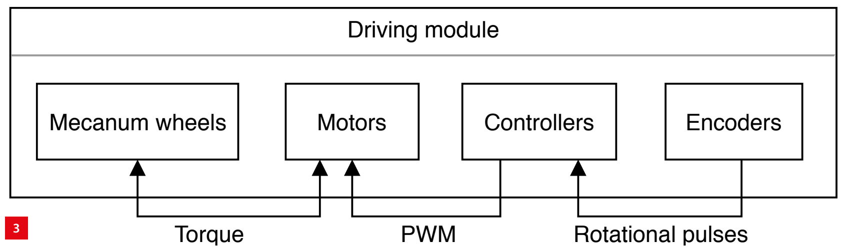

3

Driving module that contains the structural details of the hardware used and the interfaces that allow the module to connect to other modules.

Simulation in AutomationML

One of the structural elements within the robotic system is the Driving module (Figure 3), which was used for implementation in AutomationML. The module contains the structural details of the hardware used and the interfaces that allow the module to connect to other modules, which are the electronics and mechanical components that create the drive train of the mobile platform.

In the Driving module, the components are not fully defined, but their requirements and interfaces are presented in the internal structure of the module. For this module, it was known that it contains four mecanum wheels, actuated by four electric motors that in turn are controlled by a pulse-width modulation signal from motor controllers. On the motors, relative encoders are mounted offering a pulse-type signal used by the motor drivers for calculating the velocity and translation of the mobile platform.

The AutomationML file consists of four blocks, as shown in Figure 4. The block in the top left corner describes the main

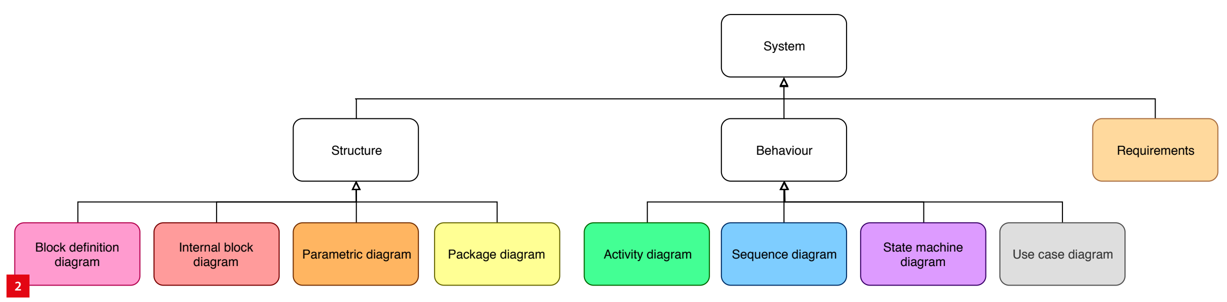

2

System structure: a high-level decomposition of the robot model.

Main hierarchy	Component library
Driving instance ▪ Mecanum wheel ▪ Motors ▪ Controllers ▪ Encoders	Driving ▪ Mecanum wheel 1, 2, 3 and 4 ▪ Motors 1, 2, 3 and 4 ▪ Controllers 1 and 2 ▪ Encoders 1, 2, 3 and 4
Role library	**Interface library**
	Interface data transfer components ▪ PWM ▪ Rotational pulses ▪ Torque

4

The main layout of the AutomationML file for the Driving module.

hierarchy of the RoboCup@Work project, featuring the mechanical, software and electrical parts. The other three blocks are the libraries for the main hierarchy, namely:

- Components library, containing all components that were used in the RoboCup@Work project.
- Role library, containing every role of the modular mobile platform.
- Interface library, containing the communication signals and connections between the parts of the modular mobile platform.

In addition, Figure 5 partially represents the implementation of the Driving module in the AutomationML environment.

Discussion and conclusions

During the process of the robot design, system engineering is often one of the challenging parts. This is mainly because there are several experts involved from different backgrounds working on several modules, which have to be assembled into one complete system. Difficulties can arise, especially in case of complex systems developed by several teams. If one calculation is wrong, every submodule must change. Theoretically, this should not be a problem, but in practice it will take hours to inform every department about the change, not to mention the time and hence costs to adjust every module to fit in the new design.

By using AutomationML as a standard format for the project, all information is placed in one structure, making it easy for every department to check it at any time. An additional benefit of AutomationML is the fact that all modules are interlinked. If one aspect in a module changes, AutomationML automatically changes all dependent modules accordingly. This will save time and costs in Industry 4.0 projects.

In this work, AutomationML has been used to separate elements of behaviour and components of the mobile platform and RoboCup environment, to create a clear overview. By adding interfaces to connect every behaviour state with the relevant components and placing every component in an orderly and proper way inside the main hierarchy, every team member from every department can see their module, connected to the other relevant modules. This helps every member to get the relevant information they need to construct a fitting module and even solve future problems in other departments. For example, an electric malfunction inside the drive train can be prevented at an early stage by a member creating the sensing part of the platform.

As studied in the Industry 4.0 framework with an example of RoboCup@Work, using model-based methodology considerably decreases the number of project communication mistakes and unnecessary handling when one component is updated, adjusted or even either added or deleted. For example, in this case the handling time required for updating a component was reduced by almost 50%. So, project time and costs can be saved, providing more budget for research allowing a better design. If something is changed in the system, it must be guaranteed that correlating components keep working properly. It can be concluded that using AutomationML leads to an appropriate decomposition of robotic systems.

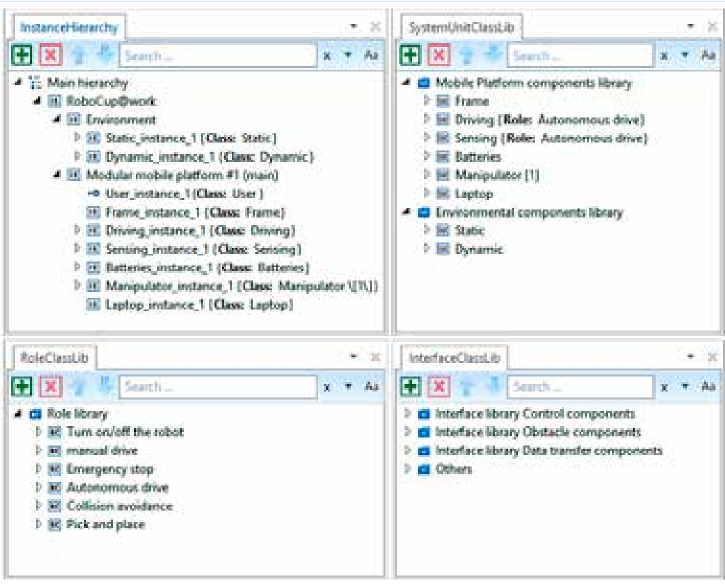

5

Implementation of the Driving module in the AutomationML environment.

REFERENCES

[1] S. Alers, D. Claes, J.-D. Fossel, D. Hennes, K. Tuyls, and G. Weiss. "How to Win RoboCup@ Work?-The Swarmlab@ Work Approach Revealed", *RoboCup*, pp. 147-158. 2013.

[2] R. Drath, A. Luder, J. Peschke, and L. Hundt. "AutomationML-the glue for seamless automation engineering", *2008 IEEE International Conference on Emerging Technologies and Factory Automation*, pp. 616-623, 2008.

[3] *www.robohub-eindhoven.nl*

[4] M. Quigley, K. Conley, B. Gerkey, J. Faust, T. Foote, J. Leibs, R. Wheeler, and A.Y. Ng., "ROS: an open-source Robot Operating System", *ICRA workshop on open source software*, 3 (2), p. 5. 2009.

[5] T. Weilkiens, *Systems engineering with SysML/UML: modeling, analysis, design*, Elsevier, 2011.

LASERS AND VACUUM BESIDES PRECISION MACHINING

As usual, the 2019 Precision Fair held in Veldhoven (NL) on 13 and 14 November showed an abundance of stands demonstrating the precision capabilities of machining specialists. But how to select from all those specialists the best to solve one's precision design problem? And which firm is ready to apply 3D-printing technology? Besides all turning, milling and grinding expertise, dedicated craftsmanship was shown in reaching ultra-high vacuum, as well as in the application of lasers to accurately cut, weld and engrave.

FRANS ZUURVEEN

How to find the right cutting/machine specialist for solving precision design problems, is one of the questions that immediately spring to mind at the Precision Fair.
When asked for reasons to select his company, Raymond Goorsenberg of Fijnmechanische Industrie Goorsenberg, a supplier of precision-engineered components and assemblies based in Nijmegen (NL), answers, "We are a family business with a workforce of only 25 men and women. If you contact us by phone, you can speak directly with the specialist behind a CNC machining centre who is making your product. You can even ask them if they will achieve the accuracies specified. After that, you can contact me to check whether your product will be delivered in time." Figure 1 shows some precision products machined by Goorsenberg Fijnmechanische Industrie. The company also utilises a 3D-printing machine for special manufacturing problems.

AUTHOR'S NOTE

Frans Zuurveen, former editor of Philips Technical Review, is a freelance writer who lives in Vlissingen, the Netherlands.

1

Some precision products machined by Goorsenberg Fijnmechanische Industrie.

2

A large precision system demonstrating the versatile manufacturing disciplines of Aalberts advanced mechatronics.

On the other hand, Aalberts advanced mechatronics (AAM), part of the Aalberts Group (Utrecht, NL), provides its own, multi-disciplinary answers. Figure 2 shows a large demo precision system product as proof of their versatile in-house manufacturing disciplines. For this complicated product, AAM companies Mogema, Lamers, IDE and Pneutec each contributed their craftsmanship. A separate Aalberts company is specialised in additive manufacturing. Thanks to the various in-house disciplines, such printed products can easily be post-processed, including surface and heat treatment, and even HIP: hot isostatic pressing.

Vacuum engineering

In addition to the many cutting specialists, the fair features a rather large number of vacuum equipment producing

Figure 3. Examples of vacuum equipment on display.
(a) A huge vacuum chamber with a large door produced by the Masévon Group.
(b) Vacuum chamber created by D&M Vacuum Systems.
(c) Vacuum assembly from Pfeiffer Vacuum Benelux.
(d) Vacuum assembly by Pink Vakuumtechnik.

firms. Wondering whether the creation of diluted air can be regarded as precision technology, one of the stand members of the Masévon Group (Hardenberg, NL) explains that their huge vacuum chamber (see Figure 3a) has been created to cover automotive products with an extremely thin layer of vacuum-evaporated or magnetron-sputtered material. With such a set-up, a sheet of gold on a plastic dashboard component may even give your car a highly luxurious appearance.

For the batch production of either critical or optional coatings, the Masévon vacuum chamber has been provided with a large door. This enables the fast loading with new, uncoated products. Large vacuum pumps then ensure the low pressure required within a short time. Vernooy Vacuum Engineering, part of the Masévon Group, delivers vacuum products *built-to-print* – according to the customer's CAD-data – or *built-to-spec*, according to CAD-data generated by Vernooy itself.

Figure 3b displays a vacuum chamber created by D&M Vacuum Systems in Budel (NL) for the epitaxial growing of layers on crystal structures, silicon or germanium, for example. Figure 3c shows a vacuum assembly with products from Pfeiffer Vacuum Benelux, based in Culemborg (NL). Two Pfeiffer turbomolecular pumps are connected to a vacuum chamber, as well as pressure measuring sensors and gas analysis equipment. This vacuum assembly was designed for performing advanced vacuum experiments. The vacuum assembly in Figure 3d is exhibited by Pink Vakuumtechnik from Wertheim, Germany.

Laser machining and TIG-welding

Many stands show the various options to apply lasers for precision machining like engraving, cutting and welding.

An impressive example is a demonstration product given away by Laser Technology Janssen in Wijchen (NL). It proves not only the capability to cut and weld, but also to microform across the complete length of a product with in-house developed tooling. The product is also provided with holes of 0.5 mm diameter with manufacturing tolerance h6, corresponding with a dimensional field of 6 μm: 0.500 to 0.506 mm. Also impressive is meeting the challenge to integrate a small stainless-steel ball in the sheet. For that purpose, a laser-pulsed continuous weld, only 200 μm wide, is deposited around the circumference of the ball; see Figure 4.

A small stainless-steel ball pulsed-laser-welded in 0.2-mm-thick sheet by Laser Technology Janssen. Width of weld 200 μm.

5

A TIG-welded biochemical-reaction vessel produced by Larsen & Buhl.

A product that might be considered the result of laser welding is a biochemical-reaction vessel produced by Larsen & Buhl in Zeewolde (NL); see Figure 5. But further inquiry reveals that this product has been TIG-welded; it can nevertheless be regarded as an advanced example of precision assembly. It serves as a test set-up for mixing fluids with bacterial reagents to develop medical vaccines, for example. When tests with this experimental vessel with several dosing entrances and a stirring mechanism are completed successfully, much larger equipment can become available for mass-producing biomedical products.

Additive manufacturing

When asked, most cutting specialists say that they are reluctant to apply 3D printing as a regular technology. But the co-operation of Micro-Machining Group Wilting in Eindhoven (NL) with 3D Systems in Leuven, Belgium – formerly LayerWise – demonstrates the opposite. Beside this, the fair shows examples of 3D-printed products that are nearly impossible to manufacture using conventional cutting technology. 3D Systems claims a density better than 99.6%, a minimum wall thickness of 200 μm and an accuracy of ±0.1% – with a minimum of ±50 μm – for their printed products.

TNO Delft shows 3D-printed products which some years ago were mounted in OMI, the TNO-developed Ozone Monitoring Instrument, now continuously traversing its elliptical orbits above our heads on board the EOS-Aura satellite. Figure 6 shows an aluminium part for the housing of several optical components. Its form resulted from topology optimisation (TO): given the fixed position and form of components, the TO program calculates a minimum amount of material to obtain the required strength and stiffness.

The product of Figure 6 was not really 3D-printed but was ultimately cast. What was printed indeed was a model from wax, which was used in a subsequent lost-wax process. The dimensions of the wax model allowed for thermal effects. For the final casting, the wax model was surrounded by a ‘slurry’ with gypsum as the main component. Subsequently the wax was melted away, resulting in a cavity for the final casting. The estimated accuracy of this sophisticated procedure amounted to 50 μm.

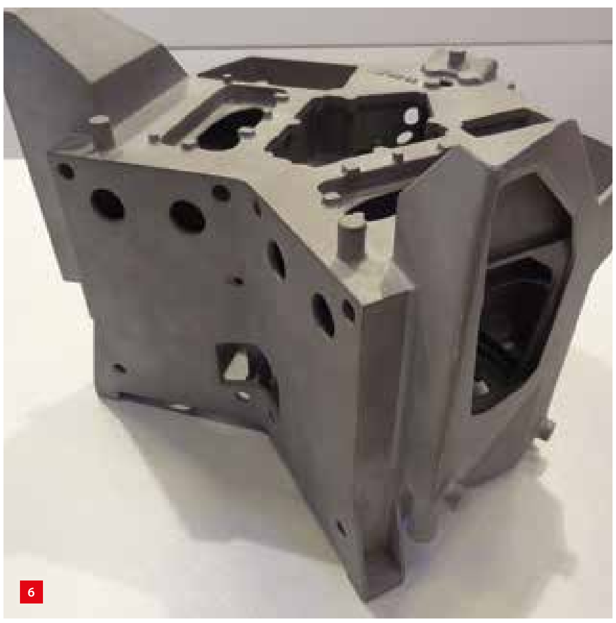

6

A complicated optical part produced by TNO for OMI, the Ozone Monitoring Instrument launched in 2004. It has been produced with a hybrid 3D-printing procedure: 3D printing a wax model and using this as a model in a subsequent lost-wax process.

7

A 3D-printed heat-exchanging system shown by Belgium company Melotte. This product is impossible to make using conventional cutting technology.

8

Exploded view of a rotational clamping device with a repetition accuracy better than 1 μm, on display in Ertec's stand.

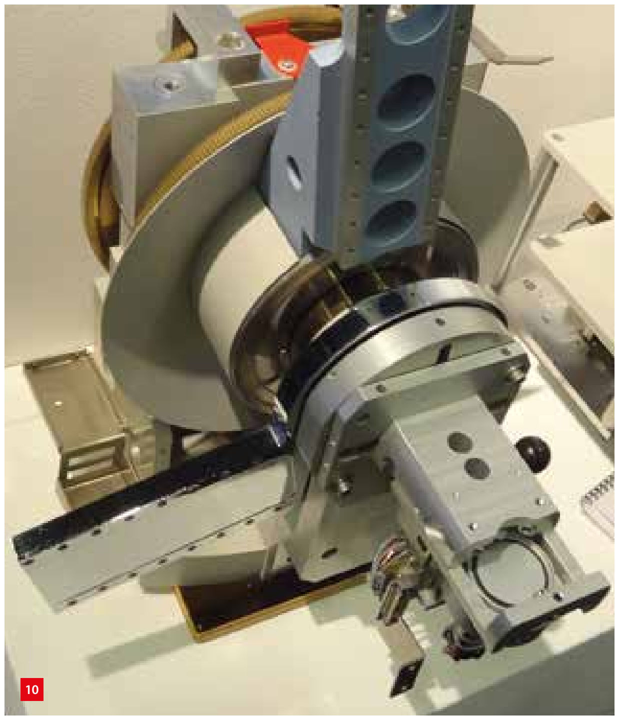

10

An angle-measuring assembly made by Nijdra Special Products for PANalytical, featuring a bearing slit of less than 2 μm.

Another 3D-printed part, impossible to make using conventional cutting, is a heat-exchanging system proudly exhibited by Melotte from Zonhoven, Belgium; see Figure 7. The main activity of Melotte is precision metal cutting, however. Melotte integrates both technologies into one product, if necessary.

Precision clamping

No precision cutting without precision clamping. Ertec Handling and Automation in Nuenen (NL) shows a chuck-like rotational clamping device with a repetition accuracy better than 1 μm; see Figure 8 for an exploded view. Such accurate workpiece holding is extremely important when reclamping for a next cutting operation in the workshop. The Ertec clamping system links the steps in a production chain through an ultra-precision coupling for both workpiece and tool holding. The parts locking force amounts to 6,000 N, with 4x90° fixed index positions.

9

An accurate parallel clamping system from Lang Technik, exhibited by Leering.

11

A Taylor Hobson roundness tester measures the out-of-roundness of a gear wheel assembly.

12

A milling tool from tungsten carbide made by Ceratizit and accurately finished by Kuitaart Slijptechniek.

Accurate parallel clamping systems from Lang Technik in Holzmaden, Germany, are exhibited by Leering in Hengelo (Ov, NL); see Figure 9. These systems were designed to accurately perform milling operations, especially when the workpiece has to be reclamped between two separate cutting processes, with or without robot handling. The crux is to avoid internal workpiece deformation due to clamping forces by gripping the piece along an only 3-mm narrow edge.

Miscellaneous

Figure 10 shows an assembly manufactured by Nijdra Special Products in Middenbeemster (NL) for PANalytical in Almelo (NL). It is, according to Bragg's law, an adjusting instrument for angles between X-ray source, sample and detector, to be used in X-ray fluorescence analysis instruments. The most difficult aspect of this assembly is achieving a bearing slit dimension of 2 μm or less. This is done by individually pairing shaft and bearing by extremely accurate machining on precision lathes.

The measuring of the out-of-roundness of gear wheels with a Taylor Hobson roundness tester is shown in Figure 11. The instrument is provided with a precision air bearing with a rotational accuracy of only 25 nm. Figure 12 shows a milling tool from tungsten carbide made by Ceratizit, headquartered in Luxembourg. The cutting edges have been accurately finished on a CNC grinding machine in the workshop of Kuitaart Slijptechniek in Kuitaart (NL).

These are just a few examples of the dazzling variety of precision products and solutions presented at the 2019 Precision Fair.

Young Talent Award

A new feature at the 2019 edition of the Precision Fair was the Young Talent Pitches event. Promising young engineers took up the challenge to explain within a short time span of three minutes only how innovative their current working tasks really are. The Young Talent Award was given for the best pitch in terms of explanation and illustration, as decided by a panel of judges chaired by Erik Puik, professor of Microsystems at HU University of Applied Sciences in Utrecht (NL). The award, consisting of a sum of money (250 euro) together with a symbolic precision artwork, went to Matthijs van Gastel, Ph.D. student at Eindhoven University of Technology; see Figure 13.
The topic of his pitch was "Sub-micron Accurate Optical Fibre Alignment for Photonic Applications". He explained the alignment and fixation of multiple single-mode optical fibres to photonic integrated circuits. Currently, this connection is a challenging, expensive and time-consuming task. Matthijs van Gastel presented a new concept for actively aligning multi-fibre arrays with sub-micrometer accuracy, fixing them to a photonic chip using UV-curable adhesive, yielding a fibre core concentricity as good as ± 0.5 μm.

13

Matthijs van Gastel (right) receiving the well-deserved Young Talent Award out of the hands of the panel of judges chairman, Erik Puik.

Other pitches on the second fair day, Thursday 14 November:

- Paul van den Hoogenhof (NTS Group)
  Design of a thermally actuated objective lens focus system
  His folded leafspring focusing system has a stroke of 2 μm with a step size within the range of 50 to 80 nm. In his work he combined analytical modelling, simulations and experimental verification.

- Dominic Scheffers (Ceratec)
  A hybrid straight guide, a revolution for UHV technology
  Thanks to the application of ceramics a non-magnetic assembly without lubrication could be realised. Compared to metallic designs his assembly exhibits less friction and is cheaper to make.

- Sven klein Avink (University of Twente)
  A flexure mechanism with increased dynamic performance by using overconstrained visco-elastic material
  The 2019 Wim van der Hoek Award winner (see page 43 ff) developed a flexure mechanism with parallel leaf springs applying numerical analysis combined with knowledge of rubber technology. He developed a visco-elastic material and used it in a set-up with an overconstrained flexure mechanism, which did not suffer from the common disadvantage of alignment errors.

- Bryan Slomp and Gerko Wilkens (Hanzehogeschool Engineering, Groningen)
  Validation of the cutting process for medical precision components manufactured by Witec BV in Stadskanaal
  For Medical Class III products in the delivery programme of Witec, the validation comprises different materials to be applied within the human body in accordance with the ISO 13485 standard.

- Salid Homayoun (VDL ETG)
  Particle contamination control solution for high-tech equipment and substrates
  The yield of manufacturing high-tech equipment is directly dependent of the density of defects generated by contamination. Therefore, particle contamination can directly impact the accuracy and productivity of high-tech equipment by either 'killing' a die or by introducing the cost of cleaning.

- Jorrit van Berkom (Silverwing)
  The future of personal and heavy-payload air transport
  Delft student start-up Silverwing is going to develop heavy-payload, autonomous and electric UAVs (unmanned aerial vehicles). The first one will be capable to carry a payload of 90 kg over 60 km. The project has achieved remarkable success in the Boeing GoFly competition, in which it ended up amongst the final five competitors out of 700 initial participating teams.

- Laurens Goverde (Inholland Composite)
  The design of a light-weight rocket
  The student team Aquilo from the Delft-based Inholland University of Applied Sciences Aviation Technology educational program has been set up to design, build and launch rocket parts from lightweight composites. New technologies such as 3D printing will be investigated to reach this ultimate goal.

- Ahmed Alazzawy (DARE)
  Why Reaching Space is the ultimate ambition of a student rocketry team
  With reaching space, the Stratos IV Delft Aerospace Rocket Engineering (DARE) Team will reclaim the European and Worldwide Amateur Rocketry Altitude Record. They are in search of partners for launching Stratos IV, which is scheduled for summer 2020. It will put the team in the history books as the first student team and the first Dutch rocket ever to reach space.

For the Wednesday pitches, see *www.precisiebeurs.nl/programma/programma-dag-1*.


14

Salid Homayoun (VDL ETG) delivering his pitch. (Photo: Mikrocentrum)

RECOATING REDEFINED

A recoater based on the principle of deposition by multiple overlapping nozzles has been designed. The design aspects of this recoater involve the nozzle configuration, the air shield and the translation system. These aspects are governed by three important physical phenomena, which are viscous jet shape, jet deflection and deposition. Based on theoretical and experimental studies on the aforementioned topics, the design aspects of the recoater have been addressed in depth and a fully-functional small-scale recoater has been designed. Experimental investigations on the designed recoater have demonstrated its ability to deposit thin, homogenous and stable layers of viscous resin at high scan speeds.

TAHMID HOSSAIN, RUUD OLIESLAGERS AND ROBIN KOLDEWEIJ

Introduction

Stereolithography is one of the most widely used additive manufacturing techniques. It relies on the solidification of resin layers by UV radiation exposure. A recoater adds these layers repetitively in between each exposure step. Various coating techniques have been studied and presented in the literature, such as slot-coating, slide-coating and curtain-coating techniques [1]. In slot-coating and slide-coating, various issues are encountered, such as resin scoop-out and non-uniformity in deposition, due to contact between the substrate and the coater. The curtain-coating technique, on the other hand, suffers from instability and breakage of the liquid curtain during the motion of the coater [2]. To overcome these issues, a new coating technology is proposed, which works on the basis of the principle of overlapping viscous jets emanated from a multiple-nozzle recoater. The contactless nature of this type of recoater minimises the possibility of resin scoop-out and non-uniformity issues. Moreover, viscous jets that are resilient to breakage while undergoing acceleration further strengthens the stability of this recoater.

Concept

The working principle of the multiple-nozzle recoater is based on the idea of a large 2D array of viscous jets overlapping each other upon deposition, which leads to coalescence and formation of a layer of resin. The motion of and deposition by the recoater are depicted in Figure 1. The basic components of the recoater are a nozzle plate,

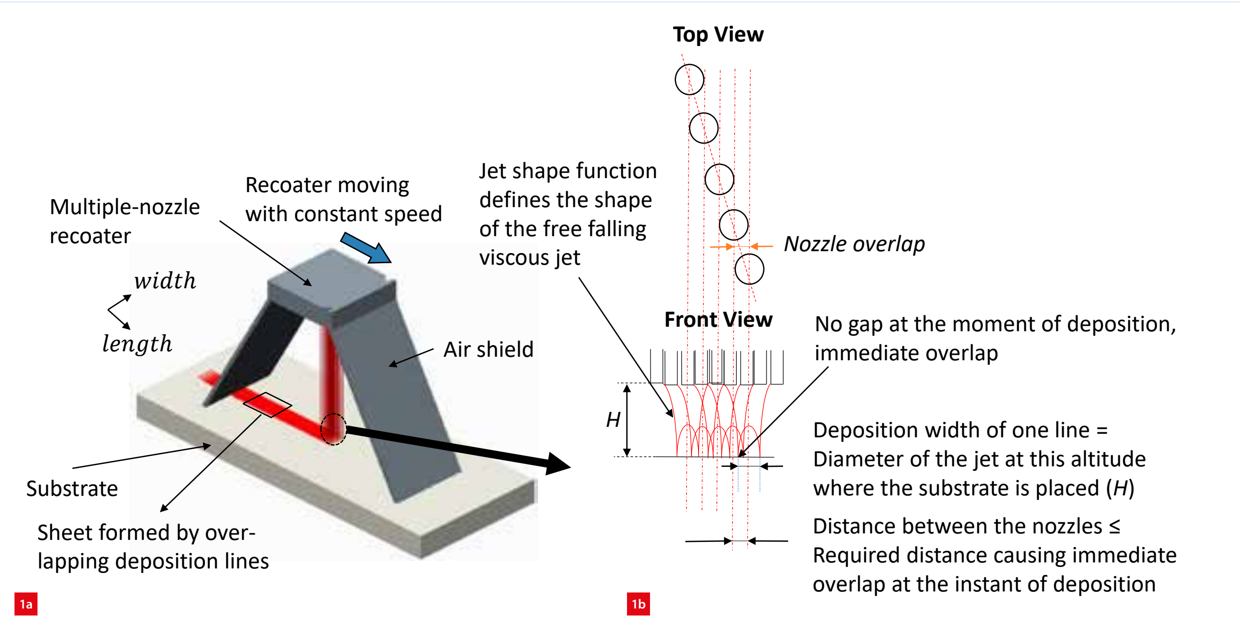

The multiple-nozzle recoater.
(a) Moving over a substrate and depositing overlapping lines that form a sheet of resin along the width direction.
(b) Top and front view schematic of the deposition overlap.

AUTHORS' NOTE

Tahmid Hossain and Robin Koldeweij are thermo-fluidic research scientists at TNO in the department of Nano-instrumentation.
Ruud Olieslagers is currently a thermo-fluidic architect at Philips Innovation Services.

tahmid.hossain@tno.nl
www.tno.nl
www.innovationservices.philips.com

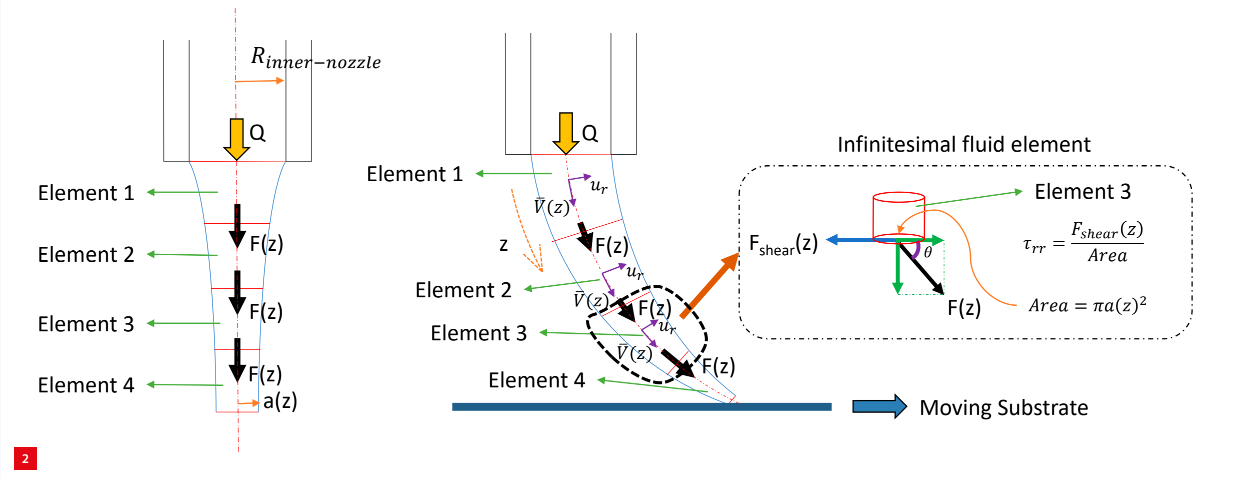

Schematic representation of jet deflection and the forces involved.

an air shield and a translation system. It is crucial to ensure overlap between the nozzles to maintain sheet formation along the width direction as the recoater transverses along the length of the substrate.

Design

The design of the multiple-nozzle recoater covers four main aspects:

1. Determination of operating conditions.
2. Design of nozzle plate.
3. Design of air shield.
4. Design of translation system.

Operating conditions

Three main parameters influence the recoater operating conditions, namely nozzle flow rate, recoater/nozzle-to-substrate height and recoater speed. It has been experimentally observed that under certain operating conditions, the emanated viscous jets exhibit deflection, with a radius of curvature that is much larger than the jet radius, as schematically depicted in Figure 2. This type of deflection can cause jet breakage and non-uniformity in the deposited layer. For the purpose of avoiding this type of deflection, a theoretical model is proposed to create a regime diagram which can be used to determine suitable operating conditions.

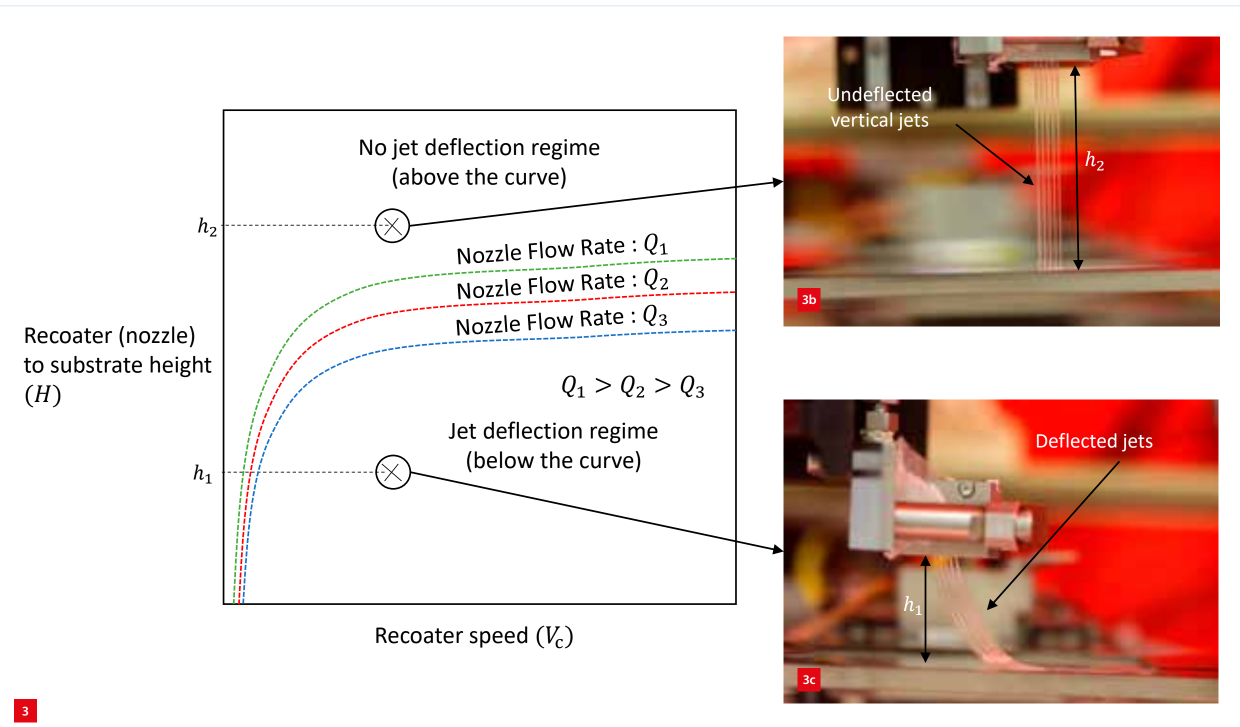

Jet deflection regimes.
(a) Schematic representation of the jet deflection regime diagram.
(b) Experimental observation of no jet deflection.
(c) Experimental observation of jet deflection.

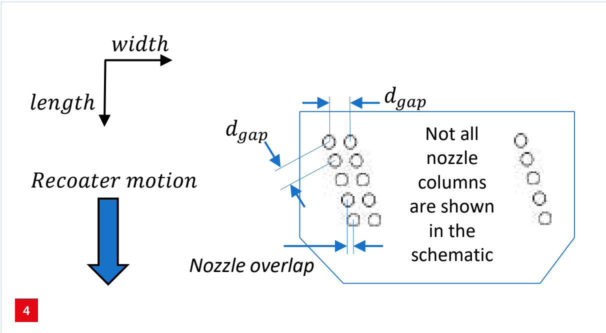

Schematic representation of the nozzle plate showing the governing design parameters, nozzle overlap and nozzle centre-to-centre distance (d_{gap}).

The primary cause of jet deflection is the interaction between fluid elements. This interaction is a force, $F(z)$, comprising the elongational force, surface tension and inertia. The other force that plays an important role in jet deflection is the radial internal shear force, $F_{shear}(z)$, which depends on the viscosity of the fluid. Here the component of gravity along the z-direction is assumed to be negligible.

To understand how these forces play their roles in jet deflection, consider the deflected viscous jet as shown in Figure 2. To simplify the problem, the free-falling jet is divided into four fluid elements. The force $F(z)$ acts between two consecutive elements. The last fluid element (element 4) is dragged along with the substrate as a result of substrate motion. As this happens due to the existing interaction force $F(z)$, this element also pulls the element before it (element 3) with an angle of inclination.

If the interaction force $F(z)$ is large enough to have a horizontal component that can overcome the radial shear force counteracting horizontal deflection, only then will the jet assume a bent and deflected shape. In a very similar way, the third element also pulls the second one, which in turn pulls the first element. As the elements get dragged away, they are essentially replaced by new elements due to the flow that enters the domain.

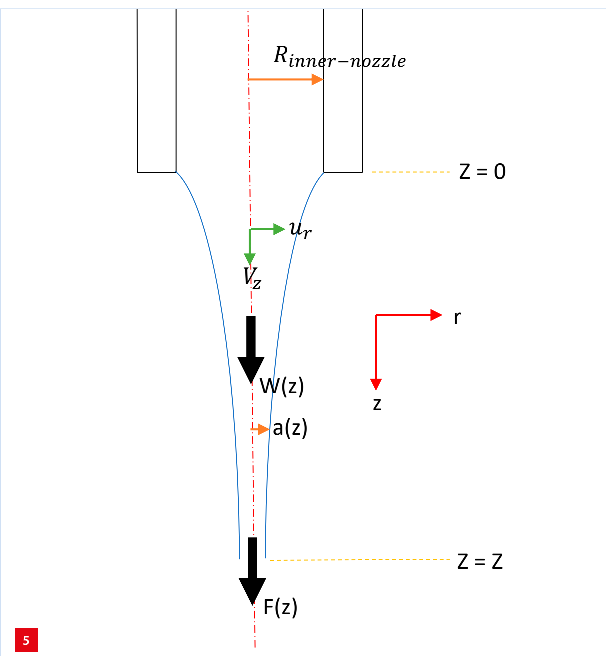

Shape of a falling viscous jet.

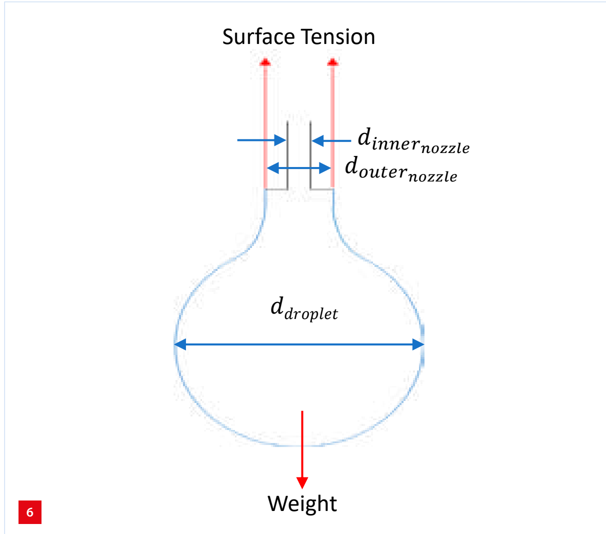

Surface tension and weight acting on a droplet about to drip from the nozzle tip.

Under certain operating conditions, when the force $F(z)$ is smaller in magnitude than the shear force $F_{shear}(z)$, the jet remains undeflected and hence vertical regardless of the substrate speed. In this case, only deflection with a curvature in the order of the jet radius is observed. This deflection does not have a significant effect on the deposition behaviour, hence it is not addressed in this study. Based on this force balance and the work of Lister & Chiu-Webster [3] and Hlod et al. [4], a regime diagram can be developed as schematically shown in Figure 3. Our experimental observations and measurements with the multiple-nozzle recoater have confirmed this theory.

In order to obtain uniform deposition, it is recommended to choose operating conditions that lie in the 'No jet deflection' regime, providing freedom of modulating the recoater speed over a wide range, while ensuring deposition of thin layers.

Nozzle plate design

With the suitable operating conditions chosen, the next step is to design the nozzle plate such that the liquid jets coalesce, leading to a homogeneous resin layer on the substrate. However, during system start-up, formation of individual jets needs to be guaranteed to maintain process stability. These two conditions can be met by designing the nozzle overlap and nozzle centre-to-centre distance (d_{gap}). Figure 4 schematically depicts these parameters for clarification.

The first and most important parameter, nozzle overlap, ensures immediate coalescence of the deposited jets and continuous sheet formation along the width within a short period of time. To reinforce this, the nozzles need to be located on the nozzle plate in a specific configuration. The jets at the substrate need to overlap, such that coalescence is ensured. Jets contract radially as they move downstream, hence the jet diameter at the nozzle plate is larger than at the substrate. To ensure immediate coalescence and continuous sheet formation, the nozzles should be located such that the distance between two consecutive nozzles in a single nozzle column is less than the width of the deposited line or the diameter of the jet, at the corresponding recoater-to-substrate height.

A theoretical model of viscous jet shape formation based on the work of Adachi et al. [5] is used to determine the jet diameter as a function of the downstream direction. Consider a jet formed at a nozzle exit falling freely in the atmosphere that contracts in the radial direction before dropping onto a substrate; see Figure 5. The velocity of the fluid increases in the downstream direction due to gravity as a result of which the cross-section area decreases in order to maintain the same mass flow rate into and out of any arbitrary control volume.

Figure 5 shows a schematic of a falling viscous jet, along with the relevant forces acting on the jet. The relevant forces $F(z)$ (interaction force) and $W(z)$ (weight of the jet) both vary with z, but their sum remains constant along the vertical axis z, as pointed out by Joseph [6]. Given these forces and the liquid properties, the shape of a falling viscous jet can be determined.

This jet shape model is used to approximate the jet diameter at a specified downstream location. Based on this model and the chosen operating conditions, a suitable value for the nozzle overlap can be determined to ensure immediate coalescence.

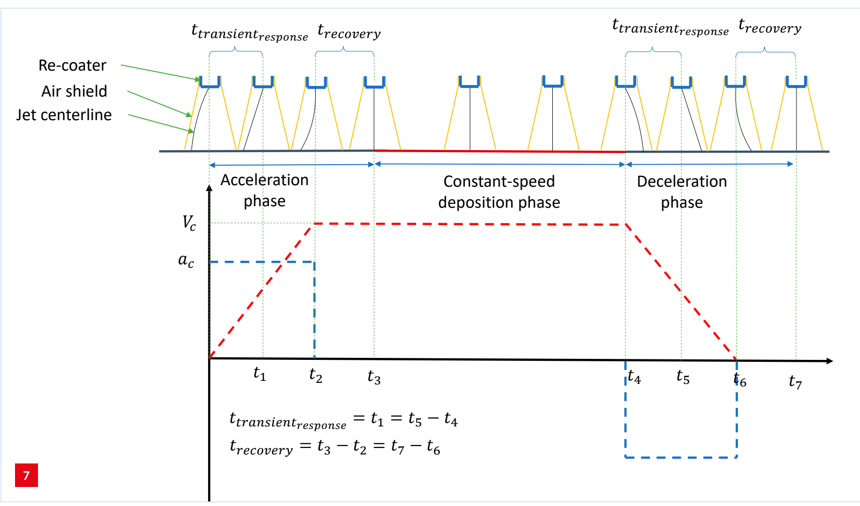

Schematic representation of the three different recoater motion phases. (Just one jet is shown for clarity.)

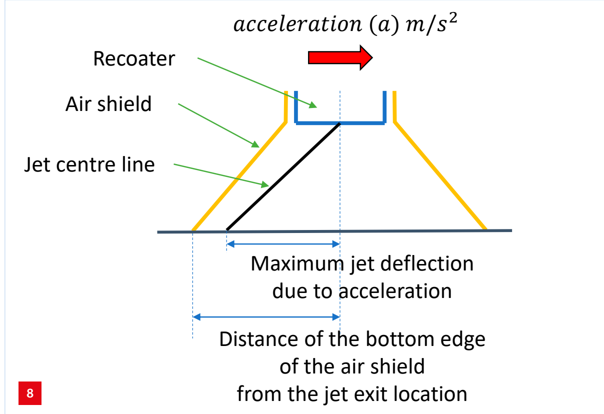

A schematic representation of the recoater with integrated air shield for eliminating aerodynamic effects. The air shield is positioned away from the deflected jet. (Just one jet is shown for clarity.)

To prevent the aforementioned early jet coalescence, the nozzle centre-to-centre distance (d_{gap}) is determined. It depends on the size of the largest droplet that can form at the nozzle tip during system start-up. To ensure the formation of individual jets, neighbouring nozzles must be located at a distance greater than the largest droplet diameter. A theoretical model is developed to determine this distance (d_{gap}) based on the fluid properties and nozzle dimensions.

As resin flow is actuated in the system, droplet formation is initiated at the nozzle tip. After a certain pressure build-up, the transition to jetting occurs. At the static equilibrium of a droplet, i.e. just before a droplet breaks off from the nozzle, the force balance between surface tension and weight (as schematically shown in Figure 6) can be used to approximate the maximum droplet diameter. The measured maximum droplet diameter can then be used to determine the nozzle centre-to-centre distance (d_{gap}).

The number of nozzle columns and the number of nozzles per column are dependent on the width of the substrate to be recoated. Based on the substrate width, the nozzle configuration for the entire nozzle plate can be established.

Translation system and air shield design

The motion of the multiple-nozzle recoater consists of an

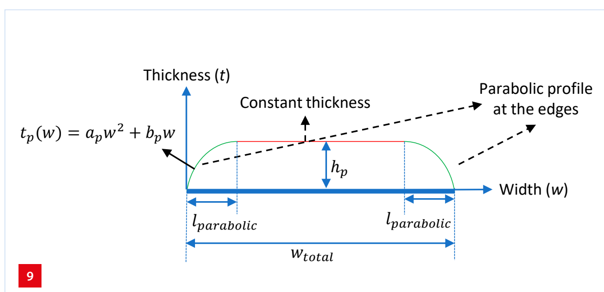

A pancake-like shape is attained by the meniscus after deposition. The parabolic profile of the edges depends on the fluid properties of the resin.

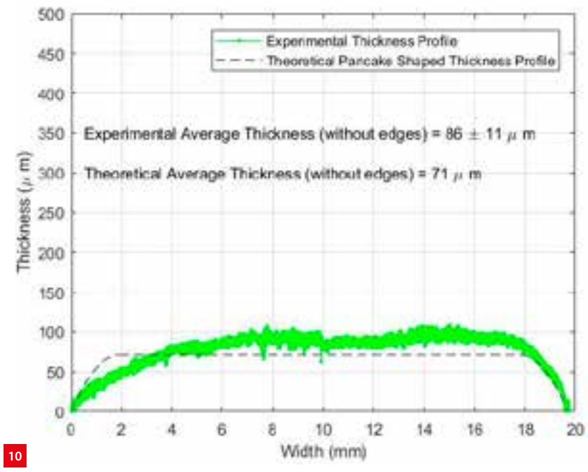

10

Achieved thickness profile with a small-scale multiple-nozzle recoater depositing at 4 m/s.

acceleration phase, a phase of constant speed and finally a deceleration phase to stop the moving recoater as shown schematically in Figure 7. Firstly, in the acceleration phase, the viscous jets emanated from the nozzles experience inertia force and exhibit transient jet deflection. This deflection must dissipate before the onset of the constant-speed phase, where liquid layer deposition occurs, to ensure a predictable and stable deposition. A similar transient jet deflection is also evident in the deceleration phase of the recoater. The distance travelled by the recoater during its transient-response and recovery phases must be taken into account while designing the translation system. In short, the length of the translation system must satisfy this inequality:

$$L_{sys} \geq d_{acc} + d_{dec} + d_{rec} + d_{trans\text{-}res} + L_{sub}$$

Where d_{acc} and d_{dec} are the distances travelled by the recoater during the acceleration and deceleration phases respectively; d_{rec} and $d_{trans\text{-}res}$ are the distances travelled during the recovery and transient-response time periods, respectively; and L_{sub} is the length of the substrate to be recoated.

During the motion of the recoater, aerodynamic drag leads to further jet deflection, which creates the need to integrate an air shield into the recoater. During the acceleration phase the jet deflects to a maximum position. This is shown schematically in Figure 8. The extent of this deflection depends on the magnitude of acceleration and the recoater-to-substrate height. The design of the air shield should be such that it does not interfere with the deflected jet, and is therefore directly dependent on the operating conditions.

Results

Taking the design aspects discussed above into account, a prototype multiple-nozzle recoater is built. To validate its functionality, early experiments are conducted.

Observations show that deposition using this recoater results in the formation of a 'pancake'-shaped thickness profile along the substrate width as shown in Figure 9.

For mathematical simplicity, the shape is assumed to have parabolic edges near the ends and a fairly constant thickness in the central region. The thickness profile of the deposited resin layer formed immediately after deposition can be predicted by the theoretical model of Pirouz et al. [7]. The pancake-shaped thickness profile (t_p, p for pancake) as a function of the substrate width (w) can be mathematically determined by using conservation of mass.

An illustrative experimental result is shown in Figure 10, where the scan speed is 4 m/s, and the viscosity and surface tension of the resin used are 5 Pa.s and 38 mN/m respectively. The correctly designed nozzle configuration based on the theoretical models resulted in immediate coalescence and formation of an instantaneous continuous sheet along the substrate width. The achieved thickness profile of the deposited layer presented in Figure 10 was measured immediately after deposition using a confocal sensor. The deposited layer is very homogeneous in the central region and reasonably consistent with the theoretical prediction.

Conclusions and outlook

A new recoating technology has been proposed and tested on a small scale. The principles of the recoater design have been explored while addressing the governing physical phenomena with theoretical models. Experiments have shown stable and homogeneous deposition of viscous resin with the designed recoater. Future work will focus on conducting experiments with a scaled-up multiple-nozzle recoater and further developing the theoretical models for better prediction.

This new recoating technology, with its unique and stable deposition concept, can be used not only in stereolithography but also in other recoating applications where the deposition of stable, uniform and thin layers is of prime importance.

REFERENCES

[1] ISO / ASTM52921-13, "Standard Terminology for Additive Manufacturing-Coordinate Systems and Test Methodologies", ASTM International, West Conshohocken, PA, USA 2013.
[2] Gilo, M., "Curtain Recoating for Stereolithography", Ph.D. thesis, Katholieke Universiteit Leuven, Belgium, 2004.
[3] Chiu-Webster, S., and Lister, J.R., "The fall of a viscous thread onto a moving surface: a fluid mechanical sewing machine", *Journal of Fluid Mechanics*, 569, pp. 89-111, 2006.
[4] Hlod, A., et al., "Mathematical model of falling of a viscous jet onto a moving surface", *European Journal of Applied Mathematics*, 18(6), pp. 659-677, 2007.
[5] Adachi, K., et al., "Steady laminar round jets of a viscous liquid falling vertically in the atmosphere", *AIChE Journal*, 36(5), pp. 738-745, 1990.
[6] Joseph, D.D., "An integral invariant for jets of liquid into air", *Archive for Rational Mechanics and Analysis*, 74(4), pp. 389-393, 1980.
[7] Pirouz, K., Ben, O., and McKinley, G.H., "Evaporatively driven Marangoni instabilities of volatile liquid films spreading on thermally conductive substrates", *Colloids and Surfaces A: Physicochemical and Engineering Aspects*, 206(1), pp. 409-423, 2002.

PRIZES FOR MULTI-DISCIPLINARY SYSTEM THINKER AND INTERESTING DDP ADDITION

During the 2019 Precision Fair, the Rien Koster Award and the Wim van der Hoek Award were presented under the auspices of DSPE. Hans van de Rijdt, the owner of Van de Rijdt Innovatie, received the Rien Koster Award 2019 for his merits as a developer of multidisciplinary and straightforward concepts for high-tech systems that score well on manufacturability and cost. The Wim van der Hoek Award 2019 was bestowed upon Sven klein Avink, who graduated from the University of Twente on the incorporation of visco-elastic elements in elastic hinge constructions to absorb the effects of overconstraining.

The Rien Koster Award is given to a mechatronics engineer/designer who has made a significant contribution to the field of mechatronics and precision engineering. The panel of judges, now chaired by Ton Peijnenburg, deputy general manager and manager systems engineering at VDL ETG, uses four criteria in the assessment: oeuvre, creativity, relevance (social and commercial) and professional appearance. The award was presented for the eighth time on Wednesday, 13 November. On behalf of the panel of judges, Rien Koster, after whom the award is named, presented the award to ing. Hans van de Rijdt, of Van de Rijdt Innovatie, based in Gemert (NL); see Figure 1.

From patient table to asparagus harvester

After his mechanical engineering studies at the HTS Eindhoven, Van de Rijdt joined Philips CFT, where he worked on many different topics, including the transport system of a placement machine for electronic components and a patient table for radiotherapy. In 1997 he started his own company, Van de Rijdt Innovatie, and since then he has worked for a variety of clients. For example, he developed the concept for a pathology scanner by Philips Healthcare, Sioux CCM and Frencken. He designed the architecture for various NXP production systems and elaborated the concept for a new ASML wafer stage. He also made important contributions to the concept of an asparagus harvester by Cerescon.

Multidisciplinary system thinking

According to the panel of judges, Van de Rijdt's concepts bear witness to multidisciplinary system thinking. "He makes careful use of mechanics, electrical engineering, metrology and

The Rien Koster Award ceremony. (Photos, unless otherwise indicated: Mikrocentrum)
(a) Hans van de Rijdt holding the award certificate and the award's namesake showing the associated trophy, made by LiS students.
(b) Prof. Rien Koster congratulating the award winner's spouse.

control technology to arrive at an optimum design. At the same time, he considers the manufacturability and the cost price, and he often manages to achieve significant cost-price reductions with his design approach. Moreover, he usually comes with multiple options, so that clients have something to choose from, and his designs are often remarkably simple. He creates no-nonsense solutions that make everyone comment, 'That's right, this is how you should do it'."

Professional and modest

On the criterion of 'relevance', Hans van de Rijdt's input leads to usable, marketable products, the production of which generates a lot of high-quality employment, the panel judged. "Finally, he combines a professional appearance with a modest attitude. Van de Rijdt Innovatie is hired by numerous companies, in many cases for just one day a week. Yet he is often the guiding factor in a design team of five to 20 people. In addition, he remains relatively modest as a person. He also offers his time to the High Tech Institute as a training coach for manufacturability. All in all, the panel of judges has every reason to award the Rien Koster Award 2019 to Hans van de Rijdt for the intelligent and intensive way in which he has been practising his profession for 30 years."

The importance of designing

With its Rien Koster Award, DSPE wants to highlight the importance of designing to the precision industry. Globally, the Netherlands plays a leading role in this industry, which can broadly be dubbed the 'high-tech systems' sector. As a group leader at Philips CFT (Centrum voor Fabricagetechnologie [Centre for Manufacturing Technology]) and a professor at the University of Twente (UT), the award's namesake Rien Koster has made a major contribution to the Netherlands' position in this sector. Koster is also the author of the renowned book "Constructieprincipes voor het nauwkeurig bewegen en positioneren" (Design Principles for Precision Movement and Positioning). The Rien Koster Award comprises a sum of money, donated by VDL ETG, and a trophy made by students of the Leidse instrumentmakers School (LiS).

Constructors Award

The second fair day, Thursday 14 November, featured the presentation of the Wim van der Hoek Award. This award (also known as the Constructors Award) was introduced in 2006 to mark the 80th birthday of the Dutch doyen of design engineering principles, Wim van der Hoek, who was the predecessor of Rien Koster. The Constructors Award is presented every year to the person with the best graduation project in the field of design in mechanical engineering at the Dutch (and Belgian) universities of technology and universities of applied sciences. This award includes a certificate, a trophy made by the LiS and a sum of

2

The panel of judges flanking the three nominees for the Wim van der Hoek Award 2019; on the left, Jos Gunsing (MaromeTech), chairman of the panel and DSPE board member.

money, sponsored by HTSC; the High Tech Systems Center at Eindhoven University of Technology (TU/e).

Three nominations

Criteria for the assessment of the graduation theses include quality of the design, substantiation and innovativeness, as well as the suitability for use as teaching materials. The panel of judges, chaired by DSPE board member Jos Gunsing (MaromeTech), received three nominations, submitted by the graduation supervisor/professor of each student concerned, from Fontys University of Applied Sciences in Eindhoven, TU/e and UT. "In all cases it concerned high-quality work in which very different

3

Sven klein Avink, winner of the Wim van der Hoek Award 2019, showing the certificate and the trophy he has just received.

themes have been systematically tackled from design to experiment", the panel of judges said. The three nominees (Figure 2) have been invited to attend the DSPE Conference on Precision Mechatronics 2020 free of charge and to contribute a poster presentation of their graduation work.

DDP worthy

The Wim van der Hoek Award 2019 eventually went to Sven klein Avink (Figure 3), who studied Mechanical Engineering at Saxion University of Applied Sciences and the UT. This spring, he graduated from the UT, in the group of Dannis Brouwer, professor of Precision Engineering, on the incorporation of visco-elastic elements in elastic hinge constructions to absorb the effects of overconstraining.

According to the panel of judges, this work adds an extra paragraph, and "explicitly a material property component", to Des Duivels Prentenboek (DDP), "The Devil's Picture Book", Wim van der Hoek's principal work.
"Sven approaches the theme analytically, numerically as well as experimentally; thereby he creates optimum understanding. The work offers extra possibilities for designers to extend the working range of leafspring constructions. He gives an excellent quantification of the visco-elastic effects down to the level of the impact on the eigenmodes / eigenfrequencies." The panel also sees opportunities for a follow-up: "We would like to propose the generalisation to other elastic hinge constructions and / or the application to a complete construction."

Wim van der Hoek

Earlier this year, Wim van der Hoek passed away at the age of 94. His widow, Aat, and son, Rouke, attended the award ceremony (Figure 4).

This year, the ceremony for the Wim van der Hoek Award was the first after the passing away of the award's namesake. His widow, Aat, and son, Rouke, attended the ceremony. Here, they are flanking the award winner. (Photo: Lambert van Beukering)

CALCULATING THE ADVANTAGES OF ADDITIVE MANUFACTURING

The post-processing of high-precision, 3D-printed metal parts is still too costly. Finding a solution to this problem led Hittech Multin to initiate research based on its own system engineering approach. This ultimately resulted in the Interreg 2 Seas 3D Flexible Post Processing (3D&FPP) project, which is aimed at designing and developing an efficient, fast and affordable post-processing solution. This article discusses a proposed generic and retrofit solution based on existing technology that can be part of an integrated system for processing printed parts. Specifically, it focuses on part positioning and the corresponding adjustment of the NC-code for milling purposes.

ATMA DE WAAL AND QIANG LI

Introduction

Additive manufacturing (AM) is rapidly moving from an emergent technology into a true and mature manufacturing capability. Exploitation, however, has been particularly limited for AM metal parts, due to the time-consuming nature and labour-intensive post-processing of AM parts. An efficient, fast and affordable post-processing solution based on existing technology, which will decrease production cost and time, will help to capitalise on the possibilities for 3D metal printing in industries that require high-precision metal parts (e.g. medical, semiconductor, maritime, aviation and cleantech industries). Considering this objective and given the Hittech Group's proprietary system engineering approach, a clear

AUTHORS' NOTE

Atma de Waal is a technical project manager at Hittech Multin, part of the Hittech Group, based in Den Haag (NL). Qiang Li is a postdoctoral research fellow at the University of Exeter, UK.

Project partners in the Interreg 2 Seas 3D Flexible Post Processing (3D&FPP) project are Hittech Multin, University of Exeter Manufacturing Enterprise Centre (XMEC), 3T additive manufacturing, Argon Measuring Solutions, TNO, RDM Makerspace, and Rotterdam University of Applied Sciences.

The algorithm and transformation study was carried out by the University of Exeter (Qiang Li), the validation by Hittech Multin (Atma de Waal and Jeroen Valentijn, system engineer) in collaboration with Argon MS (Dimitri Vanbuel, R&D manager), and editorial review by Hittech Multin (Bas Verhulp, mechatronic engineer).

adwaal@hittech.com
www.hittech.com
www.projects.exeter.ac.uk/xmec
www.argon-ms.com
www.3dfpp.eu

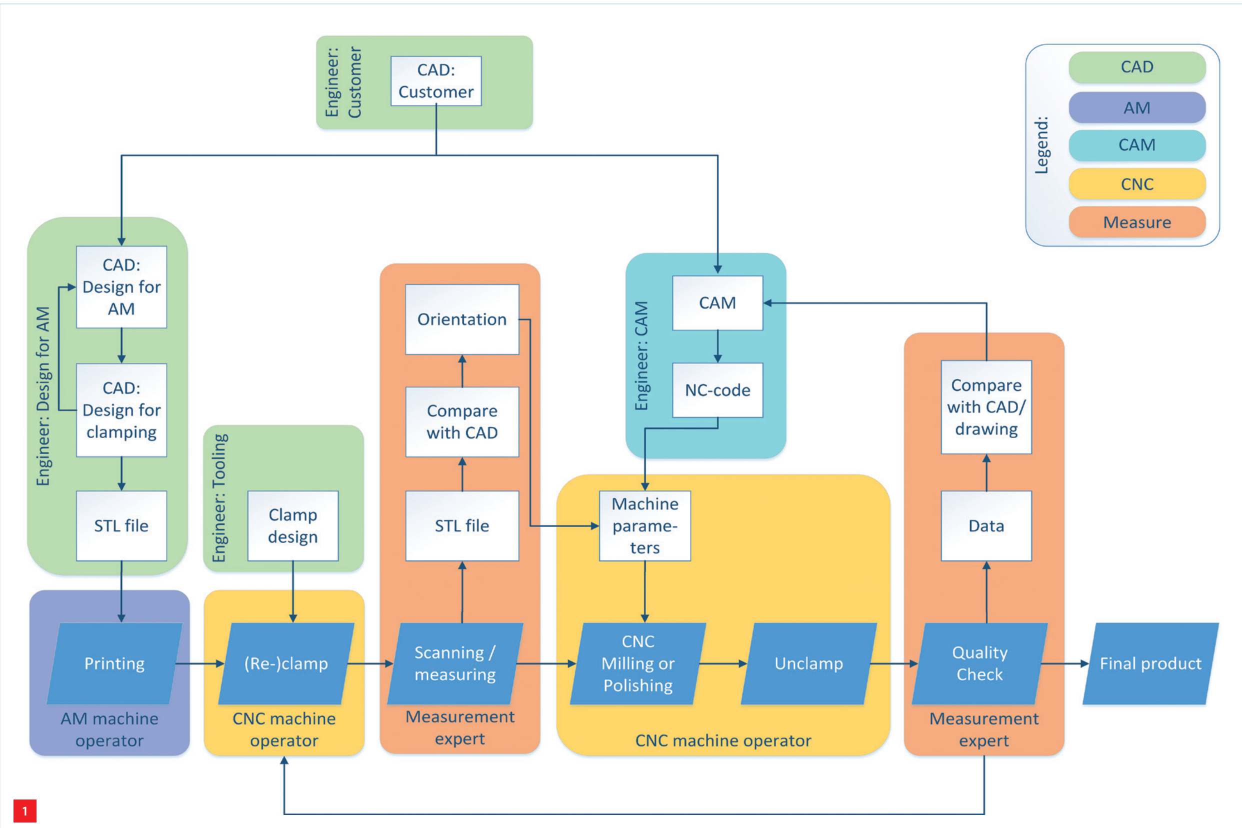

1 *Post-processing workflow.*

understanding of the process steps involved is drafted, their iterations and their interdependencies in order to conceive an integrated post-processing system that can be implemented in current production processes. The flowchart of Figure 1 shows the distinctive production steps (blue), the professions or skills involved (combined areas in various colours) and the necessary (data)communication (dotted lines).

From this understanding, four areas of research were identified in the 3D&FPP project:
1. CAD/CAM
2. Flexible clamping
3. Scanning/positioning for milling
4. Surface polishing

The project aim was to deliver at Technical Readiness Level 7 a flexible, affordable generic post-processing process for the professional CNC market (e.g. Heidenhain, Fanuc and Siemens) that will reduce production costs and production time. The application of optics for the positioning and alignment of the AM metal part proved to be a vital part of the project's solution and is therefore main focus of this article.

Methodology
In order to facilitate the positioning of 3D-printed metal parts onto a CNC machine, 3D-scanning technology is applied to obtain the digital model of a clamped part that can then be compared with the original CAD model to find the relationship between the part's real position and its theoretical position designed in the CAM program.

The purpose of the comparison, i.e. alignment, of the original CAD model and the scanned 3D model is to determine whether the printed part has enough stock to allow the AM part to be milled into its final shape. The relationship between the part's real position and its theoretical position, represented as a coordinate system transformation matrix (CSTM) or rotation & translation matrix (as depicted in Figure 2), can subsequently be used as input to the developed 'Compiler' in order to modify the NC-code matching the part's real clamping position.

Generic alignment strategy for 3D models
Calculating the difference between two 3D models (CAD and scanned) requires the 3D models to be positioned in the same coordinate system in order to align overlapping components in the data set or point cloud. For this matching, the Iterative Closest Point (ICP) approach and the Spatial Normal Vector (SNV) approach were considered; see the text box on the next page.

Matrix based on SNV analysis
Determining the rotation matrix between two 3D models requires the two 3D models to be aligned by matching their

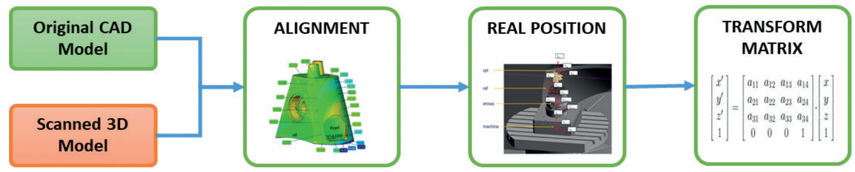

2

Basic workflow of model comparison.

corresponding feature surfaces, thus obtaining their respective spatial normal vectors, which can subsequently be compared. The rotation matrix used in this project is derived from the alignment of the spatial normal vectors of corresponding features.

Rotation matrix R
The vector of a flat surface's normal is perpendicular to its surface and is represented as surface normal vector or *SN* (see Figure 3). To establish a frame, of which two spatial normal vectors SN_1 and SN_2 are given, the vectors $\overrightarrow{OX}$, $\overrightarrow{OY}$, $\overrightarrow{OZ}$ can be calculated as follows (using the cross product ×):

$$\begin{bmatrix}\overrightarrow{OX}\\ \overrightarrow{OY}\\ \overrightarrow{OZ}\end{bmatrix} = \begin{bmatrix} SN_1 \\ (SN_1 \times SN_2) \times SN_1 \\ SN_1 \times SN_2 \end{bmatrix}$$

Note: The spatial normal vector is not the direction of the coordinate system axis, and the angle between SN_1 and SN_2 might not necessarily equal 90°. To build a coordinate system frame, either SN_1 or SN_2 is selected as $\overrightarrow{OX}$, and the plane that consists of SN_1 and SN_2 is defined as the *XY* plane. When taking SN_1 as $\overrightarrow{OX}$, the direction of $\overrightarrow{OZ}$ will be the cross product of SN_1 and SN_2. Hence, the direction of $\overrightarrow{OY}$ is the cross product of $\overrightarrow{OZ}$ and $\overrightarrow{OX}$.

Given the direction vectors of $\overrightarrow{OX}$, $\overrightarrow{OY}$, $\overrightarrow{OZ}$ and, $\overrightarrow{OX'}$, $\overrightarrow{OY'}$, $\overrightarrow{OZ'}$ the rotations angles φ, θ and ψ around *Z*, *Y* and *X*, respectively, can be calculated as follows:

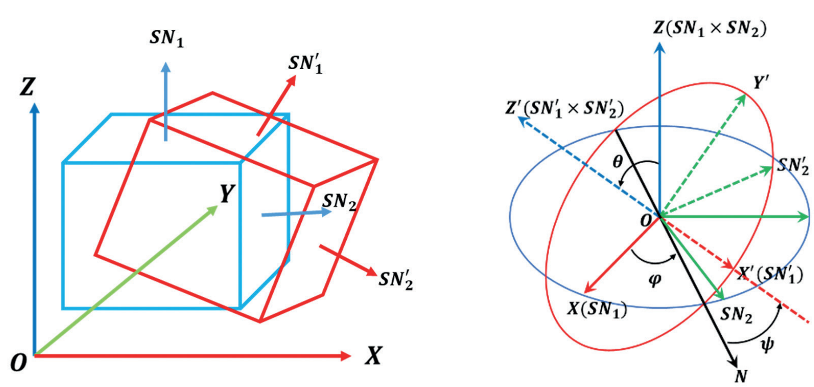

3

Illustration of spatial normal vectors.

$$\varphi = arccos\left(\frac{|\overrightarrow{OX}\cdot\overrightarrow{ON}|}{|\overrightarrow{OX}||\overrightarrow{ON}|}\right), where\ \overrightarrow{ON} = \overrightarrow{OZ}\times\overrightarrow{OZ}'$$

$$\theta = arccos\left(\frac{|\overrightarrow{OZ}\cdot\overrightarrow{OZ}'|}{|\overrightarrow{OZ}||\overrightarrow{OZ}'|}\right)$$

$$\psi = arccos\left(\frac{|\overrightarrow{ON}\cdot\overrightarrow{OX}'|}{|\overrightarrow{ON}||\overrightarrow{OX}'|}\right)$$

The rotation matrix R can subsequently be calculated as follows:

Considerations for alternative model matching processes

Iterative Closest Point (ICP) approach

Consider a finite-dimensional real vector space R^n that contains target [*E*] and source points [*S*] sets {*E*,*S*}, each with a finite number of points. The fundamental problem is to find a transformation *T*(*S*) that can be applied to *S* such that the transformed point set and *E* are properly aligned. The ICP algorithm assures that the closest point pairs between *S* and *E* are in correspondence and iteratively minimises the mean squared error of the corresponding points until convergence, so *E* and *T*(*S*) become optimally aligned:

$$argmin_{R,t}\left\{\frac{1}{|E|}\sum_i \|e_i - (Rs_i + t)\|_2^2\right\}$$

Here, $e_i \in E$ and $s_i \in S$ form a correspondence pair, and |*E*| represents the number of points in *E*, while argmin *f*(*R*,*t*) gives a position {*R*,*t*} at which *f* is minimised. Hence, an initial selection of points from two point sets must be given and their correspondence established. Whether convergence occurs and how quickly it does so depends greatly on the initial selection. Moreover, the number of points in a 3D mesh model converted from a CAD model and in a scanned model differ significantly. The scanned model usually is fragmentary in comparison, which affects the iteration step negatively.

Spatial Normal Vector (SNV) approach

The SNV approach is based on calculating the spatial normal vector of feature surfaces that consist of triangular faces in a 3D mesh model (STL file, or CAD model), instead of its respective points. A spatial normal vector is the normal vector of a planar surface or the direction vector of a cylindrical feature's central axis. This approach therefore does not require the correspondence between point sets to be established, nor does it need iteration for alignment. This approach was therefore the preferred one.

$$R = R_z(\varphi)R_y(\theta)R_x(\psi) =$$

$$\begin{bmatrix} \cos\theta\cos\varphi & \sin\psi\sin\theta\cos\varphi - \cos\psi\sin\varphi & \cos\psi\sin\theta\cos\varphi + \sin\psi\sin\varphi \\ \cos\theta\sin\varphi & \sin\psi\sin\theta\sin\varphi + \cos\psi\cos\varphi & \cos\psi\sin\theta\sin\varphi - \sin\psi\cos\varphi \\ -\sin\theta & \sin\psi\cos\theta & \cos\psi\cos\theta \end{bmatrix}$$

The correct translation value can be achieved by alignment of the scanned model through the translation along the *X*-, *Y*- and *Z*-direction:

$$x = \frac{(x_{max}^{scan} + x_{min}^{scan}) - (x_{max}^{cad} + x_{min}^{cad})}{2}$$

$$y = \frac{(y_{max}^{scan} + y_{min}^{scan}) - (y_{max}^{cad} + y_{min}^{cad})}{2}$$

$$z = \frac{z_{max}^{scan} - z_{max}^{cad}}{2}$$

In the flowchart (see Figure 4), *R* is the rotation matrix that is calculated based on the established two coordinate system frames of the scanned model and the CAD model. The three angles are Euler angles and the total rotation sequence is computed with $R = R_z(\varphi)R_y(\theta)R_x(\psi)$, which aims to set the two coordinate systems in the same orientation. Subsequently, the translation matrix is calculated based on the boundary box of the rotated CAD and the scanned model.

Automated NC-code modification

The NC-code, also known as NC-post, is independently generated by a CAM software package, its only input being the original CAD model. This NC-code defines the movements of the tools relative to the Program Zero Position (PZP), which is the coordinate zero used in the CAM software. Please note that the coordinate zero of the Tilted Working Plane (TWP) is always relative to PZP. This correlation of zero points is also called working-plane-based CNC programming.

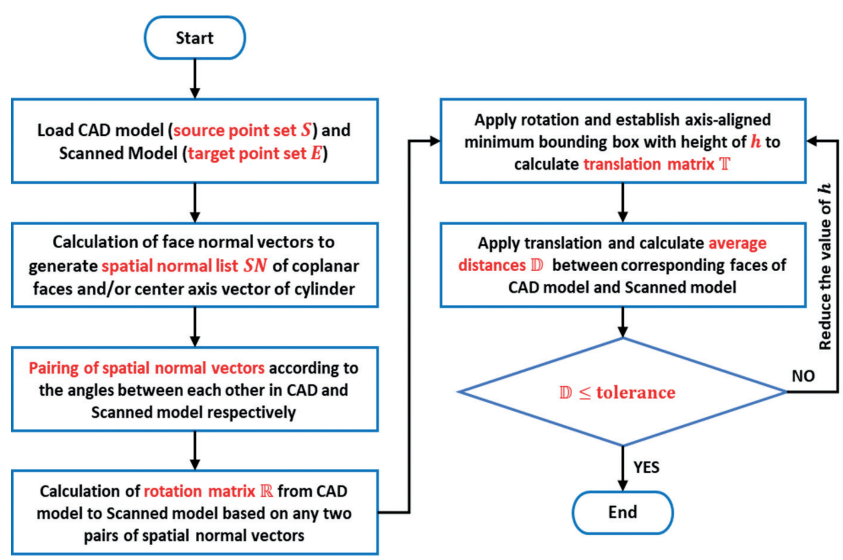

4

Flowchart of the proposed non-iterative model comparison algorithm.

Spatial angles

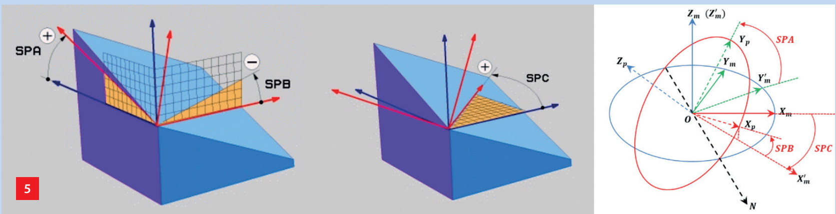

5

Depiction of SPA, SPB and SPC for which a function is used to define a TWP with up to three spatial angles.

Spatial angles define a working plane through up to three rotations in the non-tilted workpiece coordinate system (tilting sequence A-B-C).
Given the values of *SPA, SPB, SPC* (Figure 5), and vectors $\overrightarrow{OX_m}, \overrightarrow{OY_m}, \overrightarrow{OZ_m}$, the vectors $\overrightarrow{OX_p}, \overrightarrow{OY_p}, \overrightarrow{OZ_p}$ can be calculated as follows:

$$\overrightarrow{OX_p} = \overrightarrow{OX_m} \cdot ROT(SPC) \cdot ROT(SPB) \cdot ROT(SPA)$$
$$\overrightarrow{OZ_p} = \overrightarrow{OZ_m} \cdot ROT(SPC) \cdot ROT(SPB) \cdot ROT(SPA)$$

After offsetting ($O_m = O_p = O$) and given the direction vectors $\overrightarrow{OX_m}, \overrightarrow{OY_m}, \overrightarrow{OZ_m}$, $\overrightarrow{OX_p}, \overrightarrow{OY_p}, \overrightarrow{OZ_p}$, the values of *SPA, SPB, SPC* can be calculated as follows:

- *SPC*, the angle between $\overrightarrow{OX_m}$ and the intersection line ($\overrightarrow{OX_{xy}}$) of planes OX_pZ_m and OX_mY_m:

$$\overrightarrow{OX_{xy}} = \overrightarrow{OY_m} \times (\overrightarrow{OZ_m} \times \overrightarrow{OX_p})$$
$$SPC = \overrightarrow{OX_m} \angle \overrightarrow{OX_{xy}} = arccos(\frac{|\overrightarrow{OX_m} \cdot \overrightarrow{OX_{xy}}|}{|\overrightarrow{OX_m}||\overrightarrow{OX_{xy}}|})$$

Where $\angle$ represents the angle between the two vectors.

- *SPB*, the angle between the intersection line ($\overrightarrow{OX_{pxy}}$) of planes OX_pZ_m and OX_mY_m, and $\overrightarrow{OX_p}$:

$$SPB = \overrightarrow{OX_{pxy}} \angle \overrightarrow{OX_p} = arccos(\frac{|\overrightarrow{OX_{pxy}} \cdot \overrightarrow{OX_p}|}{|\overrightarrow{OX_{pxy}}||\overrightarrow{OX_p}|})$$

- *SPA*, the angle between planes OX_pZ_m and OX_pZ_p:

$$SPA = \overrightarrow{OY_p} \angle (\overrightarrow{OZ_m} \times \overrightarrow{OX_p}) = arccos(\frac{|\overrightarrow{OY_p} \cdot \overrightarrow{OZ_mX_p}|}{|\overrightarrow{OY_p}||\overrightarrow{OZ_mX_p}|})$$

Note: the angles φ, θ and ψ can differ from the angles *SPC, SPB* and *SPA*, since both angle types are calculated differently. However, the rotations $R = R_z(\varphi)R_y(\theta)R_x(\psi)$ and *ROT*(*SPC*).*ROT*(*SPB*).*ROT*(*SPA*) will result in the same reorientation of the respective coordinate systems.

Before executing the CNC program, a critical procedure is to measure the real position of the PZP within the CNC machine's coordinate system and to synchronise the actual position of the part as it relates to the machine zero position through work offsetting.
In this approach, 3D scanning is used to obtain the digital 3D model and the relationship between the part's theoretical position and its actual position, relative to the machine zero position, which is ultimately represented as a transformation matrix. The theoretical position of the 3D CAD model and the transformation matrix to align the scanned model with the 3D CAD model can be used to recalculate the geometric position of each TWP as defined in the NC-code, because the relative position of every TWP to the PZP is fixed.

However, the PZP as well as the TWPs might be represented in various formats, depending on the specifications of the NC-codes (i.e. Heidenhain, Fanuc or Siemens). They must therefore first be converted to a generic geometric format and, after applying the transformation matrix, converted back into their original format. The most commonly used TWP formats are spatial angles and projection angles; see the respective text boxes on this page and the next page.

Based on the investigation of TWP-based CNC programming and the established conversion mechanisms, a proprietary software platform for online automatic modification of TWP-based CNC programming according to the real clamping position was developed, called the Compiler.

System accuracy

The performance of such a system and its validity has been tested. Since the applied science in the Compiler is completely mathematical, it can be assumed that the application will either work or not. Therefore, the 3D&FPP approach was considered to have an overall system accuracy close to or equal to the cumulative machine accuracy of the system's set-up.

To validate the approach, test objects were mounted on an Erowa zero-point clamp system in a standard clamp and scanned. This scan data was compared to the customer's CAD model, by aligning the surfaces. The real orientation of the object with respect to the Erowa clamp resulted in a transformation matrix, which served as input to the Compiler for modification of the NC-code. The modified NC-code resulted in a post-processed object milled according to specifications (Figure 7), which was verified on a coordinate measuring machine (CMM).

These tests proved the applicability of the 3D&FPP approach to modifying the NC-code based on a transformation matrix attained by scanning. The overall accuracy (system error) of the system highly depends on the used set-up but can be as good as 10 μm, which complies with current high-precision industrial standards.

Conclusions and future work

The proposed approach is generic and backwards compatible. The approach provides insight into how to automate the repositioning of a part in an industrial environment. The operating system on the CNC machine

Projection angles

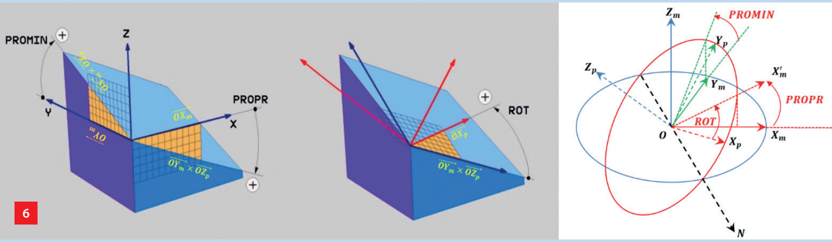

Depiction of the projection angle.

Projection angles define a TWP through two angles that are determined by projecting the first coordinate plane (*ZX* with tool axis *Z*) and the second coordinate plane (*YZ* with tool axis *Z*) onto the TWP. When applied to the machine coordinate system, they are indicated as follows (Figure 6):

PROPR: Projected angle of the TWP in the first coordinate plane of the fixed machine coordinate system (*ZX* for tool axis *Z*).
PROMIN: Projected angle in the second coordinate plane of the fixed machine coordinate system (*YZ* for tool axis *Z*).
ROT: Rotation of the tilted coordinate system around the tilted tool axis.

Given direction vectors of $\overrightarrow{OX_m}, \overrightarrow{OY_m}, \overrightarrow{OZ_m}$, $\overrightarrow{OX_p}, \overrightarrow{OY_p}, \overrightarrow{OZ_p}$, the values of ***PROPR, PROMIN, ROT***, represented as *B*, *A* and *C*, respectively, can be calculated as follows:

$$B = \overrightarrow{OX_m} \angle (\overrightarrow{OY_m} \times \overrightarrow{OZ_p})$$
$$A = (\overrightarrow{OX_m} \times \overrightarrow{OZ_p}) \angle \overrightarrow{OY_m}$$
$$C = (\overrightarrow{OY_m} \times \overrightarrow{OZ_p}) \angle \overrightarrow{OX_p}$$

$$\mathbf{PROPR(B)} = \begin{bmatrix} \cos B & 0 & \sin B \\ 0 & 1 & 0 \\ -\sin B & 0 & \cos B \end{bmatrix}$$

$$\mathbf{PROMIN(A)} = \begin{bmatrix} 1 & 0 & 0 \\ 0 & \cos A & -\sin A \\ 0 & \sin A & \cos A \end{bmatrix}$$

$$\mathbf{ROT(C)} = \begin{bmatrix} \cos C & -\sin C & 0 \\ \sin C & \cos C & 0 \\ 0 & 0 & 1 \end{bmatrix}$$

Given the values of ***PROPR (B), PROMIN (A), ROT (C)*** and vectors $\overrightarrow{OX_m}, \overrightarrow{OY_m}, \overrightarrow{OZ_m}$ the vectors $\overrightarrow{OX_p}, \overrightarrow{OY_p}, \overrightarrow{OZ_p}$, can be calculated as follows:

$$\overrightarrow{OZ_p} = \overrightarrow{OX_m} \cdot PROPR(B) \times \overrightarrow{OY_m} \cdot PROMIN(A)$$
$$\overrightarrow{OX_p} = \overrightarrow{OX_m} \cdot PROPR(B) \cdot ROT(C)$$
$$\overrightarrow{OY_p} = \overrightarrow{OX_p} \times \overrightarrow{OZ_p}$$


7

Test object milled to its final shape based on an adjusted NC-code.

must of course support the TWP way of working, however, the solution does not require an API or direct access to the operating system.

Implementation of the proven 3D&FPP concept will no doubt require, to some extent, the integration of systems (scanning system, the Compiler and the CNC machine), a clear understanding of the data management involved and, last but not least, adjustments to production processes and procedures.

Whether this approach will decrease production costs and time in an industrial environment will greatly depend on the production processes in place and on the type of products or product families being produced. For a rudimentary assessment of the applicability of the 3D&FPP approach, taking into account manufacturers' production specifics, a calculation format will be made available on the project website [12].

REFERENCES

[1] Briére-Côte, A., Rivest, L., and Maranzana, R., "3D CAD model comparison: An evaluation of model difference identification technologies", *Comput. Aided Des. Appl.*, 10, pp. 173-195, 2013, *doi:10.3722/cadaps.2013.173-195*
[2] Tam, G.K.L., et al, "Registration of 3D Point Clouds and Meshes: A Survey from Rigid to Nonrigid", *IEEE Trans. Vis. Comput. Graph.*, 19, pp. 1199-1217, 2013, *doi:10.1109/TVCG.2012.310*
[3] Maiseli, B., Gu, Y., and Gao, H., "Recent developments and trends in point set registration methods", *J. Vis. Commun. Image Represent.*, 46, pp. 95-106, 2017, *doi:10.1016/j.jvcir.2017.02.012*
[4] Jian, B., and Vermuri, B.C., "Robust point set registration using Gaussian mixture models", *IEEE Trans. Pattern Anal. Mach. Intell.*, 33, pp. 1633-1645, 2010, *doi:10.1099/TPAMI.2010.223*
[5] Rusinkiewics, S., and Levoy, M.,, "Efficient variants of the ICP algorithm", *Proc. Int. Conf. 3-D Digit. Imaging Model. 3DIM*, pp. 145-152, 2001, *doi: 10.1109/IM.2001.924423*
[6] Myronenko, A., and Song, X., "Point-Set Registration: Coherent Point Drift", *IEEE Trans. Pattern Anal. Mach. Intell.*, 32, pp. 2262-2275, 2010, *doi: 10.1109/TPAMI.2010.46*
[7] Khoo, Y., and Kapoor, A., "Non-Iterative Rigid 2D / 3D Point-set Registration Using Semidefinite Programming", *IEEE Trans. Image Process.*, 25, pp. 2956-2970, 2016.
[8] Siemens, D MC, *SINUMERIK Milling with SINUMERIK*, 2011.
[9] Apro, K., *Secrets of 5-Axis Machining*, Industrial Press, 2008.
[10] Europe FGC, *FANUC 5-Axis Machining Functions*.
[11] Heidenhain, *HEIDENHAIN iTNC 530 User's Manual*, 2005.
[12] *www.3dfpp.eu*

FOUNDATIONS AND EMERGING APPLICATIONS

Following the school for smart optics technologies in 2016, DCSC organised a second school of this type in Delft (NL), this time in the context of two international optics events that were held in conjunction. The Adaptive Optics School covered all aspects of applied adaptive optics, with special emphasis on the theoretical foundations of both real-time imaging and post-processing.

TIJMEN VAN OLDENRIJK

Recently, Delft University of Technology issued a press release announcing that researchers from DCSC and the Imaging Physics (Imphys) department have integrated two existing techniques within super-resolution microscopy into a new method (Figure 1), something many experts thought technically impossible. The new technique, SIMFLUX, combines Single Molecule Localization Microscopy (SMLM) with Structured Illumination Microscopy (SIM).

It is a recent example of what can be achieved through the skilful integration of methods and the collaborative synergy between the two departments. The kind of expertise DCSC brings to the table is itself about strongly integrating methods. Its Smart Optics Lab aims to develop new imaging instruments that maintain or increase performance while decreasing cost and maintenance complexity, and the key to optimising this trade-off is to integrate systems and control methodologies with maximum information processing through all components into the instrument design from the onset.

To make this kind of knowledge available to both wider academia and the industry, a school for smart optics technologies was organised in 2016 [1]. In October 2019, a second school was organised, within the framework of the XII International Workshop on Adaptive Optics in Industry and Medicine (AOIMXII), and the second edition of Face2Phase, a conference that addresses imaging with phase information, both of which were held at the Science Centre Delft. Imphys and DCSC seamlessly integrated the two events.

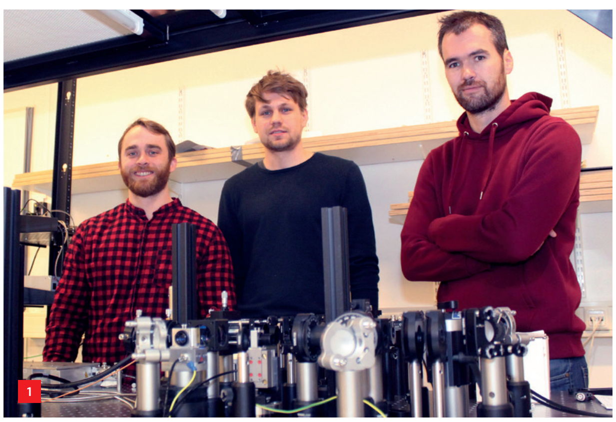

1

Post-doc Taylor Hinsdale (left) and Ph.D. candidates Rasmus Thorsen (middle) and Jelmer Cnossen (right) with the new SIMFLUX microscopy set-up.

AUTHOR'S NOTE
Tijmen van Oldenrijk is a teaching assistant at the Delft Center for Systems and Control, Delft University of Technology, Delft (NL).

t.vanoldenrijk@student.tudelft.nl
www.dcsc.tudelft.nl

Conference and workshop

The conference Fase2Phase [2], in its second edition this year, addressed imaging with the use of phase information and covered topics such as lensless imaging, aberration retrieval, adaptive and active optics, ptychography, holography, tomography, phase retrieval, and applications. It was chaired by Professor Paul Urbach of the Imphys department and Professor Martin Booth of Oxford University.

AOIMXII [3] focused on key topics related to the use of adaptive optics (AO) technology and methods, such as control for AO, wavefront sensing and correction, microscopy, computational imaging, lithography, and emerging technologies. The workshop was chaired by Professor Gleb Vdovin of DCSC.

Adaptive Optics School

The two-day School on Adaptive Optics, chaired by Professor Michel Verhaegen of DCSC, covered the use of the technology in a wide variety of applications, ranging from astronomy, ophthalmology and free-space optics to lithography and high-power lasers. This wide scope of exposure with an emphasis on the emerging applications was presented by a group of renowned, world-leading experts and attracted a decent crowd (Figure 2).

First day: fundamentals

Robert K. Tyson of the University of North Carolina in Charlotte (USA) gave an overview of AO systems, including the relationship between wavefront sensors, wavefront correctors and the integrated controls that link the

Participants of the Adaptive Optics School.

components together. After this general overview, Gleb Vdovin gave a broad and practical introduction to wavefront correction technologies. Caroline Kulcsár and Henri-François Raynaud of the Institut d'Optique Graduate School in France presented the principle of AO control for astronomical applications, ranging from the simple integral-action controller implemented in the very first operational system to high-performance controllers.

Boris Ferdman and Yoav Shechtman of Technion in Haifa, Israel, introduced image-plane-based AO optimisation, a very useful method to obtain information on phase aberrations in the pupil plane while avoiding direct wavefront sensing.

Second day: applications
Pablo Artal (University of Murcia, Spain) lectured on AO for vision and ophthalmology. He gave a review of the main optical properties of the eye and how they affect our visual capabilities, and of the use of AO technologies that enable seeing the retina with high resolution and the development of new instruments for visual testing. Then Na Ji (University of Berkeley, USA) talked about AO microscopy, including example applications to in-vivo imaging of the brain.
Jean-Marc Conan, of the French Aerospace Lab Onera, explained how free-space optical links, when compared to current radio-frequency links, offer very promising perspectives for data transfer, telecommunications and high-precision clock comparison. He detailed the key role of AO in bi-directional links and discussed the main error budget contributors that limit performance.

The final lecture was by Martin Booth, on AO for ultrafast lasers and laser machining. He discussed the problem of aberrations in laser processing and used it to outline appropriate methods for aberration correction and dynamic beam shaping and control, giving attention to scientific and industrial applications of adaptive laser machining.

State of the art

To conclude, two leading scientists from Michel Verhaegen's research group at DCSC and co-organisers of the school, Professor Gleb Vdovin and Dr. Oleg Soloviev, briefly commented on what is state of the art in AO, after the event. Both are active in academia as well as industry, and therefore have a firm grasp of both hardware and general design aspects, and optimisation and control aspects of AO systems.

What can you say about the current developments in AO?
Gleb Vdovin: "First of all, microscopy is an important area of application where AO techniques play an irreplacable role. Engineering of the point-spread function now allows for a resolution of tens of nanometers, which is much higher than the diffraction limit. Secondly, there is the area of optical communication, especially satellite communication, which because of the use of a directed beam is a peculiar means of communication, and difficult to tap. Without AO we would be completely unable to transmit to geostationary satellites.

"The third area of development is high-power lasers, which because of thermal deformations cannot operate without the adaptive instrumentation. And fourthly, there is of course the area of astronomy, which over the years has become completely grounded in AO. If we compare current developments to those discussed in our symposium three years ago there are no significant breakthroughs, just a gradual development. But if we compare them with the first conference on the topic 22 years ago, much progress has been made; one might speak of a revolution."

What developments could be interesting for precision engineers?
Oleg Soloviev: "While I guess controlling something at the level of a fraction of the wavelength of light already should sound intriguing enough for precision engineers, AO offers many interesting challenges here. During the last two decades, we have seen AO moving from correction of several first Zernike polynomials with a phase residual error of 1 rad rms and straightforward algorithms for closing the feedback loop while ignoring any dynamical aspects, to the optimal, high-performance control of several thousands of actuators, which can be adaptively tuned for high noise levels or sudden vibrations and strong wind shakes.

"In other words, while 20 years ago astronomers were glad to be able to see a double star with the help of AO, now their ambitions extend to exo-planet detection. The same holds for (in-vivo) bio-medical applications, where wavefront shaping requires principally new control techniques. These developments of course imply new challenges in the fabrication of the high-precision AO elements."

REFERENCES
[1] T. van Oldenrijk, "Open window on the future of smart optics systems", *Mikroniek*, 56 (2), pp. 42-45, 2016.
[2] *www.face2phase.nl*
[3] *www.aoimxii.org/delft*

28 January 2020, Veldhoven (NL)
CLEAN 2020
This theme day, organised by Mikrocentrum, provides an expert's view on cleanliness. Speakers from academia and industry will present new developments, discuss process and cost optimisation, review quality control and share best-practice applications.

WWW.MIKROCENTRUM.NL

26-27 February 2020, Aachen (DE)
SIG Meeting Thermal Issues
Meeting hosted by euspen, on measurement and simulation of thermal effects as a major contributor to errors on machine tools, measuring equipment and workpieces.

WWW.EUSPEN.EU

4-5 March 2020, Veldhoven (NL)
RapidPro 2020
The annual event showcasing solutions for prototyping, product development, customisation and rapid, low-volume & on-demand production.

WWW.RAPIDPRO.NL

17-20 March 2020, Utrecht (NL)
ESEF / TechiShow 2020
The premier exhibitions in the Benelux area in the field of supply, subcontracting, product development and engineering (ESEF), and industrial production technology and processing of metals and plastics (TechniShow), respectively.

WWW.ESEF.NL
WWW.TECHNISHOW.NL

21-22 April 2020, Aachen (DE)
Aachen Polymer Optics Days 2020
Conference devoted to innovations and trends in optical plastics production. The topics range from classical injection moulding to material-related issues and aspects of digitalisation in production. Organised by Fraunhofer IPT and ILT, and the Institute of Plastics Processing (IKV) in Industry and the Skilled Crafts at RWTH Aachen University.

AACHEN.POLYMEROPTICS.DE

14-15 May 2020, Aachen (DE)
30th Aachen Machine Tool Colloquium
The general topic of AWK 2020 (Aachen Machine Tool Colloquium, Aachener Werkzeugmaschinen-Kolloquium) is "Internet of Production – Turning Data into Value". The focus is on the added value of comprehensive production networking, from demand-oriented data acquisition to the application of machine learning algorithms to the fast and error-free implementation of changes in series production.

WWW.AWK-AACHEN.DE

3-4 June 2020, Veldhoven (NL)
Materials+Eurofinish+Surface 2020
At this new event, a combination of three trade fairs, product developers, product designers, engineers, R&D professionals, production staff, material specialists and researchers can meet the entire value chain; from design and materials to analysis and coating technology.

WWW.MATERIALS-EUROFINISH-SURFACE.COM

8-12 June 2020, Geneva (CH)
Euspen's 20th International Conference & Exhibition
The event features latest advances in traditional precision engineering fields such as metrology, ultra-precision machining, additive and replication processes, precision mechatronic systems & control and precision cutting processes. This 20th edition will be a landmark event at CERN, home of the largest particle physics laboratory in the world.

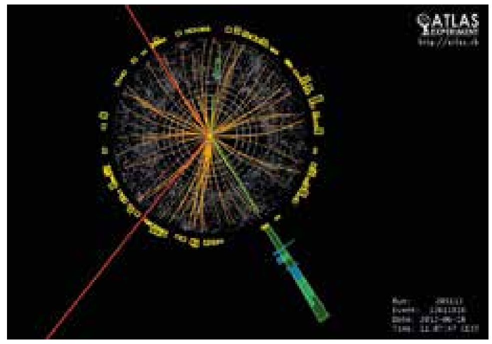

The ATLAS experiment at CERN, host of euspen's 20th International Conference & Exhibition. (Image: CERN)

WWW.EUSPEN.EU

10-11 June 2020, Veldhoven (NL)
Vision, Robotics & Motion 2020
This trade fair & congress presents the future of human-robot collaboration within the manufacturing industry.

WWW.VISION-ROBOTICS.NL

17 June 2020, Den Bosch (NL)
Dutch System Architecting Conference
The third edition of this conference features system architecting as a distinguishing discipline in the development and commercialisation of complex systems, products and machines.

WWW.SYSARCH.NL

8-9 September 2020, Sint-Michielsgestel (NL)
DSPE Conference on Precision Mechatronics 2020
Fifth edition of DSPE's conference on precision mechatronics. This year's theme is "Uncovering the Essence". The call for abstracts closes on 1 February 2020. See also page 57.

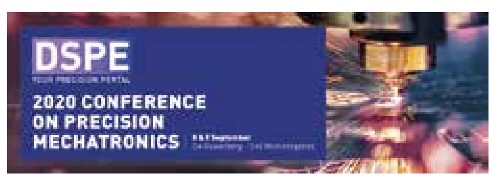

WWW.DSPE-CONFERENCE.NL

ECP² COURSE CALENDAR

COURSE (content partner)	ECP² points	Provider	Starting date
FOUNDATION			
Mechatronics System Design - part 1 (MA)	5	HTI	6 April 2020
Mechatronics System Design - part 2 (MA)	5	HTI	5 October 2020
Fundamentals of Metrology	4	NPL	to be planned
Design Principles	3	MC	11 March 2020
System Architecting (S&SA)	5	HTI	9 March 2020
Design Principles for Precision Engineering (MA)	5	HTI	22 June 2020
Motion Control Tuning (MA)	6	HTI	to be planned
ADVANCED			
Metrology and Calibration of Mechatronic Systems (MA)	3	HTI	27 October 2020
Surface Metrology; Instrumentation and Characterisation	3	HUD	to be planned
Actuation and Power Electronics (MA)	3	HTI	to be planned (2020)
Thermal Effects in Mechatronic Systems (MA)	3	HTI	23 June 2020
Summer school Opto-Mechatronics (DSPE/MA)	5	HTI	upon request
Dynamics and Modelling (MA)	3	HTI	23 November 2020
Manufacturability	5	LiS	to be planned
Green Belt Design for Six Sigma	4	HI	3 February 2020
RF1 Life Data Analysis and Reliability Testing	3	HI	30 March 2020
Ultra-Precision Manufacturing and Metrology	5	CRANF	20 January 2020
SPECIFIC			
Applied Optics (T2Prof)	6.5	HTI	18 February 2020
Advanced Optics	6.5	MC	5 March 2020
Machine Vision for Mechatronic Systems (MA)	2	HTI	upon request
Electronics for Non-Electronic Engineers – Analog (T2Prof)	6	HTI	to be planned
Electronics for Non-Electronic Engineers – Digital (T2Prof)	4	HTI	to be planned
Modern Optics for Optical Designers (T2Prof) - part 1	7.5	HTI	to be planned (Q3 2020)
Modern Optics for Optical Designers (T2Prof) - part 2	7.5	HTI	to be planned (Q3 2020)
Tribology	4	MC	10 March 2020
Basics & Design Principles for Ultra-Clean Vacuum (MA)	4	HTI	15 June 2020
Experimental Techniques in Mechatronics (MA)	3	HTI	23 June 2020
Advanced Motion Control (MA)	5	HTI	to be planned (2020)
Advanced Feedforward Control (MA)	2	HTI	to be planned (Q4 2020)
Advanced Mechatronic System Design (MA)	6	HTI	to be planned (2020)
Passive Damping for High Tech Systems (MA)	3	HTI	26 May 2020
Finite Element Method	5	MC	in-company
Design for Manufacturing – Design Decision Method	3	SCHOUT	in-company

ECP² program powered by euspen

The European Certified Precision Engineering Course Program (ECP²) has been developed to meet the demands in the market for continuous professional development and training of post-academic engineers (B.Sc. or M.Sc. with 2-10 years of work experience) within the fields of precision engineering and nanotechnology. They can earn certification points by following selected courses. Once participants have earned a total of 45 points, they will be certified. The ECP² certificate is an industrial standard for professional recognition and acknowledgement of precision engineering-related knowledge and skills, and allows the use of the ECP² title.

WWW.ECP2.EU

Course providers

- High Tech Institute (HTI)
  WWW.HIGHTECHINSTITUTE.NL
- Mikrocentrum (MC)
  WWW.MIKROCENTRUM.NL
- LiS Academy (LiS)
  WWW.LISACADEMY.NL
- Schout DfM (SCHOUT)
  WWW.SCHOUT.EU
- Holland Innovative (HI)
  WWW.HOLLANDINNOVATIVE.NL
- Cranfield University (CRANF)
  WWW.CRANFIELD.AC.UK
- Univ. of Huddersfield (HUD)
  WWW.HUD.AC.UK
- National Physical Lab. (NPL)
  WWW.NPL.CO.UK

Content partners

- DSPE
  WWW.DSPE.NL
- Mechatronics Academy (MA)
  WWW.MECHATRONICS-ACADEMY.NL
- Technical Training for Prof. (T2Prof)
  WWW.T2PROF.NL
- Systems & Software Academy (S&SA)

Euspen gains EU funding

The European Society for Precision Engineering and Nanotechnology (euspen) has been successful in gaining Erasmus+ funding from the European Union (EU). This concerns a new euspen initiative, the European Framework for Continuous Professional Development in Precision Engineering for Advanced Manufacturing.

The general aim of the project is to support continuous professional development in precision engineering, offering high-quality learning opportunities to individuals for specialised competences, in order to strengthen employability and personal development in strategic industries. This project will allow euspen to fully develop a European framework for training in precision engineering for the advanced manufacturing sector, to increase the availability of specialised trainings in multiple European countries

Currently, euspen is already running the ECP^2 program. This European Certified Precision Engineering Course Program offers a short-course assessment standard and aims at supporting continuous professional development in precision engineering from a European perspective, building on DSPE's successful Certified Precision Engineer program.

Erasmus+

Erasmus+ is the programme for education, training, youth and sport, with the EU committing € 14.7 billion to the programme between 2014 and 2020. The euspen project is funded under Key Action 2 of the programme; Cooperation for Innovation and the Exchange of Good Practices. Projects funded under this Key Action will focus on sharing, developing and transferring innovative practices in education, training and youth provision between participating countries.

WWW.EUSPEN.EU
EC.EUROPA.EU/PROGRAMMES/ERASMUS-PLUS

IBS introduces Position Inspector

IBS Precision Engineering in Eindhoven (NL) specialises in ultra-precision measurement and engineering solutions, including machine tool metrology. The latest addition to IBS's portfolio of machine tool inspection & analyzer solutions is the Position Inspector, which delivers rapid and reliable measurement of the positioning accuracy of machine tools.

The Position Inspector comes with the Trinity wireless measuring head, which is placed in the spindle, and a traceable artefact, comprising two orthogonally positioned calibrated ball beams. Using this set-up, X-, Y- and Z-errors (linearity, straightness and squareness errors) are measured simultaneously, with 0.2 μm resolution and within 5 minutes. The measurement software provides compensation data enabling corrective action to avoid wasted products. All tests are in compliance with the ISO 230 standard, "Test code for machine tools", and the sensor is calibrated and supplied with a traceable certificate.

The new metrology tool can be used for qualification of tool positioning accuracy & repeatability. A quality report is issued including quality management information and status & trend data for predictive maintenance.

The metrology concept of the Position Inspector is based on that of IBS's successful Rotary Inpector, which is used for determining (and correcting) critical geometric and dynamic performance parameters of 5-axis machines that feature two rotary axes.

WWW.IBSPE.COM

Delta robot live in digital twin

Digital twin technology is one of the key tools of today's Smart Industry for optimally designing and controlling products and systems. The engineering firm QING from Arnhem uses digital twins, which link a virtual model (3D CAD + simulations) to a physical system, to smartly integrate industrial robots into production processes, among other things.

During the Digital Twin Live event last month at the Smart Production Center (SPC) in Arnhem (NL), QING presented a number of innovative digital twin applications. The event was a joint initiative by QING, HAN Automotive Research, Visual Components and Cadmes. The SPC was developed by HAN Automotive Research, part of HAN University of Applied Sciences, specifically for the production of lightweight (composite) components for the automotive industry. Aspects covered by the SPC include continuous (24/7) production, mass production of composites, Internet of Things and big data.

The objective of the event was to show how a digital twin can be used in real-time to improve processes. That happened with a production cell in the SPC. Part of that cell is a delta robot, which places composite products in the right position and orientation so that the next robot can then place them in a press. The delta robot weighs the product along the way; a weight that is either too low or too high indicates an incorrect product, which the robot will then remove from the cell. With the help of the Visual Components software for 3D production simulation, QING programmed the delta-robot control.

The script that QING developed was custom-made for delta robots from Fanuc, but now it is easy to create scripts for every type of robot. The user only has to put the last configuration in the robot controller, for example the end point of the robot to which a tool is attached and the robot's reference frame. For the user, this is zero programming and that saves a lot of time.

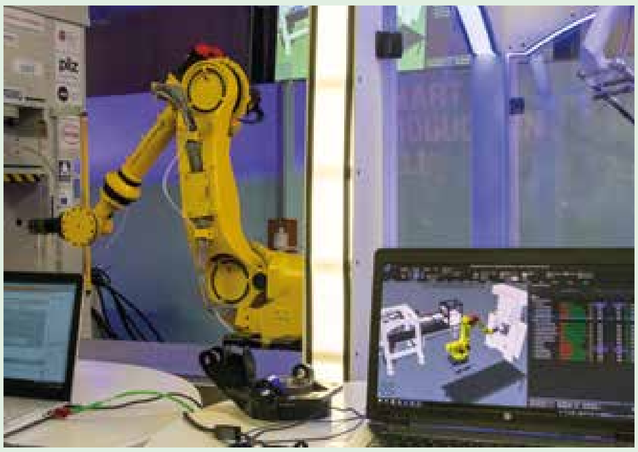

WWW.QING.NL
WWW.SPECIALS.HAN.NL/SITES/AUTOMOTIVE-RESEARCH

DSPE CONFERENCE 2020: "UNCOVERING THE ESSENCE"

"Uncovering the Essence" is the theme of the 5th edition of the DSPE Conference on Precision Mechatronics, which will be held on 8-9 September 2020, once again in conference hotel De Ruwenberg in Sint Michielsgestel (NL). The call for abstracts closes on 1 February 2020.

The theme reflects the challenge that each of us is working on, either directly or indirectly, for example by investigating the fundamentals of particle contamination or developing improved control schemes. Ultimately, precision engineering and mechatronics, i.e. the equipment it produces, is an important enabler for uncovering the essence of comprehensive phenomena such as climate change, life or even the cosmos.

All this would be impossible without electron microscopes, satellites, healthcare devices and semi-conductor equipment for manufacturing the required computing power. Therefore, traditional core topics have been supplemented with sessions on adjacent application areas. Areas of interest range from disruptive technologies and design principles to picometer stability and energy efficiency.

With three guest speakers, 21 oral presentations, many posters/demos and a social event, the DSPE Conference will offer plenty of room for networking and food for thought and discussion about the essence and its (precision) details. The target group includes technologists, designers and architects in precision mechatronics, who are connected to DSPE, Brainport Industries, the mechatronics contact groups MCG/MSKE or selected companies or educational institutes.

The deadline for short abstract submission is 1 February 2020. For accepted papers the final submission date is 15 June. Early bird registration closes on the 15th of May.

INFO@DSPE-CONFERENCE.NL
WWW.DSPE-CONFERENCE.NL

New edition of Optomechanical system design course

The DSPE Optics Week 2019 saw the successful premiere of a three-day Optomechanical system design course. As there are currently no courses on this topic being offered in Europe, DSPE decided to set one up in order to promote the importance of optomechanical system design, a truly multidisciplinary expertise that combines optical, mechanical, mechatronic, thermal, electrical, control, and systems engineering. The first edition of the course held last October with 35 participants was completely 'sold out' and the waiting list for a next edition filled quickly. Therefore, DSPE decided to organise a second edition of this course, on 9-11 March 2020, in Eindhoven (NL). Registration is still open.

The course is intended for mechanical, mechatronic and optical engineers involved in optomechanical system design. The teachers are experienced engineers, who know the tricks of the trade in optomechatronics, system architecture, system design and engineering, and optomechanical engineering. Together they draw upon more than 100 years of experience in this field at Dutch universities and research institutes, and in the high-tech industry.

WWW.DSPE.NL/EDUCATION

Impressions of the 2018 edition of the DSPE Conference.

Automation Technology

Festo BV
Schieweg 62
2627 AN DELFT
The Netherlands
T +31 (0)15-2518890
E sales@festo.nl
W www.festo.nl
Contact person:
Mr. Ing. Richard Huisman

Festo is a leading world-wide supplier of automation technology and the performance leader in industrial training and education programs.

member DSPE

Cleanrooms

Brecon Group
Droogdokkeneiland 7
5026 SP Tilburg
T +31 (0)76 504 70 80
E brecon@brecon.nl
W www.brecon.nl

Brecon Group can attribute a large proportion of its fame as an international cleanroom builder to continuity in the delivery of quality products within the semiconductor industry, with ASML as the most important associate in the past decades.

Brecon is active with cleanrooms in a high number of sectors on:
* Industrial and pharmaceutical
* Healthcare and medical devices

member DSPE

Connect 2 Cleanrooms BV
Newtonlaan 115
Zen Building
3584 BH Utrecht
Nederland
T +31 (0)30 210 60 51
E info@connect2cleanrooms.com
W www.connect2cleanrooms.nl

Developing the most appropriate cleanroom to transform your production is our passion. Our scalable and connected cleanrooms have been delivering regulatory compliance to our clients since 2002. We innovate to overcome your contamination control challenges – resulting in a new generation of scalable cleanrooms that set an unprecedented benchmark in the industry.

member DSPE

Development

TNO
T + 31 (0)88-866 50 00
W www.tno.nl

TNO is an independent innovation organisation that connects people and knowledge in order to create the innovations that sustainably boosts the competitiveness of industry and wellbeing of society.

member DSPE

Development and Engineering

Segula Technologies Nederland B.V.
De Witbogt 2
5652 AG Eindhoven
T +31 (0)40 8517 500
W www.segula.nl

SEGULA Technologies Nederland BV develops advanced intelligent systems for the High Tech and Automotive industry. As a project organisation, we apply our (engineering) knowledge to non-linear systems. This knowledge is comprised of systems architecture and modelling, analysis, mechanics, mechatronics, electronics, software, system integration, calibration and validation.

member DSPE

Education

Leiden school for Instrumentmakers (LiS)
Einsteinweg 61
2333 CC Leiden
The Netherlands
T +31 (0)71-5681168
E info@lis.nl
W www.lis.nl

The LiS is a modern level 4 MBO school with a long history of training Research instrumentmakers. The school establishes projects in cooperation with industry and scientific institutes thus allowing for professional work experience for our students. LiS TOP accepts contract work and organizes courses and summer school programs for those interested in precision engineering.

member DSPE

Electrical Discharge Machining (EDM)

CVT BV
Heiberg 29C
5504 PA Veldhoven
The Netherlands
T +31 (0)497 54 10 40
E info@cvtbv.nl
W www.cvtbv.nl

Partner high tech industry for wire EDM precision parts. Flexible during day shifts for prototyping. Outside office hours low cost unmanned machining. Call and enjoy our expertise!

member DSPE

Ter Hoek Vonkerosie
Propaanstraat 1
7463 PN Rijssen
T +31 (0)548 540807
F +31 (0)548 540939
E info@terhoek.com
W www.terhoek.com

INNOVATION OF TOMORROW, INSPIRATION FOR TODAY
Staying ahead by always going the extra mile. Based on that philosophy, Ter Hoek produces precision components for the high-tech manufacturing industry.

We support customers in developing high-quality, custom solutions that can then be series-produced with unparalleled accuracy. That is what makes us one of a kind.
It is in that combination of innovative customization and repeated precision that we find our passion. Inspired by tomorrow's innovation, each and every day.

member DSPE

Lasers, Light and Nanomotion

Laser 2000 Benelux C.V.
Voorbancken 13a
3645 GV Vinkeveen
Postbus 20, 3645 ZJ Vinkeveen
T +31(0)297 266 191
F +31(0)297 266 134
E info@laser2000.nl
W www.laser2000.nl

Laser 2000 Benelux considers it her mission to offer customers the latest photonics technologies available.
Our areas of expertise are:
- Lasers, scanners and laser machines for industry and research
- Light metrology instruments for LED and luminaire industries
- Light sources for scientific applications
- Piezo- and stepper motion products for nano- and micro positioning
- Inspection and research grade high speed cameras
- Laser safety certified products

te lintelo systems bv
photonics. our passion!
35 YEARS

Te Lintelo Systems B.V.
Mercurion 28A
6903 PZ Zevenaar
T +31 (0)316 340804
E contact@tlsbv.nl
W www.tlsbv.nl

Photonics is our passion!
Our experienced team is fully equipped to assist you with finding your best optical business solution.
For over 35 years TLS represent prominent suppliers in the photonics industry with well-educated engineers, experience and knowledge.
Over the years we became the specialist in the field of:
- Lasers
- Light metrology,
- Opto-electronic equipment,
- Positioning equipment
- Laser beam characterization and positioning,
- Interferometry,
- (Special) Optical components,
- Fiber optics,
- Laser safety

Together with our high end suppliers we have the answer for you!

member DSPE

Mechatronics Development

SOURCE OF YOUR TECHNOLOGY

Sioux CCM
De Pinckart 24
5674 CC Nuenen
T +31 (0)40 2635000
F info.ccm@sioux.eu
W www.sioux.eu

Sioux CCM is a technology partner with a strong focus on mechatronics.
We help leading companies with the high-tech development, industrialization and creation of their products, from concept stage to a prototype and/or delivery of series production.
Commitment, motivation, education and skills of our employees are the solid basis for our business approach

Sioux CCM is part of the Sioux Group.

member DSPE

MTA creating machines together

MTA
Waterbeemd 8
5705 DN Helmond
T +31 (0)492 474992
E info@m-t-a.nl
W www.m-t-a.nl

MTA is an high-tech system supplier specialized in the development and manufacturing of mechatronic machines and systems.
Our clients are OEM s in the Packaging, Food, Graphics and High-tech industries.

member DSPE

Mechatronics Development

MI-Partners
Dillenburgstraat 9N
5652 AM Eindhoven
The Netherlands
T +31 (0)40 291 49 20
F +31 (0)40 291 49 21
E info@mi-partners.nl
W www.mi-partners.nl

MI-Partners is active in R&D of high-end mechatronic products and systems. We are specialised in concept generation and validation for ultra-fast (>10g), extremely accurate (sub-nanometers) or complex positioning systems and breakthrough production equipment.

member DSPE

Metal Precision Parts

Etchform BV
Arendstraat 51
1223 RE Hilversum
T +31 (0)35 685 51 94
F info@etchform.com
W www.etchform.com

Etchform is a production and service company for etched and electroformed metal precision parts.

member DSPE

Micro Drive Systems

maxon motor benelux
Josink Kolkweg 38
7545 PR Enschede
The Netherlands
F +31 53 744 0 713
E info@maxonmotor.nl
W www.maxonmotor.nl

maxon motor is a developer and manufacturer of brushed and brushless DC motors as well as gearheads, encoders, controllers, and entire precision drive systems. maxon motor is a knowledge partner in development. maxon drives are used wherever the requirements are particularly high: in NASA's Mars rovers, in surgical power tools, in humanoid robots, and in precision industrial applications, for example. Worldwide, maxon has more than 2,500 employees divided over sales companies in more than 40 countries and eight production locations: Switzerland, Germany, Hungary, South Korea, France, United States, China and The Netherlands.

member DSPE

Micro Drive Systems

FAULHABER Benelux B.V.
Drive Systems
High Tech Campus 9
5656 AE Eindhoven
The Netherlands
T +31 (0)40 85155-40
E info@faulhaber.be
E info@faulhaber.nl
W www.faulhaber.com

FAULHABER specializes in the development, production and deployment of high-precision small and miniaturized drive systems, servo components and drive electronics with output power of up to 200 watts. The product range includes brushless motors, DC micromotors, encoders and motion controllers. FAULHABER also provides customer-specific complete solutions for medical technology, automatic placement machines, precision optics, telecommunications, aerospace and robotics, among other things.

Physik Instrumente (PI)
Benelux BV
Hertog Hendrikstraat 7a
5492 BA Sint-Oedenrode
The Netherlands
T +31 (0)499-375375
F +31 (0)499 375373
E benelux@pi.ws
W www.pi.ws

Stay ahead with drive components, positioners and systems by PI. In-depth knowledge, extensive experience and the broadest and deepest portfolio in high-end nanopositioning components and systems provide leading companies with infinite possibilities in motion control.

member DSPE

Micro Laser Services / Metal Precision Parts

Raytech
Dirk Martensstraat 3A
8200 Brugge
Belgium
T +32 (0)50 45 44 05
E info@raytech.be
W www.raytech.be

As subcontractor, Raytech produces extreme accurate components by micro laser technologies.

Motion Control Systems

Aerotech United Kingdom
The Old Brick Kiln
Ramsdell, Tadley
Hampshire RG26 5PR
UK
T +44 (0)1256 855055
F +44 (0)1256 855649
W www.aerotech.co.uk

Aerotech's motion control solutions cater a wide range of applications, including medical technology and life science applications, semiconductor and flat panel display production, photonics, automotive, data storage, laser processing, electronics manufacturing and testing.

Motion Control Systems

Newport Spectra-Physics B.V.
Vechtensteinlaan 12 - 16
3555 XS Utrecht
T +31 (0)30 6592111
E netherlands@newport.com
W www.newport.com

Newport Spectra-Physics B.V. is a subsidiary of Newport, a leader in nano and micro positioning technologies with an extensive catalog of positioning and motion control products. Newport is part of MKS Instruments Inc., a global provider of instruments, subsystems and process control solutions that measure, control, power, monitor, and analyze critical parameters of advanced processes in manufacturing and research applications.

member DSPE

Physik Instrumente (PI)
Benelux BV
Hertog Hendrikstraat 7a
5492 BA Sint-Oedenrode
The Netherlands
T +31 (0)499-375375
F +31 (0)499 375373
E benelux@pi.ws
W www.pi.ws

Opt for state-of-the-art motion control systems from the world's leading provider PI. Developed, manufactured and qualified in-house by a dedicated and experienced team. Our portfolio includes a wide and deep range of components, drives, actuators and systems and offers infinite possibilities in motion control on a sub-micron and nanometer scale.

member DSPE

Optical Components

Molenaar Optics
Gerolaan 63A
3707 SH Zeist
T +31 (0)30 6951038
E info@molenaar-optics.nl
W www.molenaar-optics.eu

Molenaar Optics is offering optical engineering solutions and advanced products from world leading companies OptoSigma, Sill Optics and Pyser Optics.

member DSPE

Piezo Systems

HEINMADE BV
Heiberg 29C
NL - 5504 PA Veldhoven
T +31 (0)40 851 2180
E info@heinmade.com
W www.heinmade.com

As partner for piezo system solutions, HEINMADE serves market leaders in the high tech industry. Modules and systems are developed, produced and qualified in-house. HEINMADE distributes Noliac piezo components.

member DSPE

Piezo Systems

Physik Instrumente (PI)
Benelux BV
Hertog Hendrikstraat 7a
5492 BA Sint-Oedenrode
The Netherlands
T +31 (0)499-375375
F +31 (0)499 375373
E benelux@pi.ws
W www.pi.ws

High-precision piezo systems and applications that perform on a sub-micron and nanometer scale: world leader PI develops, manufactures and qualifies these in-house. With a broad and deep portfolio with infinite possibilities in components, drives, actuators and systems at hand, our experienced team is dedicated to find the best solution for any motion control challenge.

member DSPE

Precision Electro Chemical Machining

Ter Hoek Applicatie Centrum B.V.
Propaanstraat 1
7463 PN Rijssen
T +31 (0)548 540807
F +31 (0)548 540939
E info@terhoek.com
W www.terhoek.com

As Application Centre we possess the required knowledge to support our clients in every phase of development and process selection.
With our own PEM800 machine we can also use PECM in-house for the benefit of our clients.

member DSPE

Ultra-Precision Metrology & Engineering

IBS Precision Engineering
Esp 201
5633 AD Eindhoven
T +31 (0)40 2901270
F +31 (0)40 2901279
E info@ibspe.com
W www.ibspe.com

IBS Precision Engineering delivers world class measurement, positioning and motion systems where ultra-high precision is required. As a strategic engineering partner to the world's best manufacturing equipment and scientific instrument suppliers, IBS has a distinguished track record of proven and robust precision solutions. Leading edge metrology is at the core of all that IBS does. From complex carbon-fibre jet engine components to semiconductor chips accurate to tens of atoms; IBS has provided and engineered key enabling technologies.

member DSPE

ADVERTISERS INDEX